RENAN LUCAS FAGUNDES

MULTIFRACTAL ANALYSIS OF THE STREET NETWORK AND POPULATION: 15 LARGEST BRAZILIAN CITIES

LAVRAS – MG
2024

RENAN LUCAS FAGUNDES

MULTIFRACTAL ANALYSIS OF THE STREET NETWORK AND POPULATION:
15 LARGEST BRAZILIAN CITIES

Dissertação apresentada à Universidade Federal de Lavras, como parte das exigências do Programa de Pós-Graduação em Física, área de concentração em Física, para a obtenção do título de Mestre.

Prof. Dr. Fabiano Lemes Ribeiro
Orientador

LAVRAS – MG
2024

Ficha catalográfica elaborada pelo Sistema de Geração de Ficha Catalográfica da Biblioteca Universitária da UFLA, com dados informados pelo(a) próprio(a) autor(a).

Fagundes, Renan Lucas
Multifractal Analysis of the Street Network and Population : 15 Largest Brazilian Cities / Renan Lucas Fagundes. – Lavras : UFLA, 2024.
144 p. : il.

Dissertação(mestrado)–Universidade Federal de Lavras, 2024.
Orientador: Prof. Dr. Fabiano Lemes Ribeiro.
Bibliografia.

1. Multifractal Analysis. 2. Urban Scaling. 3. Science of Cities. I. Universidade Federal de Lavras. II. Título.

RENAN LUCAS FAGUNDES

MULTIFRACTAL ANALYSIS OF THE STREET NETWORK AND POPULATION: 15 LARGEST BRAZILIAN CITIES

ANÁLISE MULTIFRACTAL DA REDE DE RUAS E DA POPULAÇÃO: 15 MAIORES CIDADES BRASILEIRAS

Dissertação apresentada à Universidade Federal de Lavras, como parte das exigências do Programa de Pós-Graduação em Física, área de concentração em Física, para a obtenção do título de Mestre.

APROVADA em 21 de Fevereiro de 2024.

Profa. Dra. Angélica Sousa da Mata	UFLA
Dr. rer. nat. Diego Rybski	IOER e CSH Viena
Prof. Dr. Vinícius de Moraes Netto	UFF e UP

Prof. Dr. Fabiano Lemes Ribeiro
Orientador

LAVRAS – MG
2024

À minha filha Mariê e à minha esposa Sabrina.
Dedico.

ACKNOWLEDGEMENTS

I would like to thank Prof. Dr. Fabiano for his guidance, the trust he placed in me, the coffees, the conversations, the inspiration and the encouragement to continue my studies.

To my beloved daughter Mariê, for making me the luckiest father in the world.

To my beloved wife Sabrina, for her patience, consideration, love and for always believing in me.

To my dear mother Maria Teresa and my stepfather Lourival for their unconditional support.

To my mother-in-law Eliana and my father-in-law Evaldo for their unconditional support.

To my younger brothers, Mateus and José.

To my aunts Lúcia, Cristina, Maristela, Luiza, Maria Helena, my uncle Edson, my aunt Naninha who left us too soon and all my cousins.

To my friends André, Guto and Ícaro.

To the colleagues I made at UFLA, Gabriel, Rômulo, Nathan, Eduardo, Henrique, Thiago, David and Antônia.

To Prof. Dr. Rodrigo for the learning I brought from my scientific initiation degree and for encouraging me to continue my studies.

To Profa. Dra. Angélica for her directed studies and encouragement.

To *Black Label Society* and *Ark* for the phenomenal compositions, from the oldest to the newest, making me *headband* and forget about the difficult task of writing this work.

To the truck drivers and travelers who gave me rides home and back safely.

To CNPq, CAPES and UFLA.

This work was carried out with the support of FAPEMIG.

Without data you're just another person with an opinion.
(W. Edwards Deming)

ABSTRACT

By 2050, the world's population is expected to reach 9.8 billion people. This will result in significant challenges related to housing, infrastructure, basic services, food security, health, education, employment, safety and natural resources at all urban levels. Faced with this alarming scenario, there is an urgent need to understand how cities work. This knowledge can greatly assist public agents in making decisions. However, the literature widely recognizes that cities are complex systems with many interacting components. How can we bridge the gap between decision-making and the complexity of cities? To address this question, we examined Brazil's 15 largest cities in 2010 using fractal geometry, urban scaling and network science. We sought to demonstrate that both the street network and the population show multifractal patterns, indicating the existence of a non-linear dynamic governing the behavior of these patterns, which we suspect is closely related to their multifractal spectra. We believe that the shape of these spectra is closely linked to the geography and natural elements that make up the city. Furthermore, this study suggests that some urban laws of scale can be described in terms of endogenous variables such as population, area and fractal dimension by maximizing Shannon entropy, which is used to obtain the probability of interaction between two regions of the city. In addition, the generalized dimensions of the city can be considered to extend the scaling laws that take into account the notion of fractal dimension, in order to investigate which region or regions contribute most to the prediction of gross domestic product (GDP) and total street length. In addition, we sought to demonstrate that models which take endogenous factors into account to explain the economy and returns to scale can be simplified using only macroscopic quantities such as population, total street length and urban area. This simplification was applied to the set of 5523 Brazilian cities. Finally, the data indicates that the fractal dimensions of the nodes, links and cyclomatic number of the street networks analyzed are equal to the fractal dimension of Bonacich's centrality measure. Furthermore, the relationship between the topological quantities of this type of network remains constant, regardless of its size. In addition, there must be a close relationship between decision-makers and the knowledge generated. Therefore, we believe that in order to promote quality of life in urban environments, it is important to understand how cities work. This can be achieved through the use of computational tools and a theoretical basis derived from various complex systems topics.

Keywords: Multifractal Analysis; Urban Scaling; Science of Cities.

RESUMO

Prevê-se que, em 2050, a população mundial atinja 9,8 mil milhões de pessoas. Isto resultará em desafios significativos relacionados com a habitação, infra-estruturas, serviços básicos, segurança alimentar, saúde, educação, emprego, segurança e recursos naturais a todos os níveis urbanos. Diante desse cenário alarmante, é urgente entender o funcionamento das cidades. Esse conhecimento pode auxiliar muito os agentes públicos na tomada de decisões. No entanto, a literatura reconhece amplamente que as cidades são sistemas complexos com muitos componentes que interagem entre si. Como podemos fazer a ponte entre a tomada de decisões e a complexidade das cidades? Para abordar essa questão, examinamos as 15 maiores cidades do Brasil em 2010 usando geometria fractal, leis de escala urbana e ciência de redes. Buscamos demonstrar que tanto a rede de ruas quanto a população apresentam padrões multifractais, indicando a existência de dinâmica não linear governando o comportamento destes padrões, a qual suspeitamos estar intimamente relacionada com os seus espectros multifractais. Acreditamos que a forma destes espectros está intimamente ligada à geografia e aos elementos naturais que compõem a cidade. Além disso, este estudo apresenta indicativos de que as leis da escala urbana podem ser descritas em termos de variáveis endógenas como a população, a área e a dimensão fractal partindo da maximização da entropia de Shannon, utilizada para obter a probabilidade de interação entre duas regiões da cidade. Adicionalmente, o espetro multifractal das cidades pode ser considerado para alargar estas leis, afim de investigar qual ou quais regiões contribuem mais para a predição do produto interno bruto (GDP) e do comprimento total de ruas. No entanto, é necessária mais investigação. Buscou-se demonstrar que os modelos que consideram fatores endógenos para explicar a economia e o rendimento de escala podem ser simplificados utilizando apenas quantidades macroscópicas como a população, o comprimento total das ruas e a área urbana. Essa simplificação foi aplicada ao conjunto de 5523 cidades brasileiras. Finalmente, os dados indicam que as dimensões fractais dos nós, ligações e número ciclomático das redes de ruas analisadas são iguais à dimensão fractal da medida de centralidade de Bonacich. Além disso, a relação entre as grandezas topológicas desse tipo de rede permanece constante, independentemente do seu tamanho. Para além disso, deve existir uma relação estreita entre os decisores e o conhecimento gerado. Portanto, para promover a qualidade de vida em ambientes urbanos, é importante entender como as cidades funcionam. Isto pode ser conseguido através da utilização de ferramentas computacionais e de uma base teórica derivada de vários tópicos de sistemas complexos.

Palavras-chave: Análise Multifractal; Escala Urbana; Ciência das Cidades.

LIST OF FIGURES

LIST OF TABLES

SUMMARY

1 INTRODUCTION

Experts project that the world's population (*Pop*) will reach 9.8 billion people by 2050, see Figure 1.1, and the effects of climate change are already being felt by 75% of cities, which contribute 70% of greenhouse gas emissions[1] (NATIONS, 2017). This brings enormous challenges in terms of sustainability, significantly affecting issues related to adequate housing, infrastructure, basic services, food security, health, education, decent jobs, safety and natural resources, among others, at all urban scales (NATIONS, 2016).

Faced with this alarming scenario, it is extremely urgent to understand how cities work, both from a practical and theoretical point of view (BETTENCOURT; WEST, 2010; BETTENCOURT, 2013; BARTHELEMY, 2019b; RIBEIRO; RYBSKI, 2023). The knowledge generated in this process can be of great help in decision-making by public agents, especially in the creation of public policies focused on sustainability, with the aim of mitigating the effects of climate change and solving directly or indirectly related problems (WOODCOCK et al., 2009; SALLIS et al., 2016).

An interdisciplinary approach that has proved effective in understanding urban processes involves considering that cities are complex systems (RYBSKI; GONZALEZ, 2022). A complex system is made up of numerous elements interconnected locally in a non-trivial way, whose dynamics evolve in space and time, resulting in patterns of self-organization and emergent behaviour (SAYAMA, 2015; SIEGENFELD; BAR-YAM, 2020; BIANCONI et al., 2023). For example, ant colonies, brain, global financial markets, weather, traffic, and cities are examples of complex systems (THERAULAZ et al., 2002; BASSETT; GAZZANIGA, 2011; JOHNSON; JEFFERIES; HUI, 2003; LOVEJOY, 2022; DING et al., 2019; JOHNSON, 2009). These systems[2] have the remarkable ability to adapt to external effects, which makes them particularly relevant for the analysis and management of cities in a context of climate change and *Pop* growth.

With the aim of understanding cities in the light of complex systems, a group of researchers have dedicated their efforts to establishing a new field of science known as the Science of Cities (BATTY, 2012; BATTY, 2013). In short, this new field stands out for

[1] <https://www.citiesalliance.org/newsroom/news/results/climate-change-and-cities-infographic>.
[2] See some examples in <http://www.complexity-explorables.org/>.

bringing together scientific methodology, a multidisciplinary[3] approach and the analysis of real data in the search for solutions to urgent problems such as climate change, urbanization and transport, among other crucial challenges (ALBERTI, 2017; LOBO et al., 2020). Allied to this, the development of mathematical models plays a fundamental role in this process, although there are some caveats[4]. Various models have been proposed in this context (BATTY; LONGLEY, 1994; FRANKHAUSER, 2008; BETTENCOURT; WEST, 2010; BARTHELEMY, 2019a; BARTHELEMY, 2019b; KEUSCHNIGG, 2019; MOLINERO; THURNER, 2021; MOLINERO, 2022; ARCAUTE; RAMASCO, 2022; RIBEIRO; RYBSKI, 2023), but models that consider the multifractal nature of cities, considering both the road network, the *Pop* pattern and the urban scaling, have still been little explored. In this work we chose to explore these topics using concepts involving fractal geometry, urban scaling laws and network science. In particular, we focus on the 15 largest Brazilian cities in 2010.

Figure 1.1 – World population (*Pop*) projections from historical editions of the United Nations Population Prospects. Data available: <https://ourworldindata.org/population-projections>.

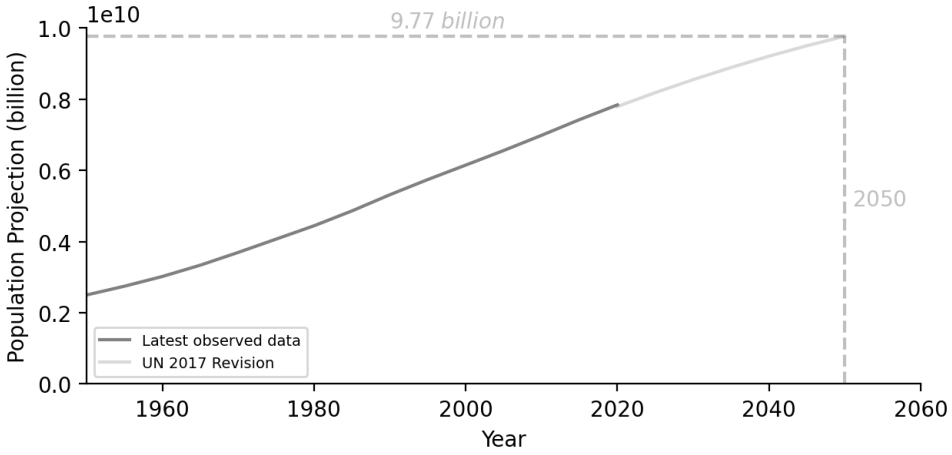

Source: United Nations, World Population Prospects (various years).

These three topics are some of the most important branches in the study of complexity science (SAYAMA, 2015). We will see that fractal geometry deals with abstract geometric objects that need to be described in terms of a different kind of geometry in which irregularity is inherent in the scales of nature. This is due to the first observations,

[3] Network and data sciences, business intelligence, artificial intelligence algorithms, internet of thing, blockchain, quantum computation, advanced robotics, renewable energy, 5G internet, to cite a few.

[4] <https://www.wired.com/2008/06/pb-theory/>.

mainly by Mandelbrot and others, that natural processes are irregular and repeat themselves on different scales of length and time (MANDELBROT, 1995; MANDELBROT; FREEMAN; COMPANY, 1983; MANDELBROT, 1986).

Figure 1.2 – Spatial pattern of the population (Pop) of Lavras in its street network (SN). We can see that the probability p in some radius (e.g 500 m) of meeting people is distributed in a multivariate normal way.

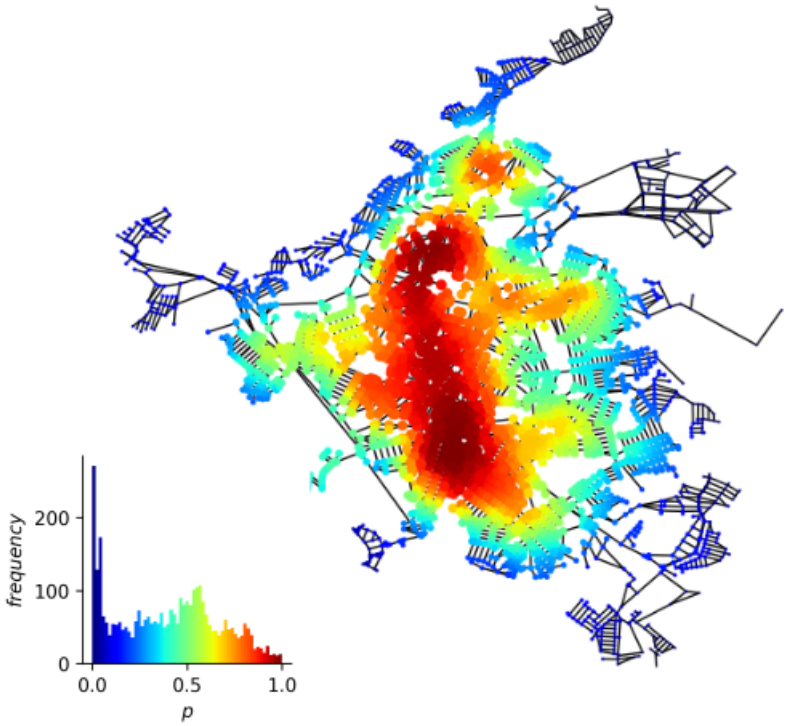

Source: Own authorship.

We show that the Pop and the street network (SN) of the largest Brazilian are multifractal structures. This means that both have local and global variability in their spatial patterns, resulting from non-linear dynamics that occur on the most varied size scales as well as in the most concentrated and rarefied parts. To capture these properties we use the multifractal spectrum and define rates (CHEN, 2018). With the spectrum it is possible to infer aggregation and diffusion processes to characterize these patterns (CHANUI et al., 2022; LONG; CHEN, 2021). An aggregation process means that both the SN and the Pop tend to concentrate in sites which are relatively larger than those occupying peripheral regions. The diffusion process tells us that peripheral places are denser in terms of people and streets than central ones.

Although it is not easy to know the dynamics of the irregularities observed in nature, it is possible to use some mathematical models to try to capture some of these processes. We will see that socio-economic activities, infrastructure resources and individual needs in cities tend to behave differently as the *Pop* grows. The difference between the three can be seen by measuring characteristic scaling exponents (BETTENCOURT; WEST, 2010).

In particular, the laws that describe the first two can be obtained by maximizing Shannon entropy – a quantity used in statistical physics to quantify uncertainty in stochastic processes – providing a general law for the probability of interaction between individuals or elements separated by a given distance, an idea first considered by Wilson (1967) to extend models of the spatial location of activities between areas of a region, and recently simplified by Batty (2021).

In addition, we will show that the model proposed by Molinero & Thurner (M&T), which allows inferring the wealth and efficiency, terms of the transport network, in the city via geometry, can be simplified heuristically considering only macroscopic variables such as area urban area, *Pop*, gross domestic product (GDP) and total street length. With such simplification it is possible to show two regimes, one linear and the other non-linear, for the scale exponent - ratio between the fractal dimensions of street network and population - that characterizes the relative spatial complexity between SN and *Pop*.

On the other hand, we will see that the street network of cities, indispensable for transporting information, goods and access to different regions, has very similar characteristics to a group of computers connected to the internet network, but that both can exhibit non-trivial properties of their own, allowing us to classify and characterize them (ERDÖS; RÉNYI, 1959; WATTS; STROGATZ, 1998; BARABASI; ALBERT, 1999; NEWMAN; WATTS; STROGATZ, 2002; MATA, 2020). In fact, some networks can exhibit properties very similar to the distribution of wealth and the irregular pattern of *Pop* occupation, that is, they have a power law behavior.

Therefore, fractal geometry, scaling laws and network science can help us to generate knowledge in order to guide decision-making in solving problems that can be found both in central regions - where the probability of finding people, stores, markets, hospitals, bakeries, bars, restaurants is higher and there are relatively few of them - and in the peripheral regions - where the probability of finding people is lower, the basic infrastructure

conditions is inadequate and where the majority of residents are partially excluded from the socio-economic benefits of growing cities (ARVIDSSON; LOVSJO; KEUSCHNIGG, 2013). See Fig. 1.2 for illustration.

This work attempts to unite these three topics and is divided as follows: in Chapter 2 we discuss the theoretical foundations involving fractal geometry, urban scale laws and network science. In particular, we will focus on the dimensions of capacity, information, correlation and the corresponding generalized dimensions. Also in this Chapter, we present the definition of skewness and aggregation-diffusion index, as well as spatial filling rates, where the above dimensions are extremely relevant. We will present the main centralities and topological measures associated to networks, in particular we will highlight some models and their properties. We end this Chapter by presenting some of the most important intra-city models recovered from the definition of the interaction probability, which in turn can be obtained via entropy maximization; in Chapter 3 we present the objectives that motivated the research and the justification; in Chapter 4, we present the materials and methods used in the work; in Chapter 5, we present the results of the research and discuss the findings; Chapter 6 presents the conclusions. Next, we present the bibliography consulted throughout the work. Finally, we present the appendices with information that complements the text.

2 THEORETICAL FOUNDATIONS

In this Chapter, we will provide a brief overview of fractal geometry and focus particularly on the main fractal dimensions used in the analysis of complex systems. These dimensions include the capacity dimension or box-counting dimension d_B, information dimension d_I, correlation dimension d_C, and generalized dimensions D_q of order q. It is possible to establish equivalences between the first three dimensions and the generalized dimensions for values of q equal to 0, 1, and 2, respectively. Details can be found in Appendix D.

We will also discuss the basics of multifractal theory and explain how the sandbox method can be used to approximate generalized dimensions. Additionally, we will introduce the concepts of skewness and aggregation-diffusion index and define terms such as spatial filling, redundancy, and correlation rates.

Furthermore, we will demonstrate how intra-city models can be deduced from entropy maximization and give an overview of the primary intra-city models that take fractal dimension into account.

Finally, we will review the three primary models used in network science: the random or Erdös-Rényi model (ER), Barabási-Albert (BA), and Watts-Strogatz (WS). We will also discuss several centrality and topological measures.

2.1 Fractal Geometry

Fractal geometry is the study of fractal or fractal structures that exhibit the remarkable property of being self-similar at different lengths and time scales – for example, landscape, rivers, earthquakes, lungs, blood vessels, distribution of asteroids, turbulence in fluid dynamics, percolation structures, the surface of solids, street networks (SN), population (Pop), etc (STANLEY; MEAKIN, 1988; TAKAYASU, 1990; SCHROEDER, 1991; APPLEBY, 1996; HARTE, 2001; ROSENBERG, 2021).

Howeever, the study of fractal structures is closely linked to the idea of scale invariance, a concept that will be discussed in detail in the next section. Researches in this topic dates back to Bachelier, Frish, Kolmogorov, and Mandelbrot (LOPES; BETROUNI, 2009). Zmeskal et al. (2013) note that the foundations of fractal geometry can be traced back to Leibniz in the 17th century, who studied the concept of recursive self-similarity. These authors, as well as Falconer (2013), agree that the first fractal structure was pro-

posed by Karl Weierstrass in 1872, a curve that is impossible to tangent and has a fractal dimension equal to 1[1], but according to Schroeder (1991), the first real fractal structure was generated by Lichtenberg in 1777 using electrical discharges in an insulator.

A fractal structure stands out for having a non-integer dimension, which may initially seem surprising. How is it possible for an object to occupy a certain space if its dimension, say, is 0.631 or 1.263?. The dimension of a fractal structure is a measure that quantifies the degree of complexity of patterns that repeat from the smallest to the largest scale. This dimension is greater than the dimension of the topological space and less than the dimension of the Euclidean space underlying the fractal structure in question (FALCONER, 2004).

As an illustration, consider that an object has b similar shapes of size $1/a$, then is possible to define it's similarity dimension by (TAKAYASU, 1990)

$$d_s = \frac{\log b}{\log a}, \tag{2.1.1}$$

If we consider the Cantor set, see Figure 2.1, obtained by removing the middle third of a unit line segment at each iteration, and the Koch curve, obtained by removing the middle third and replacing it with an equilateral triangle of the same size, then the similarity dimension of the Cantor set can be obtained when $b = 2$ and $a = 3$. Analogously, for the Koch curve we have $b = 4$ and $a = 3$.

On the other hand, according to Rosenberg (2021), real fractals have a finite scale which distinguishes them from artificial fractals and a single fractal dimension is not sufficient to characterize the complexity of the patterns in a system (FRANKHAUSER, 2008; MURCIO et al., 2015). In this context, it is essential to generalize the notion of fractal, as certain structures can exhibit completely different patterns depending on the region of analysis (i.e. there is a local dependency). Therefore, a more comprehensive analysis of these structures must take into account a spectrum of dimensions that the system can take on, allowing for the classification of more sparse regions as well as more densely packed regions of the geometric object under study.

One approach that meets these requirements is known as multifractal analysis, in which it is possible to generalize the notion of fractal dimension. This approach offers a deeper and more detailed understanding of complex structures, taking into account their

[1] <https://mathworld.wolfram.com/WeierstrassFunction.html>

Figure 2.1 – The Cantor set a) and the Koch curve b) are sets with fractal dimensions of 0.631 and 1.262, respectively. The Cantor set can be obtained by removing the middle third of a unit line segment at each iteration and the Koch curve can be obtained by removing the middle third and replacing it with an equilateral triangle of the same size. Note that the former has a dimension less than 1 and the latter has a higher value. This means that the Koch curve is spatially more complex than the Cantor set, because the former occupies much more two-dimensional space than the latter.

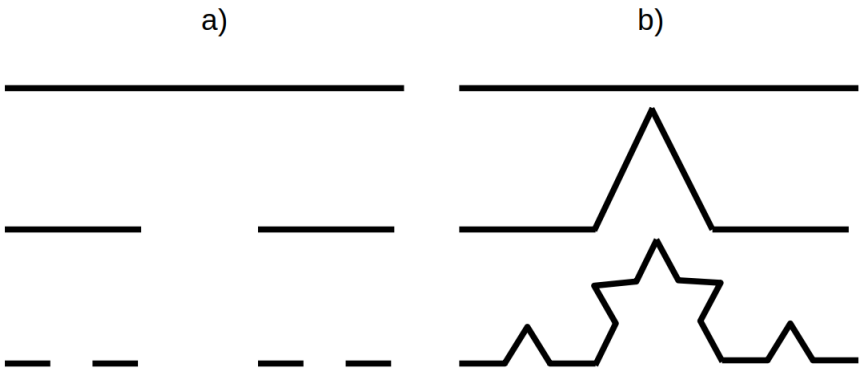

Source: Own Authorship.

local variation and allowing for a more precise characterization of their multifaceted complexity (WANG; YU; ANH, 2012; CHEN; WANG, 2013; MURCIO et al., 2015; CHEN, 2016; CHEN, 2018; LONG; CHEN, 2021; SONG; CHEN; BO, 2023).

A simple example that can be used to illustrate the notion of a multifractal structure is to consider Iteration Function Systems (IFS) with memory in the plane given by (BARNSLEY; DEMKO, 1985; HARTE, 2001; FALCONER, 2004; FRAME; NEGER, 2022)

$$\begin{cases} T_1(x,y) &= \left(\frac{\sqrt{2}}{2}x+1, \frac{\sqrt{2}}{2}y+1\right), \\ T_2(x,y) &= \left(\frac{\sqrt{2}}{2}x+1, -\frac{\sqrt{2}}{2}y+1\right), \\ T_3(x,y) &= \left(\frac{\sqrt{2}}{2}x+1, -\frac{\sqrt{2}}{2}y+1\right), \\ T_4(x,y) &= \left(-\frac{\sqrt{2}}{2}x+1, -\frac{\sqrt{2}}{2}y+1\right). \end{cases} \tag{2.1.2}$$

Thus, by assigning a probability p_i $(i = 1, 2, 3, 4)$ and a contraction factor (or the size of the self-similar segment that makes up the fractal) $r_i = 1/2$ $(i = 1, 2, 3, 4)$ to each transformation, we can use the generalized Moran equation (see Appendix A) to obtain the multifractal spectrum of the system satisfying (FEDER, 1988; SCHROEDER, 1991; ROSENBERG, 2021; FRAME; NEGER, 2022)

$$\sum_i p_i^q r_i^{\tau(q)} = 1, \tag{2.1.3}$$

a transcendental equation that restricts the orders $q \in \mathbb{R}$ of the probabilities of each transformation and their respective contraction factors. The quantity $\tau(q)$ is the mass exponent which will be discussed in section 2.1.4. Thus, without loss of generality, by choosing $p_1 = p_2 = p_3 = \frac{1}{10}$ and $p_4 = \frac{7}{10}$, which means that T_4 is seven times most frequent that T_1, T_2 and T_3. Then, it is possible to obtain the following multifractal spectrum in terms of the moments of order q

$$f(q) = \frac{\left(\frac{7^q}{3+7^q}\right)\log 7^q + \log\left(\frac{10^q}{3+7^q}\right) - \log 10^q}{\log 1/2}. \tag{2.1.4}$$

The pattern and the multifractal spectrum are presented in the Figure 2.2.

Figure 2.2 – (Top left) Spatial pattern generated by an Iterated Function System (IFS) with memory with probabilities $p_1 = p_2 = p_3 = 1/10$, $p_4 = 7/10$ and shrinkage factor $r_i = 1/2$ $(i = 1, 2, 3, 4)$. (Top right) Theoretical multifractal spectrum associated with the pattern with 50,000 points. (Bottom left) Spatial pattern formed by the points representing the population of the city of Brasília, DF, restricted to the geometries of the census tracts. Each point represents 500 people. (Bottom right) Empirical multifractal spectrum of this representation. α and $f(\alpha)$ characterize the local and global complexities of these systems.

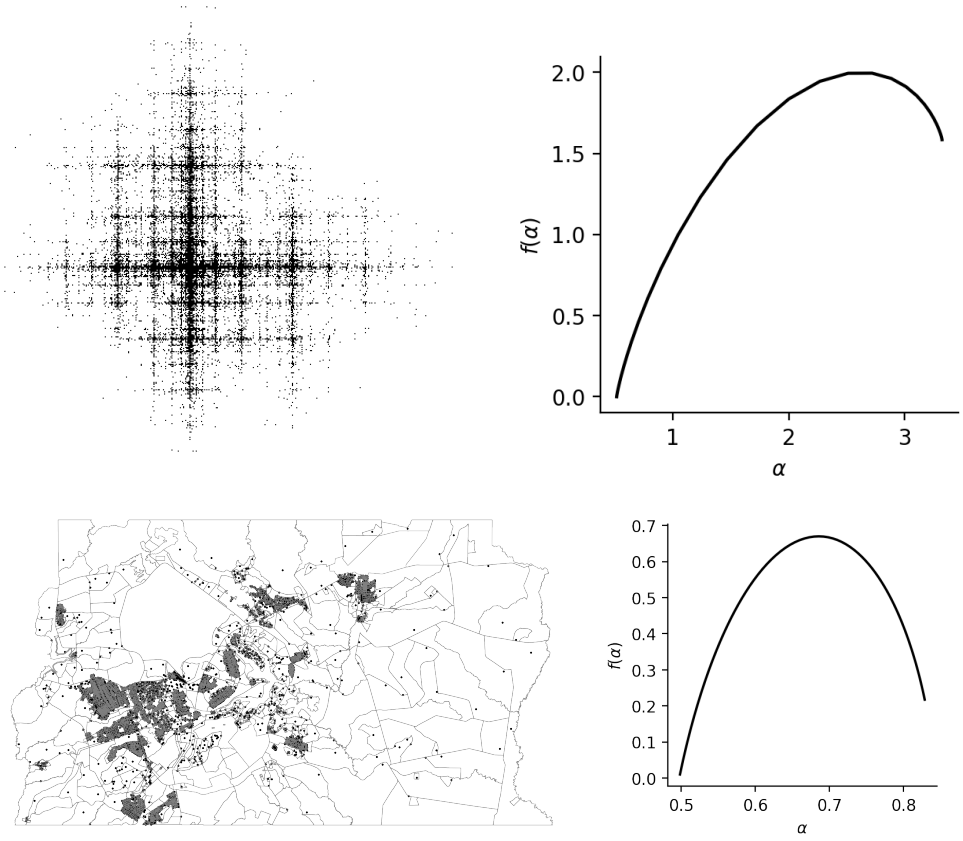

Source: Own Authorship.

Therefore, one of the first distinctions between a monofractal structure (one dimension) and a multifractal structure (many dimensions) is that the latter has an infinity of dimensions.

In addition, the pattern generated by the IFS with memory is dictated the most frequent dynamic represented by the transformation T_4, which also means that there is a dynamical process generating the spatial pattern of the fractal.

In this work, we will see that the shape of this special multifractal spectrum is a consequence of these self-similar dynamics, and the shape of the multifractal spectrum is the result of microscopic processes (as the nonlinear dynamics represented by the similarity transformations presented above) that occur in space, particularly in two-dimensional space. These processes, although difficult to know when considering real systems, e.g. SN and Pop, are encapsulated in the shape of the spectrum given by its skwennes χ or its aggregation-diffusion index ξ. Such a shape can appear in different ways. One shape exhibiting a process of the aggregation type $\chi < 1$ ($\xi > 1$), one of the diffusion type $\chi > 1$ ($\xi < 1$) and another exhibiting none of the previous types, or of the symmetric type $\chi = \xi = 1$.

Since a multifractal structure has an infinite number of dimensions, it is possible to define filling rates, redundancy, and correlation in relation to two-dimensional space. These quantities inform us about how much the structure under study fills the space, how much its elements repeat, and how much they repeat across scales.

2.1.1 Capacity Dimension

In this section, we will define the capacity dimension, which will be useful for defining the spatial filling rate that we will use to know how much the SN and the Pop fill the space in two dimensions.

First, let $N(\epsilon)$ be the number of boxes of side ϵ needed to perfectly cover a line of length L. The number of boxes in this case can be shown to be given by the product between L and the scale of the boxes $1/\epsilon$, that is, $N(\epsilon) = L(1/\epsilon)$. Now let $N(\epsilon)$ be the number of boxes, at a given scale, needed to cover a plane. It can be shown that this quantity is given by $N(\epsilon) = L^2(1/\epsilon)^2$. Analogously, the number of boxes, at a given scale, needed to cover a cube is given by $N(\epsilon) = L^3(1/\epsilon)^3$. In this sense, the number of boxes

needed to cover an object in a space of dimension d is given by

$$N(\epsilon) = L^d(1/\epsilon)^d. \tag{2.1.5}$$

Applying the natural logarithm to both sides of the above equation results in

$$d = \frac{\ln N(\epsilon)}{\ln L + \ln(1/\epsilon)} \tag{2.1.6}$$

so that for $L \gg \epsilon$ it is possible to define (BAKER; GOLLUB, 1996)

$$d_B = \lim_{\epsilon \to 0} \frac{\ln N(\epsilon)}{\ln(1/\epsilon)} \tag{2.1.7}$$

as the box-counting or capacity dimension, see Figure 2.3.

Figure 2.3 – Illustration of a square lattice of side L overlapping the street network (SN) of the city of Lavras, MG. a) 4 filled boxes of size $L/2^1$ overlapping the street grid. b) 13 filled boxes of size $L/2^2$ overlapping the street grid. c) 34 filled boxes of size $L/2^4$ overlapping the street grid. d) 108 filled boxes of size $L/2^6$ overlapping the SN. Choosing $L = 50$ units of length, it is not difficult to show that the box-count dimension of Lavras' SN is $d_B = 1.46$.

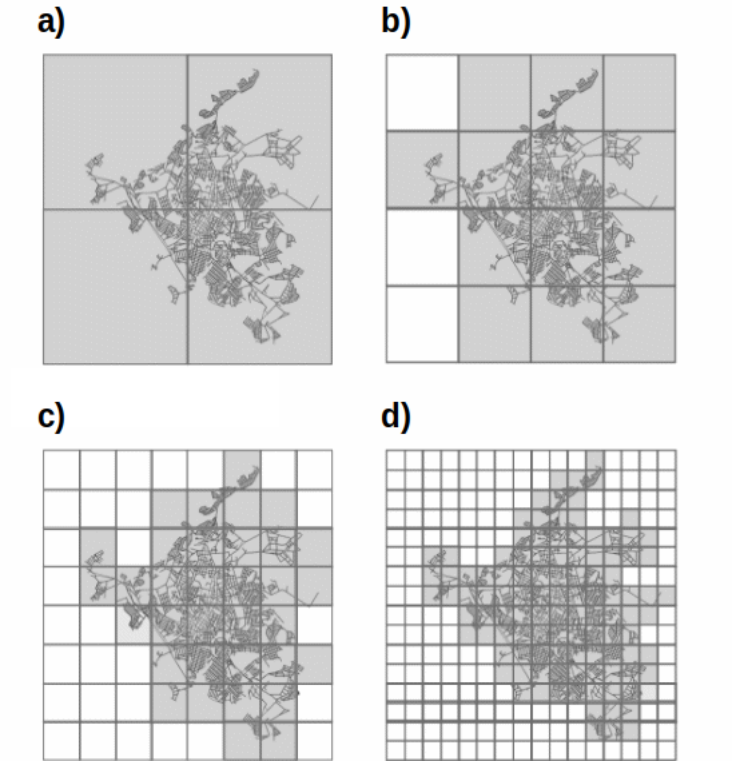

Source: Own authorship.

Although the box-counting dimension has many applications in the literature (MANDELBROT, 1986; MOORE; DASI, 2013; ABID; TORTUM; ATALAY, 2021; FERNANDES; FILHO; LOPES, 2020; CHEN, 2020; NATALIA et al., 2023; WEN; ZHANG; DENG, 2023; MARTÍNEZ; SEPÚLVEDA; MANRÍQUEZ, 2023), it is unfeasible when the measurement scale of the system is very small and when the system has a large number of components (e.g. dynamic processes occurring in spaces with dimensions greater than 3) (ROSENBERG, 2021). This is because it counts the number of boxes needed to cover the fractal structure at various scales of measurement, but does not provide information on the spatial distribution of the system's elements. In fact, we will see in the following sections that the information and correlation dimensions overcome this problem, allowing us to study systems in which the spatial distribution of points is asymmetrical or non-uniform.

2.1.2 Information Dimension

In this section, we will define the information dimension, which will be useful for defining the spatial redundancy index that we will use to find out to what extent the SN and Pop repeat in space in two dimensions.

According to Hidalgo (2015), cities, firms, and teams are the embodiment of pockets where species accumulate the capacity to produce information, which is highly uneven. In the context of dynamical systems and chaos, this property of highly uneven behavior leads to some asymmetries reflected in a chaotic attractor with fractal measurement (FARMER, 1982).

If we consider, for instance, a traveler who must go from node A to node D, but does not know which way to go, that is, he does not have any information available, Figure 2.4, but if someone advises him to go up (Top = 0) or go down (Down = 1) he acquires a little information in each instruction received. So, if someone instructed him to follow the path A-B-C-D, the amount of information he received was 3 bits. In general, the number of destinations is $m = 2^n$, where n is the number of bits of information needed to cross the m branches.

On the other hand, if we need to specify a point in a unit length line segment with some precision $\epsilon = 2^{-k}$, the number of bits of information needed is k. In general, the number of bits to specify a point in a d dimensional space is $S(\epsilon) = d \log_2 \epsilon$, where ϵ is

the accuracy of the measurement. If we consider $S(\epsilon)$ as the entropy associated with the precision ϵ, then 2^S is the number of states available in the system and a positive metric entropy can be considered as a definition of chaos (FARMER, 1982).

If we consider the Shannon entropy

$$S(\epsilon) = -\sum_i p_i(\epsilon) \ln p_i(\epsilon), \tag{2.1.8}$$

where $p_i(\epsilon)$ is the probability associated to the measurement in the i-th box of size ϵ in a square lattice, then we can define the information dimension by

$$d_I = \lim_{\epsilon \to 0} \frac{S(\epsilon)}{\ln(1/\epsilon)}. \tag{2.1.9}$$

Figure 2.4 – Consider a traveler who must go from node A to node D, but does not know which way to go, that is, he does not have any information available. If someone advises him to go up (Top = 0) or go down (Down = 1) he acquires a little information. So, if someone instructed him to follow the path A-B-C-D, the amount of information he received was 3 bits. In general, if n represents the number of branches and m the number of destinations, then $m = 2^n$, because each branch requires 1 bit of information and n branches require n bits.

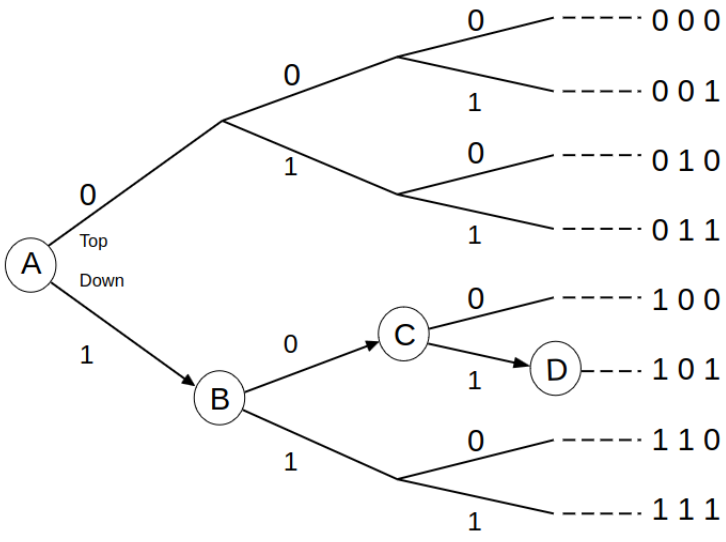

Source: Own authorship.

This dimension was introduced by Balatoni and Renyi in 1956 and the idea behind of this quantity is it allows an observer to estimate the information gained when a measurement is made at a given level of precision (FARMER, 1982; KAK, 2020). It counts the number of points within circles with radii smaller than or equal to the threshold and is

related to the spectral dimension, which counts the number of sites in a fractal structure with a certain number of visitors after infinite steps (PITSIANIS; BLERIS; ARGYRAKIS, 1989).

This quantity is important in the study of dissipative dynamic systems and chaos (dynamic processes occurring in spaces in dimensions greater than 3) which have non-trivial probability measures. It depends on the metric properties of a set and allows characterize the asymmetry of the probability distribution associated with the fractal measure. When this measure is evenly distributed the information dimension converges to the box-counting dimension, otherwise we have $d_I \leq d_B$. An interesting interpretation of the information dimension it's an box-counting dimension of the smallest set which contains the most part of the fractal structure or attractor (OTT, 2002).

2.1.3 Correlation Dimension

In this section, we will define the correlation dimension, which will be useful for defining the spatial correlation index that we will use to find out to what extent the SN and the Pop are correlated in space in two dimensions.

Defining the correlation integral by (ROSENBERG, 2021)

$$C(r) \equiv \frac{1}{N(N-1)} \sum_{i}^{N} C(x_i, r) \tag{2.1.10}$$

where

$$C(x_i, r) \equiv \sum_{j=1, j\neq i}^{N} H(r - d_{ij}) \tag{2.1.11}$$

gives the number of different points of x_i at a distance d_{ij} less than or equal to r and $H(\cdot)$ is the Heaviside step function equal to 1 if $r - d_{ij} \leq 0$ and zero otherwise.

With this, it is possible to define the correlation dimension using

$$d_C = \lim_{r\to 0} \lim_{N\to\infty} \frac{\ln C(r)}{\ln r}. \tag{2.1.12}$$

The correlation dimension is one of the most commonly used dimensions in the study of dissipative dynamical systems and chaos theory, see Figure 2.5. It is important because it characterizes the degree of correlation between neighbouring points in the

system and in estimating the size of isolated and sparsely distributed points in a given region (systems like these are called dusts) (ROSENBERG, 2021).

Among other properties of the correlation dimension is that it can capture variations in the density of points on small scales (BAKER; GOLLUB, 1996). The interpretation of positively correlated points means that the increase in the intensity of the dynamics occurring in the vicinity of a point A is directly proportional to the intensity of the dynamics in the vicinity of a point B with $A \neq B$. On the other hand, negatively correlated points mean that the increase in the intensity of the dynamics occurring in the vicinity of a point A is inversely proportional to the intensity of the dynamics in the vicinity of a point B.

Another interpretation is that it is related to the probability of pairs of independent events occurring in the same box and measures the dispersion of the data, (SALAT; MURCIO; ARCAUTE, 2017). d_B, d_I and d_C satisfy the relation $d_C \leq d_I \leq d_B$, i.e. d_C is a lower limit for d_I and d_B, while d_B is an upper limit for d_I and d_C.

In addition, it is interesting to highlight that the dimensions d_I and d_C have a strict relationship with the Kaplan-Yorke conjecture (still open), which suggests relating the dynamics of non-linear systems exhibiting chaotic behaviors to the geometric properties of the system via Lyapunov exponents λ. This quantities permits to known in which regime the system has periodic $\lambda < 0$, chaotic behaviour $\lambda > 0$ or exhibits both in the critical value $\lambda = 0$, see for example (CHLOUVERAKIS; SPROTT, 2005; NICHOLS et al., 2003; TEL; GRUIZ, 2006).

2.1.4 Generalized Dimensions

In this section, we will define the concept of generalized dimensions of q order, which are extremely important in the study of multifractal structures. They will be useful in trying to generalize, even if *ad hoc*, some of the main intra-city models discussed in (RIBEIRO; RYBSKI, 2023).

According to Feder (1988), multifractal structures are related to the study of physical or other quantities on a geometric support, allowing a hierarchical analysis of systems that exhibit complex morphological patterns at different observation frequencies (DROZDZ; OSWIECIMKA, 2015; YAHIA et al., 2021). Parisi and Frisch have been attributed to the term multifractal formalism, while the mathematical foundations, involv-

Figure 2.5 – Lorenz attractor. In evidence are a representative circle centered on the i-th point x_i of the attractor. All points in the circle are counted by the Heaviside step function and all points out of the circle are not.

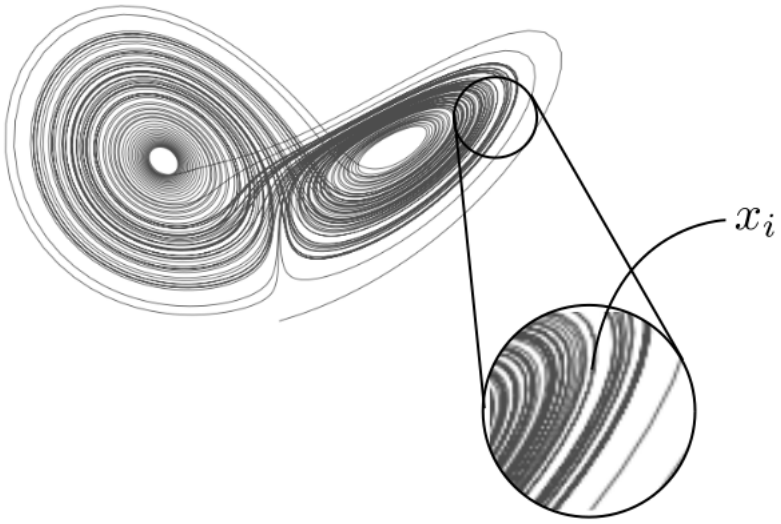

Source: Own authorship.

ing the notions of generalized dimension and multifractal spectrum, have been attributed to Rényi (1955) and Halsey et al. (1986), respectively.

In Benzi et al. (1984), it is mentioned that multifractal ensembles play a crucial role in describing turbulent flows. To explain this, the authors introduce an extension of the beta model proposed by Frisch, Sulem, and Nelkin in 1978, called the random beta model, which incorporates the notion of intermittency. Furthermore, the authors present numerical simulations involving strange attractors to illustrate the relationship between multifractal theory, dynamic systems, and chaotic attractors.

In Halsey et al. (1986), the concept of the singularity index and an associated quantity characterizes the intensity of this index is introduced. The formalism defines the intensity index, which describes the density of values assumed within the multifractal structure under investigation, and the second index quantifies the local intensity of this index in the structure. This enables the introduction of two smooth functions to characterize the structure. The authors apply these concepts to investigate some dynamical systems and also suggest that, based on the results obtained, this formalism can be used to investigate universality phenomena in experimental situations that are different from those arising from dynamical systems.

These ideas were used by Paladin & Vulpiani (1987), who reviewed several concepts such as chaotic attractor, Lyapunov exponents, Rényi entropy's, anomalous scaling, including the notion of the phenomenon of intermittency in the study of turbulence. This work reveals that the multifractal formalism has significant importance in the study of the theory of dynamic systems, turbulence in disordered and condensed matter systems.

For works involving the mathematical formalization of fractal and multifractal theory, as well as the proposition of new strategies for estimating D_q in artificial and real systems see (TEL; VICSEK, 1987; FEDER, 1988; TEL; FULOP; VICSEK, 1989; THEILER, 1990; TAKAYASU, 1990; SCHROEDER, 1991; FALCONER; LAMMERING, 1998; VICSEK, 1992; BAKER; GOLLUB, 1996; HARTE, 2001; FALCONER, 2004; ZMESKAL; DZIK; VESELY, 2013; SALAT; MURCIO; ARCAUTE, 2017; ROSENBERG, 2021).

Interesting applications involving the generalized dimension in real systems, in particular human settlements and racial segregation, see (APPLEBY, 1996; SEMECURBE; TANNIER; ROUX, 2016; STEPINSKI; DMOWSKA, 2020). In hydrology studies we have the work of (HUBERT, 2001) and in rivers we have that of (BARTOLO; GAUDIO; GABRIELE, 2004; XIANG et al., 2019). Studies involving applications of fractal dimension in data mining and stochastic field theory are those by (SKKUMAR, 2003) and (SCHERTZER; LOVEJOY; HUBERT, 2002), respectively. You can also find studies applied to data analysis (WENDT; ABRY, 2006), time series (IHLEN, 2013) and the bitcoin market (FILHO; MAGANINI; ALMEIDA, 2018).

For applications in medicine, especially vaccine performance testing (COVID-19) see (MOORE; DASI, 2013; ÖZDEMIR, 2023). For applications of D_q in complex networks, street networks (SN), urban systems and spatial analysis see (WANG; YU; ANH, 2012; CHEN; WANG, 2013; MURCIO et al., 2015; CHEN, 2016; CHEN, 2018; LONG; CHEN, 2021; SONG; CHEN; BO, 2023). Applications in studies of climatic and atmospheric systems such as daily variability of sunspot numbers, precipitation, meteorology, and solar radiation see (DROZDZ; OSWIECIMKA, 2015; LIU et al., 2015; PAVÓN-DOMÍNGUEZ; JIMÉNEZ-HORNERO; RAVÉ, 2015; ALVES et al., 2015; HE, 2017; SALAT; MURCIO; ARCAUTE, 2017; SILVA et al., 2023; ZHAO; LIU; ZHOU, 2023; SANTOS et al., 2023; NATALIA et al., 2023).

Multifractal analysis features quantum field theory, fields and astrophysical systems (DEPPMAN; MEGÍAS; MENEZES, 2020; YAHIA et al., 2021; CHANUI et al., 2022).

Therefore, it is possible to see that the multifractal theory has a wide versatility and, in this work, we will use this tool to analyze the spatial complexity of the SN and the population (Pop) of the largest Brazilian cities in 2010, in order to characterize them and to understand closely the irregularities emerging from these systems.

We are now in a position to introduce the notion of multifractality by first principles. To introduce this notion and its related quantities we follow Stanley & Meakin 1988, because it is more intuitive.

First, consider a lattice of size L defined over a fractal structure with boxes size R, such that the relative size between L and R is given by $\epsilon = R/L$. If we denote the number of points in the i-th box by M_i and assuming the number of elements the fractal has is $M_0 \equiv \sum_i M_i$, then we can denote the probability of finding a point in box i by

$$p_i = \frac{M_i}{M_0}. \tag{2.1.13}$$

Defining the probability distribution function with the set p_i by $n(p)$ when $n(p)\delta p$ is the number of p_i in the range $[p, p + \delta p]$, we can define the partition function associated to $n(p)$ by

$$\mathcal{Z}_q \equiv \sum_p n(p) p^q. \tag{2.1.14}$$

It is worth highlighting that q are the moments associated with the measurements p and when $q \ll 0$ we have regions in in which the measurements are rarefied, while $q \gg 0$ are concentrated (BARTOLO; GAUDIO; GABRIELE, 2004; ROSENBERG, 2021).

However, we can express the eq. (2.1.14) in terms of relative system size ϵ by

$$\mathcal{Z}_q \sim \epsilon^{-\tau(q)} \tag{2.1.15}$$

where $\tau(q)$ are mass exponents that relates the relative system size and the its mass.

Now, consider that this partition function is the form

$$\mathcal{Z}_q = \sum_p e^{F(p)} \tag{2.1.16}$$

with

$$F(p) = \log n(p) + q \log p. \tag{2.1.17}$$

The sum of the eq. (2.1.16) has a typical value in $p = p^*$ when $F(p = p^*)$ have a maximum, such that the following approximation is valid.

$$\mathcal{Z}_q \sim e^{F(p^*)} = n(p^*)(p^*)^q. \tag{2.1.18}$$

If we fix q, then p^* and $n(p^*)$ depends on the relative size ϵ of the system and we can write the scaling laws

$$p^* \sim \epsilon^{-\alpha(q)}, \qquad n(p^*) \sim \epsilon^{f(\alpha(q))}, \tag{2.1.19}$$

when $\alpha(q)$ are the singularity indexes and $f(\alpha(q))$ are the singularity spectrum or multifractal spectrum. In this context $f(\alpha(q))$ is though as a Hausdorff dimension of the fractal set and $\alpha(q)$ it's local version. Figure 2.6 illustrates the multifractal spectrum, the regimes when $q < 0$ and $q > 0$, the variation of the spectrum Δf, the α_{min}, α_{max}, α_0, α_1 and the corresponding dimensions that we will discuss below. α_{min} and α_{max} correspond to the singularity indexes in the rarefied and densest regions of the fractal structure, while α_0 and α_1 correspond to the largest and smallest regions which contain most of the fractal structure, respectively.

Figure 2.6 – Typical multifractal example diagram. Illustration of the multifractal spectrum, the regimes when $q < 0$ and $q > 0$, the variation of the spectrum Δf, the α_{min}, α_{max}, α_0, α_1 and the corresponding dimensions.

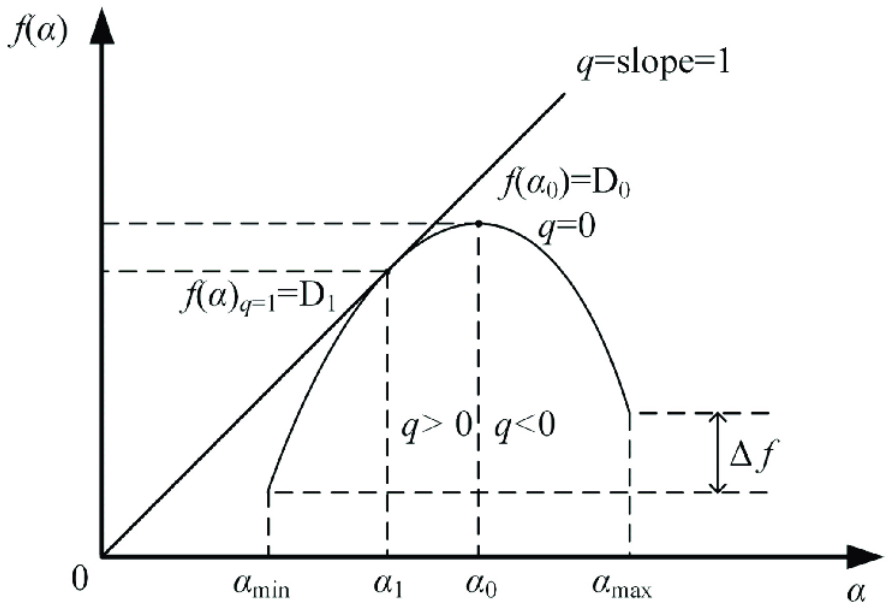

Source: (XIANG et al., 2019).

In this consideration, then we obtain

$$\mathcal{Z}_q \sim e^{F(p^*)} = \epsilon^{f(\alpha(q))-\alpha(q)q} \tag{2.1.20}$$

and comparing the eqs. (2.1.15) and (2.1.20), we have

$$\tau(q) = f(\alpha(q)) - \alpha(q)q = -(1-q)D_q \tag{2.1.21}$$

and we can define

$$D_q = \frac{\tau(q)}{q-1} \tag{2.1.22}$$

as the generalized dimensions of q order, which is related to the Rényi entropy and free energy (RÉNYI, 1955; ZMESKAL; DZIK; VESELY, 2013; BAEZ, 2022).

From the equation eq. (2.1.21) we can write $d\tau(q) = -\alpha(q)dq$ or $d\tau(q) = -\alpha(q)dq - qd\alpha(q) + qd\alpha(q)$ or $d(\tau(q) + \alpha(q)q) = qd\alpha(q)$ and we define a function of the $\alpha(q)$ variable

$$f(\alpha(q)) = \tau(q) + \alpha(q)q \tag{2.1.23}$$

as the sigularity spectrum or multifractal espectrum.

However, in this study we follow the approach described in (TEL; VICSEK, 1987; BARTOLO; GAUDIO; GABRIELE, 2004; TEL; FULOP; VICSEK, 1989; ZHAO; LIU; ZHOU, 2023), witch's use the *sandbox* method to obtain the multifractal quantities. The idea of this method is to obtain the generalized dimensions and the multifractal quantities considering an average over some randomly chose points in the fractal structure.

Moreover, is possible to extend the eq. (2.1.13) and to write

$$\sum_{boxes\, i} \mu_i^q \propto \epsilon^{(q-1)D_q} \tag{2.1.24}$$

where μ_i is the normalized mass defined by $\mu_i = M_i/M_0$ with M_0 the total mass of the fractal structure. In this work, there is two kind of mass, the intersections of the SN and the Pop. Analogously, $\epsilon = R/L$ is the normalized size of the box of the square lattice of size L that superpose the fractal object.

To correct inconsistencies when the orders moment are negative, $q < 0$, Tel, Fulop and Vicsek (1989) proposes the following modification to obtain the generalized dimen-

sions

$$\sum_i \left(\frac{M_i}{M_0}\right)^{q-1} \frac{M_i}{M_0} \propto \left(\frac{R}{L}\right)^{(q-1)D_q}. \tag{2.1.25}$$

The idea behind of this modification is to calculate the moments q of the average mass over random select points centred on the object with $R \ll L$, so that

$$\left\langle \left[\frac{M(R)}{M_0}\right]^{q-1} \right\rangle \propto \left(\frac{R}{L}\right)^{(q-1)D_q} \tag{2.1.26}$$

yielding the generalized dimensions

$$D_q = \frac{1}{q-1} \lim_{R/L \to 0} \frac{\ln \left\langle \left[\frac{M(R)}{M_0}\right]^{q-1} \right\rangle}{\ln\left(\frac{R}{L}\right)}, \qquad q \neq 1. \tag{2.1.27}$$

Viczeck (1992) argues that the inconsistencies that occur in the sparse regions of the fractal are consequences of the size of the boxes or radii used in calculating the number of elements living within them. When the box or radius is very small we have many empty boxes, which have a greater contribution to the average value for $q \to -\infty$.

However, this dimensions are interesting because its have some important special cases that can encounter in many application fields in science, engineering, computational and natural and social science. They are:

- Capacity, Hausdorff, box-counting or space-filling dimension: it is denoted by D_0 when $q = 0$. Measures how much space is filled by the fractal set. A geometric interpretation of the capacity dimension can be obtained from the intersection of a horizontal line passing through the maximum of the multifractal spectrum. The capacity dimension is the point of intersection between these two curves;

- Information dimension: it is denoted by D_1 when $q = 1$. Measures the smallest set which contains the most part of the fractal structure (OTT, 2002). A geometric interpretation of the information dimension can be obtained from the intersection of a straight line of slope 1 that is tangent to the multifractal spectrum. The information dimension is the point of intersection between these two curves;

- Correlation dimension: it is denoted by D_2 when $q = 2$. Measures how much the fractal elements relate to each other and their nearest neighbors: it manages to capture the intensity of the local relationship between its elements;
- Minus infinity dimension: it is denoted by $D_{-\infty}$ when $q \to -\infty$. Measures the spatial distribution of the fractal in the rarefied regions;
- Plus infinity dimension: it is denoted by D_{∞} when $q \to \infty$. Measures the spatial distribution of the fractal in the densest regions.

In addition, we can also define the multifractal correlation exponent, which describes the radial dependence of the generalized correlation function defined by

$$G_q(r) = \frac{1}{N_b N_{b_r}} \sum_{b} \sum_{b_r} \mu^q_{b(R)} \mu^q_{b_r(R)} \tag{2.1.28}$$

where $\mu_{b_r(R)}$ is the measure of the ball $b_r(R)$ of radius R at a fixed distance $r - R$ from $b(R)$. N_b (N_{b_r}) is the number of balls $b(R)$ ($b_r(R)$) and $\sum_{b_r}$ is the sum over all balls $b_r(R)$. The multifractal correlation exponent can be defined as (NAKAYAMA; YAKUBO, 2003)

$$z(q) = D_0 + 2\tau(q) - \tau(2q). \tag{2.1.29}$$

On the other hand, an interesting fact is that D_1, D_2 do not necessarily exist (PERES; SOLOMYAK, 2000). However, the authors proved that for D_1 and D_2 to exist, the measure μ^q must be self-conforming[2], or even self-similar subject to $q > 0$ and $q \neq 1$. They also point out that showing the existence of D_0 for any self-similar measure is still an open problem. But recently, Ngai & Xu (2023) proved that, for any self-similar measure subject to $q > 0$ and $q \neq 1$, D_q also exists for fractal structures embedded in a non-Euclidean space, in particular, in Riemannian manifolds, a fundamental mathematical structures in the development of Einstein's Theory of General Relativity.

Although generalized dimensions are based on Rényi's idea of entropy, some work has shown a more natural relationship with non-extensive statistics in which system properties are described in terms of generalized versions of functions traditionally used to

[2] A self-conformal measure is a measure invariant under a set of conformal mappings. Conformal maps preserve both angles and the shapes of infinitesimally small figures, but not necessarily their size or curvature. Source :<https://en.wikipedia.org/wiki/Conformal_map>.

describe typical behavior of systems. accessible states of the system (TSALLIS, 1988). In this formalism, the entropy of two interacting systems is greater than the sum of the individual entropies, which translates into the fact that the whole is more than the sum of its parts. In this sense, this also in processes of self-organization that occur in space and emergence that occur along the scales of the system and that exhibit multifractality have a natural mathematical formalism (LYRA; TSALLIS, 1998).

In addition, we can also define the skewness of the singularity spectrum by (CHANUI et al., 2022)

$$\chi = \frac{|\alpha_{max} - \alpha_0|}{|\alpha_{min} - \alpha_0|}, \tag{2.1.30}$$

which measures the dominance of fluctuations on the system scales. When $\chi > 1$ (right-skewed), $\chi < 1$ (left-skewed) and $\chi = 1$ (symmetric), the system scale is dominated by small, large and no fluctuations. In analogy to the author's work, small and large fluctuations correspond, in the present context, to higher ($q \to -\infty$) and lower ($q \to \infty$) generalized dimensions. This means that the spatial distribution of the fractal elements in the more and less rarefied regions exhibit large and small fluctuations when the scale of the system is varied.

However, to conform to the work of Long & Chen (2021), we define

$$\xi = 1/\chi \tag{2.1.31}$$

to represent the process of spatial aggregation ($\xi > 1$) and spatial diffusion ($\xi < 1$) in the SN and in the spatial distribution of the Pop, see Figure 2.7.

According to these authors, who analyzed the multifractality of the SN of twelve Chinese megacities, they argue that, using the definition eq. (2.1.31), $\xi > 1$ and $\xi < 1$ are closely related to non-trivial processes occurring in the formation and evolution of these structures. A spectrum with $\xi < 1$ ($\chi > 1$) implies a process of diffusion or spatial decentralization, while a spectrum with $\xi > 1$ ($\chi < 1$) involves a process of aggregation or spatial concentration. In the diffusion process, the peripheral regions are relatively larger and denser than the central regions, which are more sparse and small. In the aggregation process, the central regions are relatively larger and denser than the peripheral regions, which are more sparse and small. In the present context, $\xi > 1$ means that both the SN and Pop exhibit a greater concentration (of streets and people) in the central regions,

Figure 2.7 – Spectrum diagram of the skewness and aggregation-diffusion process.

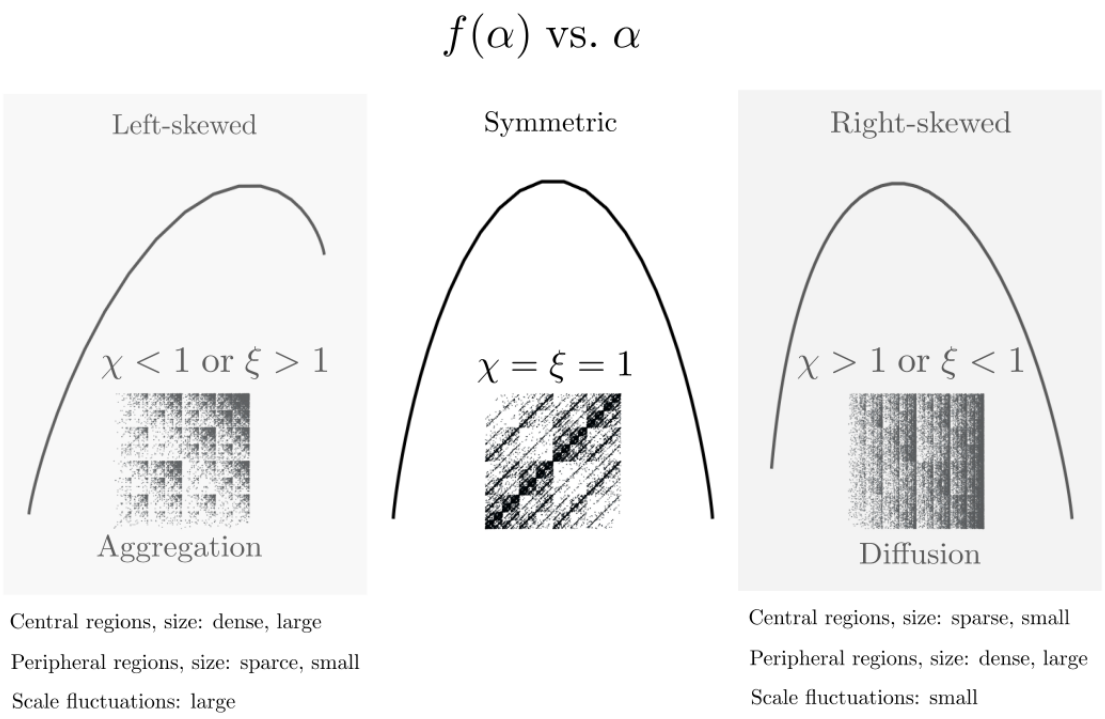

Source: Own authorship.

being relatively larger than the more peripheral regions, which are more sparse and small. $\xi < 1$ means that both the SN and Pop exhibit a greater concentration (of streets and people) in the peripheral regions, being relatively larger than the more central regions, which are more sparse and small.

Therefore, systems exhibiting large fluctuations in the scale of the system have left-skewed which is governed by a aggregation process, while systems exhibiting small fluctuations have right-skewed which is governed by an diffusion process.

In addition, according to Chen & Huang (2018) we can define the following rates:

i) Space-filling rate:

$$u = D_0/2; \tag{2.1.32}$$

ii) Spatial redundancy rate:

$$v = 1 - D_1/2. \tag{2.1.33}$$

Here, i) it measures the extent to which the embedded space is filled with fractal structure. ii) it measures the extent to which fractal structure is repeated along spatial scales.

In analogy to i) and ii), we propose a third rate:

iii) Spatial correlation rate:

$$w = 1 - D_2/2, \tag{2.1.34}$$

which measures how correlated the elements of the fractal structure are across spatial scales.

For the details of the algorithm see Section 4.3. In the Appendix C we present the mathematical construction used in the implementation of the generalized dimensions, eq. (2.1.27), the SN and the Pop. Also we show the equivalences between the generalized dimensions, according to the *sandbox* method, and the capacity, information and correlation dimensions.

2.2 Intra-city Models

In this section, we give a brief overview, albeit still incomplete, of some of the main works consulted in the literature involving urban systems. We will introduce the concept of scaling law and illustrate how these ideas combined with the notion of fractal dimension can be used to obtain urban scaling laws. We demonstrate a derivation of the interaction probability, discussed by Ribeiro & Rybski (2023), which allows us to obtain some intra-city models in which the fractal dimension is an important element. To obtain these models, we use the principle of maximizing entropy and the choice of which mechanism to maximize. Intra-city models take into account internal city processes or only endogenous factors.

Opening with one of the main mathematical ingredients in urban systems analysis, where many elements of cities are closely connected and inseparable, we have the laws of scale, which seek to capture the non-linear behavior between urban indicators and the size or Pop the city. Studies involving laws of scale date back to the late 19th century, with the analysis of income and wealth distributions by Pareto (1897). Another interesting work, published in 1932, is by George Kingsley Zipf. In it, the author studies the frequency distribution of English words and discovers a power law type behavior

(ZIPF, 1949; CORRAL; BOLEDA; FERRERI-CANCHO, 2015). He applies the same reasoning to the size distribution of cities, discovering a similar behavior, although studies show that this idea was already explored by Erich Auerbach around 1913 (RYBSKI; CICCONE, 2023).

Some of the works that played important roles in the development of urban systems theory are, for example, the work of Walter Cristaller with the proposition of Central Place Theory, see Caves (2004). The work of Huff (1963), who proposed a spatial model to try to predict the behavior of consumers who visit certain places with intense buying and selling activity based on the gravitational idea. The proposition of the first Law of Geography by Tobler (1970), stating that everything is related to everything else, but closer things are more related than more distant things.

On the other hand, inspired by the ideas of Benoît Mandelbrot et al. (1983) on fractals, Batty & Longley (1994) wrote a book presenting, for the first time, ideas on how to apply knowledge of fractal geometry in urban planning and in understanding, from a physical point of view, the spatial form of cities and their various functionalities.

Other works include (BATTY, 2008; BETTENCOURT; WEST, 2010; BATTY, 2013; BETTENCOURT, 2013; ARCAUTE et al., 2015) and more recently, (ROSNI; NOOR, 2016; LEE; BARBOSA; YOUN, 2017; STRANO et al., 2017; BARTHELEMY, 2019b; MOLINERO; THURNER, 2021; SANTOS; CRUZ; SANTOS, 2022; ARCAUTE; RAMASCO, 2022; GUO et al., 2022; RIBEIRO; RYBSKI, 2023; CZYŻA et al., 2023; WEN; ZHANG; DENG, 2023; MARTÍNEZ; SEPÚLVEDA; MANRÍQUEZ, 2023).

Scaling laws play a fundamental role in fractal geometry and urban systems, it focus on investigating and describing the relationships formed between the system's variables occurring between order and chaos (BATTY; XIE, 1999; GLERIA; MATSUSHITA; SILVA, 2004; CHEN; ZHOU, 2008; SIEGENFELD; BAR-YAM, 2020).

Formally, scaling laws are mathematical relationships with property of scale invariance. For instance, a function $f(x)$ is scale invariant if it can be scaled as $f(\lambda x)$ for all λ (TAKAYASU, 1990). This means that there exists a function $C(\lambda)$ such that

$$f(x) = C(\lambda)f(x). \tag{2.2.1}$$

Differentiating both sides of eq. (2.2.1) and eliminating $C(\lambda)$, we get

$$f'(x)/f(\lambda x) = \lambda f'(\lambda x)/f(\lambda x). \tag{2.2.2}$$

By substituting $x = c$, when c is a constant, and integrating the previous expression in λ, it is possible to obtain

$$f(x) = f(c)x^{\alpha}, \qquad \alpha = f'(c)/f(c). \tag{2.2.3}$$

where α is the scaling exponent which characterize the nonlinear behavior of the model, see Figure 2.8.

Figure 2.8 – Power laws for some exponents α. If $\alpha < 0$ as x increases, $f(x)$ decreases non-linearly. If $\alpha > 0$ as x increases, $f(x)$ increases non-linearly and if $\alpha = 0$ as x increases, $f(x)$ remains constant.

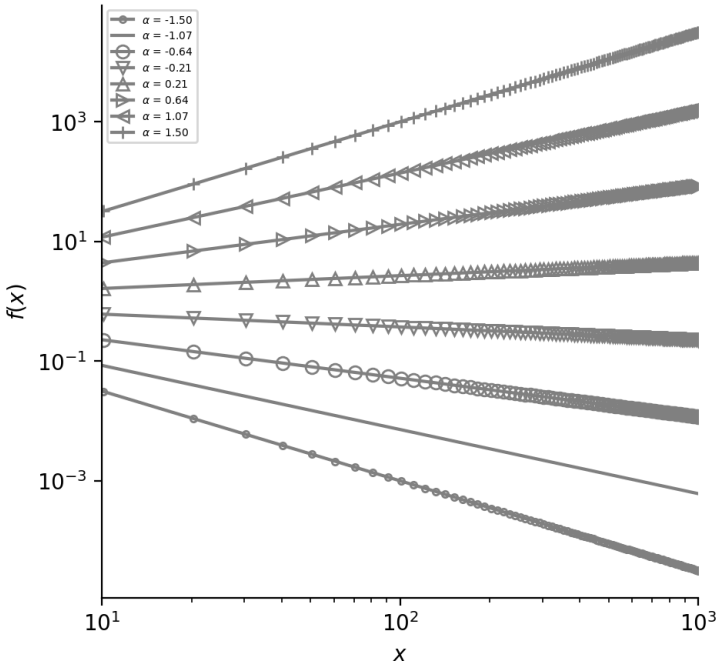

Source: Own Authorship.

If we use the notion of fractal dimension and scale theory together with empirical city data, for example *Pop* or size N, gross domestic product (GDP) Y and total street length L, it is possible to observe that as cities grow, they become richer and more efficient in terms of street infrastructure. In fact, this translates into the phenomena of economies of scale, in which GDP per capita undergoes a non-linear increase, while the total length of streets per capita decreases (RIBEIRO; RYBSKI, 2023). General models

that capture these effects can be established by assuming that the spatial patterns of the city's population (Pop) and street network (SN) have fractal dimensions D_p and D_i, respectively. Therefore, from fractal theory we can derive the following mathematical relationships

$$N = N_0 r^{D_p}, \qquad L = L_0 r^{D_i}, \tag{2.2.4}$$

where N_0, L_0 are constants and r is the Euclidean distance between the center and the periphery of the fractal structure. Eliminating r from eq. (2.2.4), we can express the economy of scale phenomenon as

$$L \sim N^{\beta_{sub}}, \qquad \beta_{sub} = \frac{D_i}{D_p} \tag{2.2.5}$$

where $\beta_{sub} < 1$, a scale exponent characteristic of the model. Empirical data suggests a value of ≈ 0.85 (RIBEIRO; RYBSKI, 2023).

However, if we can consider, for example, a circle of radius r centered on the city and an infinitesimal ring dr, see Figure 2.9, and if we assume that the rate of change of economic activities – an input of resources, a production process and an output of products (goods or services) – in relation to the square of the Pop is proportional to the probability of interaction given by $p_{intt}(r) \sim 1/r^{D_i}$, which decays with the distance r between individuals with an exponent given by the fractal dimension of the SN ,D_i, then

$$\frac{dY(r)}{d\left[N^2(r)\right]} \sim p_{intt}(r). \tag{2.2.6}$$

Thus, assuming that $p_{intt}(r)$ and $N(r)$ are independent of polar angle, integrating the economic activities from R_{min} to a radius R_{max}, it follows

$$Y(R_{max}) = Y(R_{min}) + 2\pi k \int_{R_{max}}^{R_{min}} p_{intt}(r) d[N^2(r)] \tag{2.2.7}$$

where k is a proportionality constant and 2π is because the polar invariance.

Now, using the first expression of eq. (2.2.4) and the fact that $\frac{N}{N_0} = R_{max}^{D_p}$ and $Y(R_{max}) = Y$, results in

$$Y = Y(R_{min}) + \frac{4\pi k D_p N_0^{\frac{D_i}{D_p}}}{(2D_p - D_i)} \left[N^{2-\frac{D_i}{D_p}} - N_0^{2-\frac{D_i}{D_p}} R_{min}^{D_p(2-D_i/D_p)} \right] \tag{2.2.8}$$

Figure 2.9 – Illustration of the radius of interaction, the spatial patterns of the population (Pop) and the street network (SN) in accounting for economic activities in a city.

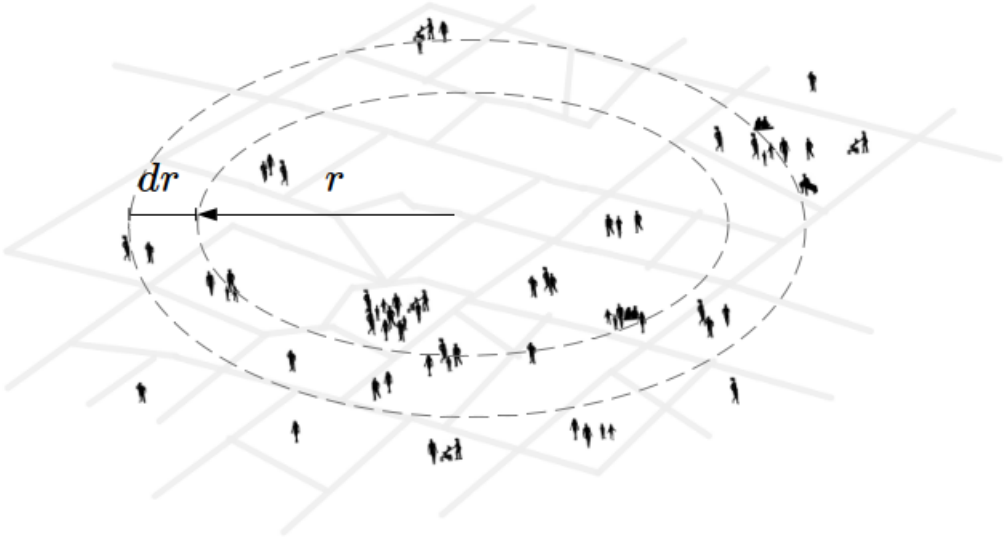

Source: Own authorship.

which leads

$$Y \sim N^{\beta_{sup}} \tag{2.2.9}$$

with $\beta_{sup} = 2 - \frac{D_f}{D_p}$.

In this way, it is possible to relate the exponent of yield and economy of scale by means of (RIBEIRO et al., 2017)

$$\beta_{sup} + \beta_{sub} = 2. \tag{2.2.10}$$

An schematic visualization of urban scaling laws is show in the Figure 2.10. The eqs. (2.2.5) and eq. (2.2.9) were presented by Molinero & Thurner (2021) to explain economy and increasing returns to scale.

The previous results show that the phenomenon of economies of scale can be explained by the spatial complexities of the SN and the Pop, which tend to become more concentrated in larger cities due to agglomeration processes, generation of innovative ideas, specialization of markets and work, opportunities and economic growth. For example, in Lucas (1988), the economic growth of cities is due to the agglomeration process resulting from human capital externalities. Other authors argue that this is due to stochastic processes or the Gibrat process (BERRY; GARRISON, 1958; STEINDL, 1965; MARSILI; ZHANG, 1998).

Figure 2.10 – Urban scaling laws infographic. Urban scaling laws describe the non-linear relationship between urban indicators (e.g. total street length, water consumption, gross domestic product, etc.) in terms of city size or population (Pop). This infographic illustrates the i) sublinear, ii) linear and iii) super-linear scaling regimes, which describe the behavior of infrastructure indicators (e.g. total street length L), basic individual needs (e.g. water consumption C) and those associated with socio-economic activities and interaction between individuals Y as a function of Pop N. In fact, if the Pop doubles in size, there is i) a per capita saving in the variable associated with infrastructure resources, ii) a linear increase in the variable associated with resources associated with basic individual needs and iii) a per capita increase in the variable associated with socio-economic resources.

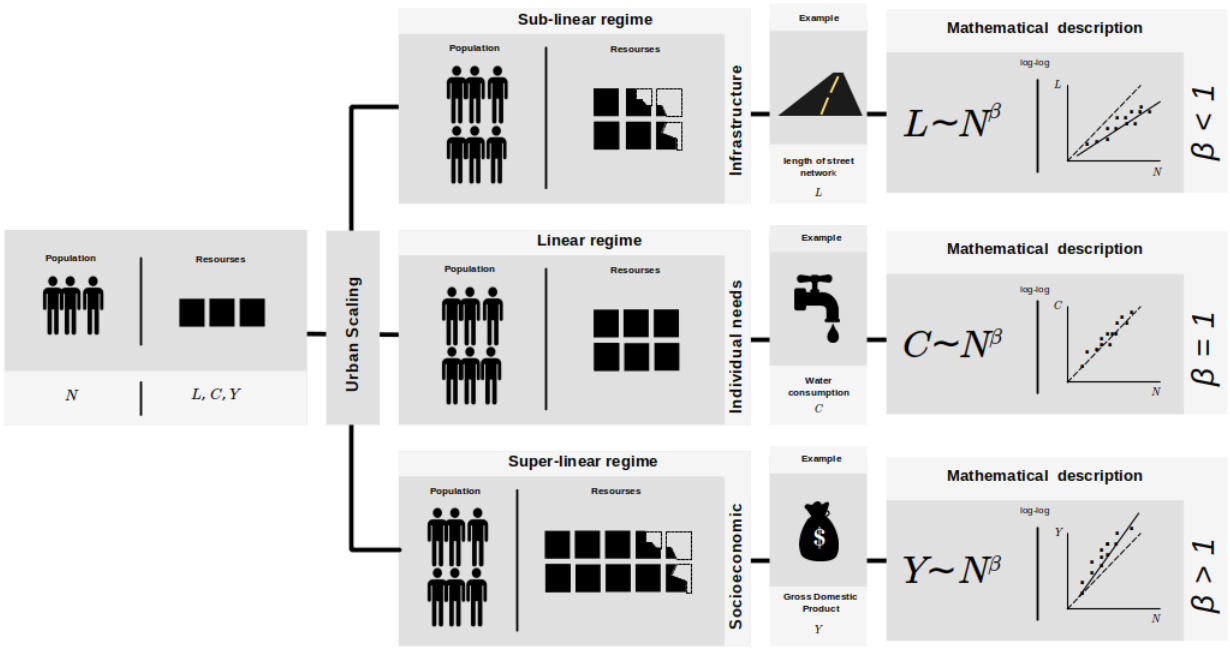

Source: Own authorship.

We now move on to derive the probability of interaction between the elements (e.g. individuals or regions) of cities, which is closely related to the type of intra-city model considered. We show that this probability decreases with the inverse of the distance raised to an arbitrary exponent, which can be chosen according to which mechanism you want to maximize, resulting in the main models, in which the notion of fractal dimension plays a crucial role in explaining economies and returns to scale.

We point out that intra-city models can be obtained in terms of the entropy maximization principle (BECK, 2009). The idea of using this principle in modeling urban systems is due to Wilson (1967, 2010), who observed the similarity between applications of the Newtonian gravitational model by engineers and the partition function method ap-

proach used in statistical mechanics. Here we use the same idea, but we use it to obtain the probability with which two regions interact with each other.

If we define the probability of interaction between two city regions (i, j) by

$$p_{ij} = \frac{T_{ij}}{\sum_i \sum_j T_{ij}} \tag{2.2.11}$$

where T_{ij} is the interaction between these regions. According to Cipoani (2023) and Wilson (2010), T_{ij} can be migration, trade flows, air travel or a general matrix of flows, while $\sum_i \sum_j T_{ij}$ is the sum of these interactions discussed by Munroe & Biles (2005) and Batty (2021).

Imposing that the restriction on the average amount of travel is $\langle \ln r \rangle = \sum_i \sum_j p_{ij} \ln r_{ij}$, with r_{ij} the Euclidean distance between i and j, we can maximize Shannon entropy subject to the restriction $\langle \ln r \rangle$, considering a Lagrangian of the form

$$\mathcal{L} = -\sum_i \sum_j p_{ij} \ln p_{ij} - \gamma \left(\sum_i \sum_j p_{ij} \ln r_{ij} - \langle \ln r \rangle \right). \tag{2.2.12}$$

The choice of the average value of the trip to be a logarithmic function of distance is a consequence of the fact that costs increase non-linearly with distance. In logistics, this effect is known as long haul, i.e. when there is: i) an increase in fuel costs due to a long-distance journey; ii) the maintenance of hours of service for fleet drivers and iii) greater chances of products being damaged due to the long distance (RODRIGUE, 2020).

Under these conditions, imposing that $\frac{d\mathcal{L}}{dp_{ij}} = 0$ and simplifying, the interaction probability p_{ij} can be approximated by

$$p_{intt}(r) \sim \frac{1}{r^{\gamma}}, \tag{2.2.13}$$

showing that the interactions between any two regions of the city decrease with the Euclidean distance between them, raised to an exponent γ, which in turn can be interpreted as a characteristic of the city's endogenous constituents, see Figure 2.11.

We will see in the following sections that this parameter can take on expressions depending on, for example, the urban area, the fractality of the street network (SN) and the population (Pop), or even the degree of influence and the level of productivity of the actors that make up the city.

Figure 2.11 – Geometric interpretation of the probability of interaction. T_{ij} is the field interaction between two sites (i, j) in the city and r_{ij} is the Euclidean distance between them. There are three routes highlighted, one in yellow, one in red and one in green. Below is an illustration of the cost function $C(r) = \ln r$ as a function of the distance r, where you can see that the yellow route has the lowest travel cost, while the green route has the highest cost.

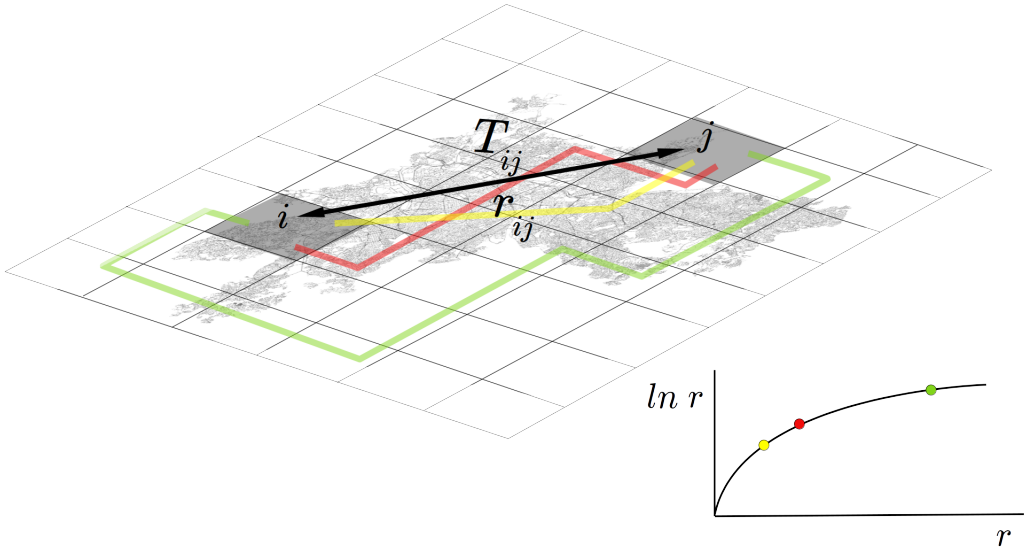

Source: Own authorship.

2.2.1 Bettencourt Model

To recover the model of Bettencourt (2013), see also Ribeiro & Ribski (2023), we can consider $\gamma = \frac{\ln(A/a)}{\ln(r)}$ where a is the area accessible to an individual, a quantity independent of scale, and A the area of the city. With this in mind, we can write the following laws of scale as a function of city size N, involving economic activities and infrastructure resources

$$L \sim N^{\frac{D_f+1/2}{D_f+1}}, \qquad Y \sim N^{2-\frac{D_f+1/2}{D_f+1}}, \tag{2.2.14}$$

where D_f is the fractal dimension of the city's urban area. This means that the choice of the γ parameter, mentioned above, is a direct consequence of the fact that the mechanism that prevails in individual interactions is closely linked to the maximization of information associated with the proportionalities between the cost of transport to get from one point to another and the socio-economic output of the individuals living in the city. Thus, one of the characteristics of this type of model is the emphasis on human interactions.

2.2.2 Molinero & Thurner (M&T) Model

On the other hand, if we choose $\gamma = D_{infra}$, then the M&T model can be obtained considering that the phenomena of income from scale and the economy of scale can be expressed in terms of the size of the city by means of the following relationships (MOLINERO; THURNER, 2021; RIBEIRO; RYBSKI, 2023)

$$L \sim N^{\frac{D_{infra}}{D_p}}, \qquad Y \sim N^{2-\frac{D_{infra}}{D_p}}, \tag{2.2.15}$$

where D_{infra} and D_p are the fractal dimensions of the SN and city Pop, respectively. In this case, the choice of the γ parameter as the fractal dimension of the SN can be explained by the maximization of the information associated with the relative spatial complexity between the Pop and the SN in the city. Thus, the yield and economy of scale are consequences of the fact that $D_{infra}/D_p < 1$, that is, the spatial complexity of Pop is slightly greater than the spatial complexity of the SN. This implies that Pop can occupy one more dimension than SN. The Pop has greater freedom to occupy, interact and move around the urban space, including not only the streets themselves, but also buildings or skyscrapers. In addition, this model is part of the class of models that take into account human interactions and transportation infrastructure, revealing in a simple and elegant way that Pop and SN are essential elements in socio-economic and urban analysis.

2.2.3 Macroscopic Molinero & Thurner (M&T) Model

As a novelty, if we define the quasi-dimensions of the street network (SN) and population (Pop) described by Chen (2020), we can to write the relations

$$N^{1/D'_p} \propto A^{1/2}, \qquad L^{1/D'_i} \propto A^{1/2}, \tag{2.2.16}$$

where N and D'_p are the Pop and its quasi-dimension and A the urban area; L and D'_i are the total street length and it's quasi-dimension. Using the transformation described in (Chen 2013, 2020), we have the Pop and SN fractal dimensions

$$D_p = 1 + \frac{1}{D'_p}, \qquad D_i = 1 + \frac{1}{D'_i}, \tag{2.2.17}$$

In this sense, if we have $\gamma = D_i$, then simplifying the fractal ratio D_i/D_p, and in analogy to the M&T model, we can write the following scaling laws

$$L \sim N^{\frac{1+\ln A/(2\ln L)}{1+\ln A/(2\ln N)}}, \qquad Y \sim N^{2-\frac{1+\ln A/(2\ln L)}{1+\ln A/(2\ln N)}}. \tag{2.2.18}$$

In this model, the mechanism is the same as that of M&T, except that the role of scaling up and economies of scale has the effect of maximizing the information associated with the spatial complexity of the Pop and the SN described in terms of the N itself, the L and the A of the city. In addition, the M&T model obtains both sub-linear and super-linear exponents from a transversal asymptotic limit, considering the city system.

2.2.4 Yakubo et al. Model

However, if we now consider $\gamma = m(\alpha - 1)$, where m is a parameter associated with the geometric properties of the city, α is a parameter related to the degree of influence of individuals in the city and D_p it's the fractal dimension the Pop, then according to this model, the increasing return to scale can be expressed by means of (YAKUBO; SAIJO; KOROVSAK, 2014; RIBEIRO; RYBSKI, 2023)

$$Y \sim N^{2-\frac{m}{D_p}(\alpha-1)+\frac{\eta}{D_p}} \tag{2.2.19}$$

where we can consider, in addition to the geometric properties and influence of its inhabitants, that the socio-economic production of the city is a distance-dependent quantity. When $\eta < 0$ production decreases, when $\eta > 0$ production increases, and when $\eta = 0$ production is independent of distance. Therefore, considering γ as a function of the intrinsic properties of the city and the degree of influence of its individuals means that we are choosing to maximize information associated to the degree of influence of those individuals who have a significant fraction (hubs) in the network formed by social interconnections in the city. So, this model falls into the class of econometric models based on the gravitational idea.

2.2.5 Fabiano et al. Model

Now, if the objective is to maximize the information associated to the condition that people in cities choose to shop in places closer to where they live or where they are temporarily settled in the city, for example, during work or college, we have that the γ parameter is identically equal to the parameter in the Fabiano et al. model (RIBEIRO; RYBSKI, 2023). This means that the economy and increasing returns in cities can be expressed by the relationships

$$L \sim N^{\frac{\gamma}{D_P}}, \qquad Y \sim N^{2-\frac{\gamma}{D_P}} \tag{2.2.20}$$

which can be classified as a type of gravitational model with D_P is the Pop fractal dimension. In Chapter 5, section 5.4 we present the results of the intra-city models of Bettencourt and M&T.

2.3 Complex Networks

In this section we will briefly review some of the main works involving network science. The term complex network is used more commonly in physics because of the emphasis on the physical interpretation of its elements. For example, in a social network, the nodes are the people and the links are the friendship ties. In a family network, the nodes are the people who make up the family group, while the links are the ties of kinship. On the other hand, in a street network (SN), the nodes are the intersections or dead ends, while the links are the street segments. Other examples of complex networks are,

for example, the nervous system, the internet, power transmission lines and radio signals, biochemical and food chains, gene proteins, WWW, coworkers and scientific collaborators (ALBERT; BARABASI, 2002; COSTA et al., 2007; NEWMAN., 2016).

Basically, complex networks are structures made up of a set of nodes interconnected through relationships or connections. These networks are characterized by non-trivial properties, such as the presence of clusters and the non-uniform distribution of connections between their nodes, see Figure 2.12.

In particular, we highlight three of the main network models, namely the Erdös-Rényi random network model, the Watts-Strogatz small world model and the Barabási-Albert model. We end with the geographic network model that can be used to simulate a transportation network. For simplicity and elegance, we consider the model discussed in (COSTA et al., 2007).

Figure 2.12 – Topological representation of the internet in the 21st century. Note the lighter points in the image, they are called hubs because they have a significant fraction of the network's links. This is a real example of a scale-free network. In particular, the scaling exponent of the Internet's degree distribution is $\gamma = 3.42$, which means that it is a network that is in the random regime with the small world property. Recent results indicate that this property comes from rules associated with mechanisms of cooperation and altruism between individuals.

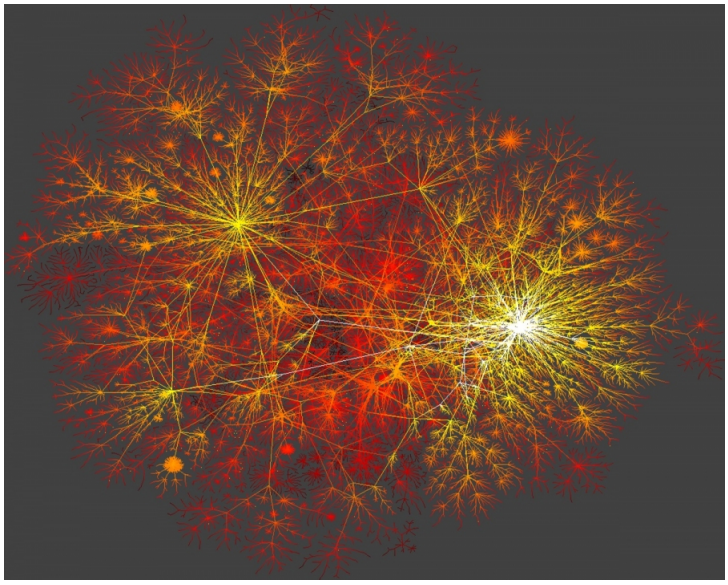

Source: A.L. Barabási, Network science <http://networksciencebook.com/>.

The origins of the study of complex networks can be traced back to graph theory, which began with Leonard Euler's solution to the problem of the seven bridges of Konigsberg and was published in 1736 (SACHS; STIEBITZ; WILSON, 1988; MALLION, 2007).

Although graph theory originated from the solution of the problem of the seven bridges of Konigsberg, it was only at the beginning of the 20th century that work involving measurements and calculations began to gain notoriety. In particular, in 1926, Otakar Borůvka proposed an algorithm for obtaining the minimum spanning tree of a graph, when there is no physical meaning attached to the network (BORUVKA, 1926). An interesting fact about this algorithm is that it was applied as a method to build an efficient power grid for Moravia, a historical region of the Czech Republic.

The applications of graph theory were not limited to engineering, but were also applied to social studies. In 1932 and 1934, Moreno (1932, 1934) published an article with collaborators and a book presenting his socio-metric studies[3]. Moreno's work, together with Helen H. Jennings, is considered one of the first to involve the analysis and visualization of social networks (GRANDJEAN, 2015; GIACOMUCCI, 2021).

With regard to what is now known in complex network theory as centrality measures, the 1948 and 1958 works, among others, by Bavelas, constitute some of the first work in this area (BAVELAS, 1948; BAVELAS, 1950). In particular, Bavelas is credited with proposing the measure of closeness centrality.

Other interesting works motivated by the applications of graph theory in social and biological studies are those by Rapoport (1957) and Erdös & Rényi (1959, 1960). In these works, you can find some of the first studies on the distribution of connections or degrees. In particular, these works are the forerunners of the study of random networks, whose degree distribution is of the Poisson type. We'll see an example of this type of network in the following sections.

In 1956 Price 1965 published a paper containing a particularly important mechanism for building network models. In this work, the author presents the rudiments of the notion of preferential attachment, i.e. some of the nodes in the network may have a higher probability of receiving connections. In particular, this mechanism is essential in the construction of complex network models, e.g. the Barabási-Albert model which we will discuss in the following sections.

In 1959, another very relevant paper in graph theory and complex networks was published by Dijkstra 1959. This paper presents an algorithm for finding the shortest path ℓ between any two nodes in a network, when the network has a positive weight.

[3] Link to the sociograms constructed by Moreno and collaborators:<https://github.com/grandjeanmartin/sociograms>.

To obtain the shortest path between two nodes in a network with a negative weight, the Bellman-Ford algorithm is used[4]. In this sense, the idea of shortest path takes into account the topology of the network under study and is different from distances such as Euclidean, Manhattan, Minkowski, etc.

In the literature, the term chemical distance is common to refer to the shortest path between the nodes of a complex network. In fact, if we relate, for example, the chemical distance and the corresponding distance in a network, it is possible to obtain the relation $\ell \sim r^{D_{min}}$, where r is the Euclidean distance, and D_{min} is the fractal dimension that characterizes the efficiency of the network. It describes a kind of "run" that passes through all the nodes once between any of the network's start and end nodes. It's as if there were an expert marathon runner who has run all the possible routes between nodes u and v of an arbitrary network, considering that each node has been crossed only once, with the exception of nodes u and v, and who is interested in the route on which he performed best. The route on which the marathon runner performed best is the shortest path (BUNDE; HAVLIN, 1992; BUNDE; HAVLIN, 1994; HERRMANN; STANLEY, 1999; ZHOU et al., 2012). For example, in Garrison 1960 and Kansky 1963 we have the first applications of graph theory ideas to the study of transportation networks at a time when data availability, computing power and modeling techniques were still quite limited.

Other very important works in the consolidation of complex network theory are Milgram's (1967) work on the six degrees of separation, see also Barabási (2002). We also have the Merton's (1968) work, who propose the Matthew effect, which seeks to capture the social phenomenon in which the rich get richer and the poor get poorer. In 1973, Granovetter 1973 propoded the theory of weak ties, which governs the behavior of connections between relatively distant and close groups.

In addition, the use of graph theory to assess the shape and physical structure of the city, in particular its street network, began with some dissidents, such as Alexander (1964,1965) and Bill Hillier (1989), who were the first to propose a theory of space syntax, relating street networks (which they called "axial maps") to the distribution of people, meetings and land uses. Sergio Porta, at Strathclyde Glasgow, and Andres Sevtsuk, at MIT, in the early 2000s, with regard to urban morphology, as "street network

[4] <https://en.wikipedia.org/wiki/Bellman%E2%80%93Ford_algorithm>.

analysis" (CRUCITTI; LATORA; PORTA, 2006; SEVTSUK; RATTI, 2010; SEVTSUK; MEKONNEN, 2012).

Figure 2.13 – The four main types of complex networks. Vertically we have directed and undirected networks. Horizontally we have unweighted and weigthted network.

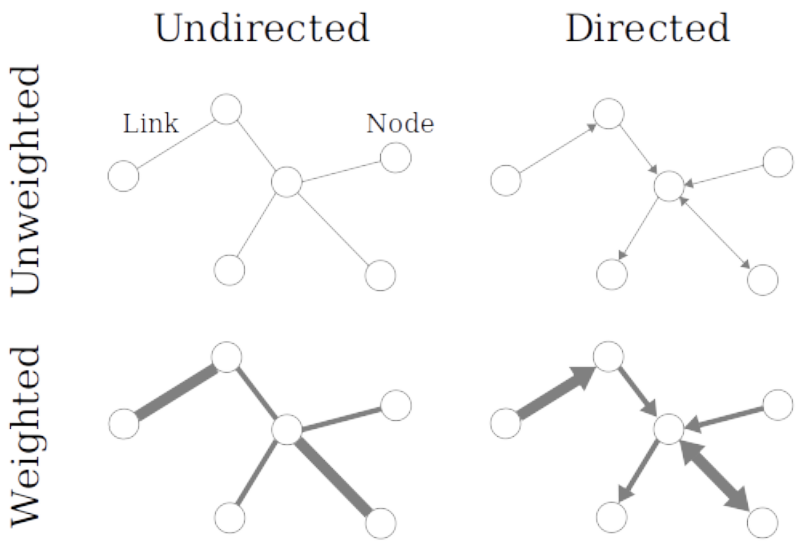

Source: Own authorship.

Now, we review some common centrality measures essential to study network science. The first is the *degree centrality*. The higher the degree of a node, the more central it is. The degree of a node is the sum of its *in-degree* and *out-degree* or the number of links that in and out the node. We define the degree as

$$k_v = \sum_u A_{vu} \tag{2.3.1}$$

where k_v is the number of connections of node v and A_{vu} is the adjacency matrix, 1 if v and u have a connection and zero otherwise (COSTA et al., 2007; NEWMAN., 2016; MATA, 2020).

The second measure is the *betweenness centrality*, it can be used to detect the amount of influence a node has over the flow of information in a graph. Its definition is

$$c_B(v) = \sum_{s,t \in V} \frac{\sigma(s,t|v)}{\sigma(s,t)} \tag{2.3.2}$$

where $\sigma(s,t|v)$ is the number of shortest path between s and t going through v, $\sigma(s,t)$ is the number of shortest path between s and t, while V is set of nodes (COSTA et al., 2007; NEWMAN., 2016; MATA, 2020). In addition, this measure also captures the dependence of other nodes on a given node in the network (BRANDES; BORGATTI; FREEMAN, 2016).

The third centrality that we will present is the *closeness centrality*, it measures its average farness (inverse distance) to all other nodes. Nodes with a high closeness score have the shortest distances to all other nodes

$$\frac{1}{c_C(v)} = \frac{1}{n-1}\sum_{u\in V\setminus v} d_{uv} \tag{2.3.3}$$

where n is the number of nodes and d_{uv} is the shortest path between u and v.

Is possible to form a relation between closeness and average path length through that

$$\langle \ell \rangle = \frac{1}{n}\sum_{v}\frac{1}{c_C(v)} = \frac{1}{n(n-1)}\sum_{v}\sum_{u\in V\setminus v} d_{u,v} \tag{2.3.4}$$

and a relation between closeness and degree centrality as (EVANS; CHEN, 2022)

$$\frac{1}{c_C(v)} = -\frac{1}{\ln z}\ln k_v + \beta, \tag{2.3.5}$$

where z is some measure of the rate of exponential growth of the shortest-path tree. β is a parameter which depends of z and the number of nodes n as

$$\beta(z,n) = \left(\frac{1}{z-1} + \frac{\ln(z-1)}{\ln z}\right) + \frac{\ln n}{\ln z}. \tag{2.3.6}$$

This implies that measuring proximity is generally redundant, unless our relationship is used to eliminate dependence on the degree of proximity, and most networks can be approximated by shortest-path trees. In fact, closeness centrality also captures the independence of a given node from the other nodes in the network, which means that there is a dual relationship between the centralities of closeness and betweenness given by (BRANDES; BORGATTI; FREEMAN, 2016)

$$\frac{1}{c_C(v)} = n - 1 + c_B(v). \tag{2.3.7}$$

The third measure is the *Bonacich centrality*. The ideia behind of this centrality is the more connections the actors in your neighborhood have, the more central you are. The fewer the connections the actors in your neighborhood, the more powerful you are. This can be express in the following way

$$c_v(\phi, \theta) = \sum_u (\phi + c_u\theta) s_{vu} \tag{2.3.8}$$

where ϕ and θ reflects the degree to which an individual's status is a function of the statuses of those to whom he or she is connect and s_{vu} is the matrix of relationships (BONACICH, 1987).

We also have some topological measures, for example, the *cyclomatic number*, α, β, and γ numbers. The cyclomatic number describes the number of edges that must be removed from a graph to ensure that no graph cycle remains (SHARIFI, 2019)

$$\mu = e - n + 1. \tag{2.3.9}$$

However, the α number measures the ratio between the number of circuits (loops) to the maximum number o circuits in the network with the same number of nodes (SHARIFI, 2019)

$$\alpha = \frac{\mu}{2n - 5}, \tag{2.3.10}$$

and the β number measures the frequency of connections based on the ratio between the number of links and the number of nodes in the network

$$\beta = \frac{e}{n}. \tag{2.3.11}$$

Finally, the γ number measures the frequency of links and is defined as the ratio between the number of links and the maximum possible number of links

$$\gamma = \frac{e}{3(n-2)}. \tag{2.3.12}$$

After reviewing some of the main works on complex networks and looking at some of their main measures, we then present three types of networks: random, scale-free, small-world, and finally we give the example of a geographic network. We also highlight some of the key

ingredients in characterizing such networks, except for the geographic network, namely the degree probability distribution, the average shortest path length, and the clustering coefficient.

The degree probability distribution tells us the probability of finding a node with a given number of links. The average length tells us the average distance between two nodes in the network, while the cluster coefficient tells us the average number of links a node has.

2.3.1 Random Networks

One of the first studies of random networks was done by Erdös and Rényi. A random or Erdös-Rényi (ER) network can be constructed as follows: a value is set for a parameter p, or the probability associated with the creation of a connection between any two nodes in the network. For each pair of randomly selected nodes, a random number r is generated according to a uniform distribution. At each step, the relationship $p > r$ is tested. If the relationship is true, a connection is added between the selected nodes, but if the relationship is false, nothing is done (NEWMAN., 2016). Random networks are widely used in modeling real-world networks, such as social networks, financial networks, percolation theory, to name a few (CALLAWAY et al., 2000; NEWMAN; WATTS; STROGATZ, 2002; DEPREZ; WÜTHRICH, 2015).

An ER network has a given degree distribution of Poisson type

$$p(k) = e^{-\langle k \rangle} \frac{\langle k \rangle^k}{k!} \tag{2.3.13}$$

where $p(k)$ is the probability of finding a node with degree k in the network G. It also has an average path length of the following expression

$$\langle \ell \rangle \sim \frac{\ln n}{\ln \langle k \rangle} \tag{2.3.14}$$

and a cluster coefficient given by

$$c(k) = \frac{\langle k \rangle}{n}. \tag{2.3.15}$$

2.3.2 Small-World

The second model we'll look at next is the Watts-Strogatz (WS) model, which has the small-world property. The Watts & Strogatz proposed in 1998 a complex network with small-world property, which means that the shortest average path of the network grows linearly with the logarithm of the number of nodes (WATTS; STROGATZ, 1998). A recent study has shown that evolutionary rules such as cooperation and altruism are some of the ingredients that allow this phenomenon to emerge (SAMOYLENKO et al., 2023). Examples of this type of network include: road maps, food chains, electricity networks, metabolite processing networks, brain neuron networks, voting networks, phone call graphs, and gene regulatory networks (NEWMAN., 2016).

A strategy used to generate such a network is as follows: i) create a circular network with n nodes connected to k neighbors. ii) select some nodes and rewrite some of its links so that each of the original links has a probability p (fixed in advance) of having one of its links moved to a new randomly chosen node.

The probability distribution of a WS network is given by

$$p(k) \sim e^{-\beta\langle k\rangle} \tag{2.3.16}$$

where $0 \leq \beta \leq 1$ is a parameter that controls the regularity of the network ($\beta = 0$: regular network or a; $\beta = 1$ Erdös-Rényi).

The average path length between two nodes in a network is.

$$\langle \ell \rangle \sim \frac{\ln n}{\ln\langle k\rangle} \tag{2.3.17}$$

and its clustering coefficient is

$$c(k) = const. \tag{2.3.18}$$

Note that the average path lengths of ER and SW are the same, but the cluster coefficients and the degree probability distributions are different.

2.3.3 Scale-Free

In 1999 Barabási & Albert proposed a model presentig a network whose degree distribution follows a power law and where its exponent informs the degree of hetero-

geneity of the network - whether the network is anomalous, scale-free (SF) or random (BARABASI; ALBERT, 1999). In these scale-free networks, it is possible to find a very small fraction of nodes containing significantly many connections. Nodes with this characteristic are called hubs. With the publication of this work, the term network science has come to the fore in recent decades, paving the way for applications in various areas of science. In this sense, a flurry of articles and textbooks on this line of research began to be published in specialized journals, publishers with an academic tradition and even personal blogs (ALBERT; BARABASI, 2002; BARABASI, 2002; COSTA et al., 2007; NEWMAN., 2016; BARABASI, 2016; MATA, 2020). Examples of scale-free networks are: the Internet, scientific collaboration networks, networks of actors in movies, and protein interactions (BARABASI, 2016).

A SF network can be generated by starting with a small network of with m_0 nodes. At each step, a new node u is added to the network, connecting it to $m \leq m_0$ of the existing nodes $v \in V \in G$. In addition, it is necessary to impose that the probability of connecting node u to node v is proportional to the degree of v. In other words, nodes with a higher number of connections are more likely to receive new connections, a process known as preferential attachment.

The degree distribution of a SF is a power law

$$p(k) \sim k^{-\alpha}. \tag{2.3.19}$$

Its average path length is

$$\langle \ell \rangle \sim \frac{\ln n}{\ln \ln n} \tag{2.3.20}$$

and with cluster coefficient

$$c(k) = \frac{(\ln n)^2}{n}. \tag{2.3.21}$$

Moreover, it is possible to relate the degree of heterogeneity of a scale-free network to its fractal properties. To see this, let's consider the notion of renormalization, which is a technique that consists of creating small replicas of a given object in order to preserve the main structural features of the original object. Basically, the idea is to obtain copies with simpler structures to facilitate analysis which is closely related to the property of self-similarity.

The renormalization, see for example Rosenberg 2021, procedure in a complex network consists of: i) covering the entire network with boxes of size (side length) ϵ; ii) replacing each box with a single node and connecting two nodes if and only if there is at least one link between two boxes in the original network; iii) applying steps 1 and 2 to the renormalized network until a single node is obtained, yielding a connected network (all nodes have links).

Thus, if we consider a network G to be a scale-free network, then its degree probability distribution is given by eq. (2.3.19) and for a renormalized network G' is given by $p'(k) \sim k^{-\alpha}$.

This means that a scale-free network has a degree probability distribution invariant by renormalizations, where the renormalization process can be understood as synonymous with the transformation (MOLONTAY, 2015). In fact, the sequence of k times renormalized networks $\{G'_n\}_{n\in\mathbb{N}}$,$\{G''_n\}_{n\in\mathbb{N}}$, ...,$\{G_n^{(k)}\}_{n\in\mathbb{N}}$, ... has the same scaling exponent α.

Empirical data suggests that by plotting the degree $k(\epsilon)$ of each node in the renormalized network against the degree k_{max} of the most connected node in the corresponding box of size ϵ, it is possible to obtain a linear scaling law

$$k(\epsilon) \sim s(\epsilon) \cdot k_{max} \tag{2.3.22}$$

where $s(\epsilon)$ is a scaling factor. Furthermore, this factor s ($s < 1$) scales with ϵ and defines an exponent d_k (fractal dimension of the degree distribution).

$$s(\epsilon) \sim \epsilon^{-d_k} \tag{2.3.23}$$

so that the degree exponent for a network sequence $\{G_n\}_{n\in\mathbb{N}}$ is given by

$$d_k = \lim_{\epsilon \longrightarrow 0} \lim_{n \longrightarrow 0} \frac{\ln s^n(\epsilon)}{\ln(1/\epsilon)} \tag{2.3.24}$$

where $s^n(\epsilon)$ is the scale factor of the mesh G_n and the side box ϵ. Assuming that $\frac{N}{N(\epsilon)} \sim \epsilon^{d_f}$ where N is the number of nodes in the network, $N(\epsilon)$ is the number of boxes needed to perfectly cover the entire network, ϵ is the size of the box, d_f is the fractal dimension of the network, and denote the degree probability distributions of the non-renormalized

network G and the renormalized network G', respectively, by

$$p(k) \sim k^{-\alpha}, \qquad p'(k') \sim k'^{-\alpha}, \tag{2.3.25}$$

we can write

$$NP(k)dk \sim N(\epsilon)p'(k')dk'. \tag{2.3.26}$$

This expression means that the probability of finding a given number of nodes with degree between $k + dk$ in a non-renormalized network G of size N is numerically equal to the probability of finding a given number of nodes with degree between $k' + dk'$ inside $N(\epsilon)$ boxes of size ϵ which perfectly overlap a renormalized network G'.

In this sense, we can write

$$Np(k) \sim N(\epsilon)p'(k')\frac{dk'}{dk} \tag{2.3.27}$$

and imposing that $k = k_{max}$ will result in

$$Np(k_{max}) \sim N(\epsilon)p'(s(\epsilon)k_{max})s(\epsilon). \tag{2.3.28}$$

Using the eq. (2.3.25), we have

$$Nk_{max}^{-\alpha} \sim N(\epsilon)k_{max}^{-\alpha}s(\epsilon)^{-\alpha}s(\epsilon) \Longrightarrow \frac{N}{N(\epsilon)} \sim s(\epsilon)^{-\alpha+1} \Longrightarrow \epsilon^{d_f} \sim (\epsilon^{-d_k})^{-\alpha+1} \tag{2.3.29}$$

which implies

$$\alpha = 1 + \frac{d_f}{d_k}. \tag{2.3.30}$$

These results show that the scale exponent α can be explained by the complexity of the spatial and geometric patterns of the network d_f and the complexity of the connection patterns between its links d_k. When $d_f = d_k$ we have the first critical regime A, see Figure 2.14, when $\alpha = 2$, while when $d_f = 2d_k$ we have the second critical regime B when $\alpha = 3$. Note that most real scale-free networks have scaling exponents in the interval $2 < \alpha < 3$, which is characterized by the ultra-small-world property. Furthermore, using

the expression for α it follows that $-\frac{d_k}{d_f} = \frac{1}{1-\alpha}$, hence

$$s(\epsilon) \sim \left(\frac{N}{N(\epsilon)}\right)^{\frac{1}{1-\alpha}} \Longrightarrow \frac{k(\epsilon)}{k_{max}} \sim \left(\frac{N}{N(\epsilon)}\right)^{\frac{1}{1-\alpha}} \Longrightarrow k_{max} \sim N^{\frac{1}{\alpha-1}}, \tag{2.3.31}$$

which tells us that the hub with the largest number of links scales with the size of the network with the exponent $\frac{1}{\alpha-1} = \frac{d_k}{d_f}$, or even that the formation of hubs is closely related to the relative complexity between the local and global structure of the network when it reaches a critical size.

Figure 2.14 – Regimes of the scaling exponent α. $\langle k \rangle$ is the average number of links or central tendency of k, $\langle k^2 \rangle$ is the associated second moment or variance of k with respect to the average, $\langle d \rangle$ is the average diameter of the network, and k_{max} is the number of links of the largest hub in the network. Note that most real scale-free networks have scaling exponents in the range $2 < \alpha < 3$, which is characterized by the ultra-small-world property. A network has the small-world property if it has relatively few long-distance links, but a small average path length relative to the total number of nodes. 1) $\alpha < 2$ means that the number of links connecting to the largest hub in the network grows faster than the size of the network. 2) $2 < \alpha < 3$ means that the number of links connecting to the largest hub in the network grows with the size of the network. 3) $\alpha > 3$ indicates that the average distance between nodes converges to the small-world formula.

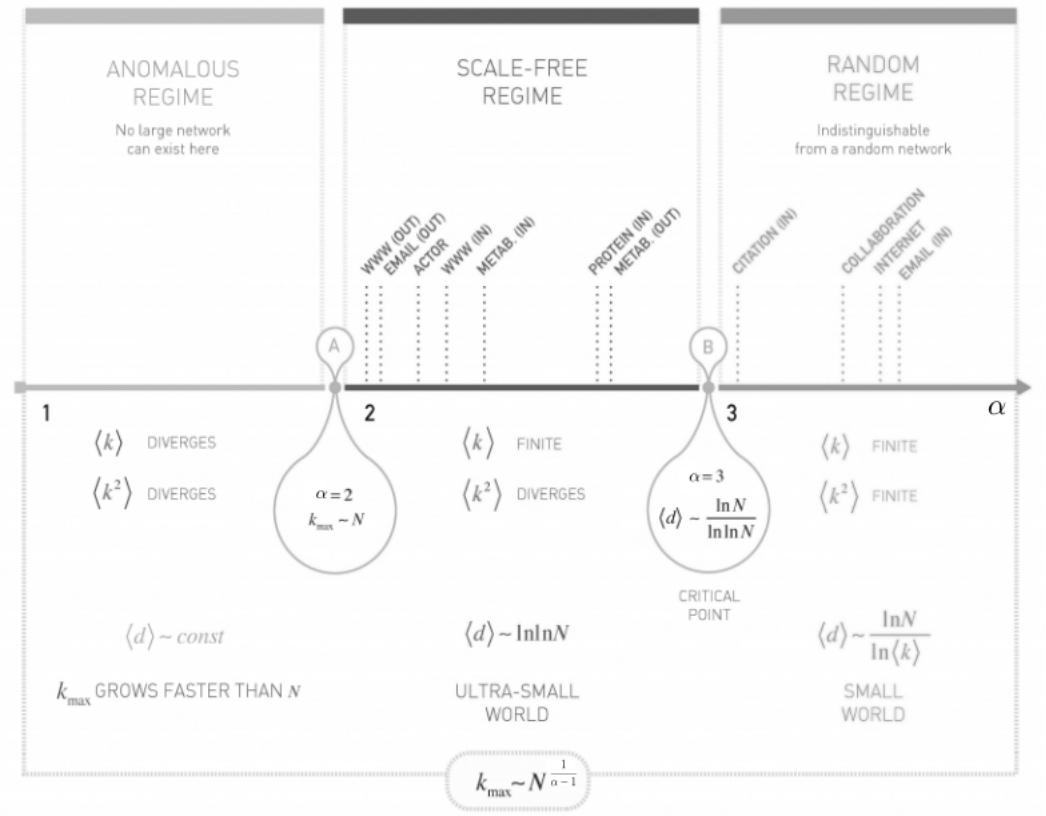

2.3.4 Spatial Network

Another example of a complex network is a spatial network. Some of the main examples of these networks are transportation systems, electricity grids, communications, infrastructures and brain activity (AMIT et al., 2023). In particular, urban streets can be generated from the following interaction probability (COSTA et al., 2007)

$$p_{ij}(r) \sim e^{-\lambda r_{ij}} \tag{2.3.32}$$

where r_{ij} is the Euclidean distance between nodes i and j and λ a scaling factor that controls the size of the links between the nodes of the network.

In fact, the above interaction probability can be obtained from the maximization of Shannon entropy

$$\mathcal{L} = -\sum_i \sum_j p_{ij} \ln p_{ij} - \lambda \left(\sum_i \sum_j p_{ij} r_{ij} - \langle r \rangle \right). \tag{2.3.33}$$

subject to the constraint $\langle r \rangle = \sum_i \sum_j p_{ij} r_{ij}$, in analogy to eq. (2.2.12).

Other interesting works involve how street networks (SN) can be modeled by mimicking biological systems or by taking into account endogenous quantities such as accessibility, income of the individuals who make up the city, transport costs, betweenness as well as the topological property of the network, see (BARTHELEMY; FLAMMINI, 2009; TERO et al., 2010; COURTAT; GLOAGUEN; DOUADY, 2011).

3 OBJECTIVES AND JUSTIFICATIONS

In this Chapter we present the questions that motivate our study, give some justifications and point out the general and specific objectives.

- **Problem formulation**:

What are the fractal dimensions of space filling, information, and correlation of Brazilian cities with a population (Pop) greater than or equal to 1 million inhabitants? What are the similarities and differences between the multifractal spectrums of the street network (SN) and the Pop? Is it possible to expand econometric models that take fractal theory into account from a multifractal perspective? If so, what are the models and what are the main implications? What are the main information measures on the Brazilian city network, such as degree, closeness, betweenness centralities and some topological quantities? What is the relationship between the network measurements of Brazilian cities and the corresponding Pop?

- **Justification**:

We see in the Chapter 2 that application of multifractal analysis, urban scaling law and network science can be applied in several fields of science and engineering. So, the need to understand urban systems, in particular, cities as a complex adaptive system in light of statistical, non-conventional, computational methods that take into account real data is mandatory. Because we need to generate new knowledge that allows the insertion of empirical results in decision-making at the local and global level, seeking to improve people's lives in cities (NATIONS, 2016). In addition, because a multifractal analysis of the SN and Pop, taken together, of cities in developing countries has not yet been carried out.

- **Objectives**:

General objectives: Investigate the multifractality of the Pop and SN of the 15 largest Brazilian cities and extend the main intra-city econometric models. *Specific objectives*: 1) Estimate the fractal dimensions (capacity, information, correlation, minus and plus infinity) of the Pop and SN of the 15 largest Brazilian cities using multifractal analysis and 2) Empirically verify the sub-linearity and super-linearity of the scale exponents

between infrastructure and socio-economic variables using econometric models, comparing their results. 3) calculate the following measures of centrality of the SN of the Brazilian municipalities: a) degree; b) closeness ; c) betweenness; d) Bonacich; f) α number; g) β number; h) γ number and i) cyclomatic number μ; j) number of nodes and links.

4 MATERIALS AND METHODS

This Chapter describes the materials and methods used throughout the research.

Before we go any further, it is worth highlighting the characteristics of the research: i) *Purpose*: applied, as we believe that the knowledge generated directly or indirectly from this research can be used to support decision-making in urban systems in the short, medium and long term. ii) *Nature*: experimental because we use real data involving population (SN), the street network (SN) and other statistical measures of the city; iii) *Approach*: quantitative, as the physical quantities of interest were: 1) the spatial distribution of the *Pop*; 2) the spatial distribution of the SN (number of streets, corners, area, perimeter, etc.), the degree, betweenness, closeness, Bonacich centrality's besides some topological measures; 3) the generalized dimensions for the SN and the *Pop*; 4) scale exponents between urban metrics and *Pop*; iv) *Technical Procedures*: documental (review of textbooks and scientific articles) and laboratory (simulation of experiments using computational tools); The programming language used was Python, as it is one of the most widely used languages for data analysis and exploration today. In particular, I highlight that throughout the master's degree several computer simulations were carried out, generating codes ranging from graphical and statistical analyses, as well as the creation of agent-based models with the intention of enriching the learning of complex systems.

In addition, a self-explanatory flowchart was constructed, Figure 4.1, to better visualize the path that was traced from data collection to the preparation of this work.

4.1 Data Avaliability

In this section we highlight the databases used in our analysis and the variables of interest. We would point out that our analysis would be greatly compromised if the data we will refer to next had not been made publicly available, which reinforces the importance of public data in order to conduct scientific research.

Below are two of the main institutions and one foundation where data was collected for the research.

The first[1] was the Instituto Brasileiro de Geografia e Estatística (IBGE), which is the country's main provider of data and information, meeting the needs of the most

[1] <https://www.ibge.gov.br/>

Figure 4.1 – Flowchart of the path that was traced, from data collection to the preparation of this work.

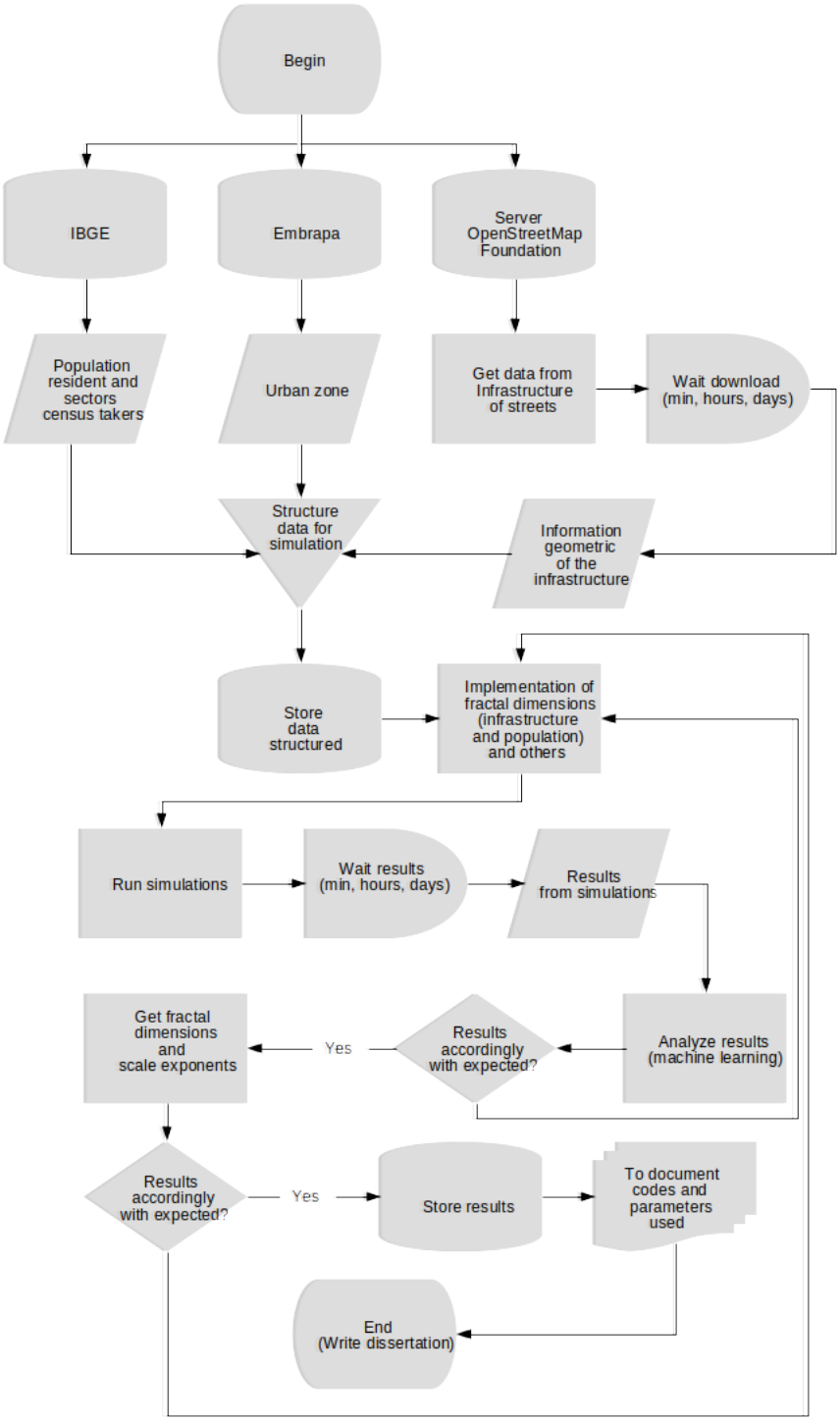

Source: Own authorship.

diverse segments of civil society, as well as federal, state and municipal government bodies.

The second[2] company was the Empresa Brasileira de Pesquisa Agropecuária (Embrapa), which is an innovation company focused on generating knowledge and technologies for Brazilian agriculture. Thirdly[3], was the *OpenStreetMap Foundation*, an open initiative to create and provide free map data to anyone who wants it.

Initially, data[4] was collected involving the census sectors of the 5570 Brazilian municipalities available in the IBGE database. The reference year was 2010.

The variables of interest were:

- Resident people (Information base of the 2010 Demographic Census: results of the Synopsis by census sector);
- Total *Pop*;
- Census mesh and its geometry (`Polygon`)[5]

After collecting the data mentioned above, the Brazilian urban area was collected, where the information on the delimitations of the geometry of the urban area can be found in the database[6] made available by Embrapa.

In this data set, the variables of interest were:

- Urban sprawl - referring to the year 2015 and its geometry (`Polygon` or `MultiPolygon`);
- Geocode (municipality code according to IBGE);
- Urban area;
- Urban perimeter.

For the municipal SN data, the library `osmnx`[7] was used (BOEING, 2017). With this package, with the geometries of the urban areas from Embrapa's data and after

[2] <https://www.embrapa.br/>.
[3] <https://wiki.osmfoundation.org/wiki/Main_Page>.
[4] Link to access the data: <https://www.ibge.gov.br/geociencias/organizacao-do-territorio/malhas-territoriais/26565-malhas-de-setores-censitarios-divisoes-intramunicipais.html?edicao=26589&t=acesso-ao-produto>.
[5] For more details on the types of variables used go to: <https://shapely.readthedocs.io/en/stable/geometry.html>.
[6] Data access link: <http://geoinfo.cnpm.embrapa.br/layers/geonode%3Aareas_urbanas_br_15>.
[7] A Python package for downloading, modeling, analyzing and visualizing SN and other geospatial elements. Link to access: <https://osmnx.readthedocs.io/en/stable/>.

developing codes in Python, it was possible to extract the SN of 5523 Brazilian cities, which were stored in files in the (comma-separated values) csv format. Two files were generated for each city, the first containing information identifying the nodes (intersections and dead-end streets) of the SN, geographical location in EPSG format 4326[8], Cartesian coordinates and geometry in `Point` type. The second is the file containing information on the links (street segments) of the SN, the identification of the end nodes of the links, the weight of the links or length in meters and the associated geometries of the `LineString` type. Thus, the variables of interest were:

- Osmid (node identification according to `osmnx`);
- Cartesian coordinates (x, y), geographic (epsg format: 4326) of SN nodes and geometry (`Point`);
- Links (u, v) of the SN where u and v are the nodes, their weights w and geometry (`LineString`);

4.2 A Python Package: FractalCity

In this section we introduce the Python packages that were used throughout the research and provide a tutorial along with a `FractalCity`[9] package created specifically to automate the processes of obtaining the generalized dimensions of the street network (SN) and the population (Pop). To see the codes developed.

In order to automate, facilitate data analysis, disseminate and generate new data, `FractalCity` was developed, a Python package with classes and methods to help with the simulations. The ICN/DFI Departamento de Física cluster was used to carry out the simulations (the cluster descriptions are shown in the Table 4.1) and a personal computer with 4 CPU(s), model Intel(R) Core(TM) i3-2310M CPU @ 2.10GHz and Zorin OS 15.3 operating system.

The following main packages were used as aids:

- `networkx`[10]: network analysis and visualization, including `osmnx`;

[8] <https://pt.wikipedia.org/wiki/WGS84>.
[9] Link to access codes and tutorial: <https://www.dropbox.com/scl/fi/pevlue8vlp1tax519f1t2/FractalCity-code-and-graphs.zip?rlkey=nflraas61jrcjfr4yhtq941hm&dl=0>.
[10] <https://networkx.org/>.

Table 4.1 – The DFI computer cluster consists of 1 server and 19 calculation nodes, the machines have the configurations described below.

Machine	Configuration by machine
1 Head node	- CPU 1x Intel(R) Core(TM) i7-2600K CPU 3.40GHz - 6 GB de RAM, 64 bit, DDR3, 1333MHz - Storage 1x HD - 1.8 TB (home), 1x HD 500 GB (backup)
8 Compute nodes	- CPU 1x Intel(R) Core(TM) i7-2600K CPU 3.40GHz - 16 GB de RAM, 64 bit, DDR3, 1333MHz.
1 Compute node	- CPU 2x Intel(R) Xeon(R) X5650 CPU 2.67GHz - 24 GB RAM, 64 bit, DDR3, 1333MHz.
3 Compute nodes	- CPU 2x Intel(R) Xeon(R) CPU E5-2640 2.50GHz - 32/8/110 GB RAM, 64 bit, DDR3, 1333MHz.
7 Compute nodes	- 1x Intel(R) Core(TM) i7 CPU 3.60GHz - 32 GB RAM, 64 bit, DDR4

Source: Own authorship.

- `numpy`[11]: for numerical calculations and statistics;
- `powerlaw`[12]: for proper estimation of power law exponents;
- `pandas`[13] e `geopandas`[14]: for reading, processing and manipulating of data and maps;
- `dask`[15]: for reading, processing and manipulating extensive data;
- `shapely`[16]: for creating, manipulating and measuring geometric objects;

[11] <https://www.google.com/search?channel=fs&client=ubuntu&q=numpy>.
[12] <https://pypi.org/project/powerlaw/>.
[13] <https://pandas.pydata.org/>.
[14] <https://geopandas.org/en/stable/>.
[15] <https://www.dask.org/>.
[16] <https://shapely.readthedocs.io/en/stable/manual.html>.

- `scipy`[17] e `scikit-learn`[18]: for modeling and machine learning;
- `matplotlib`[19], `pylab`[20], `seaborn`[21] e `plotly`[22]: for data visualization;
- `jupyter`[23]: for creating and viewing codes;
- `geobr`[24]: for visualizing geospatial data of the Brazilian territory.

4.3 Sandbox Method and Abnormal Spectra

In this Section we present the algorithm for the *sandbox* method and present the criteria used to choose the spectra of the street network (SN) and population (Pop), because depending on the choice of point where the measurements are made, the spectra show abnormalities at the left and right ends, which can compromise the estimates of the generalized dimensions. Basically, this translates mathematically in a bound condition for the dimensions discussed in section 2.1.4.

$$D_2 \leq D_1 \leq D_0. \tag{4.3.1}$$

Finally, we also present the values of the parameters used in the simulations.

In order to meet specific objective 1, presented in Chapter 3, we chose the *sandbox* method to estimate the generalized dimensions of the SN and the Pop, see Figure 4.2.

The justification for the choice is that this method provides good estimates compared to the box-counting method for generalized dimensions, which allows us to deal with effects occurring in more rarefied regions of the fractal $q < 0$, where q are the moments of order associated with the fractal measure (TEL; VICSEK, 1987) (BARTOLO; GAUDIO; GABRIELE, 2004) (TEL; FULOP; VICSEK, 1989) (ROSENBERG, 2021).

Basically, the method consists of:

[17] <https://scipy.org/>.
[18] <https://scikit-learn.org/stable/>.
[19] <https://matplotlib.org/>.
[20] <https://www.tutorialspoint.com/matplotlib/matplotlib_pylab_module.htm>.
[21] <https://seaborn.pydata.org/>.
[22] <https://plotly.com/>.
[23] <https://jupyter.org/>.
[24] <https://github.com/ipeaGIT/geobr>.

Figure 4.2 – Illustration of the sandbox method. The method consists of calculating the average number of structural elements between the radii of each point and then performing a linear regression and obtain the inclination of a curve in a log-log scale for each moment order q. A more detailed description can be shown in the Appendix C.

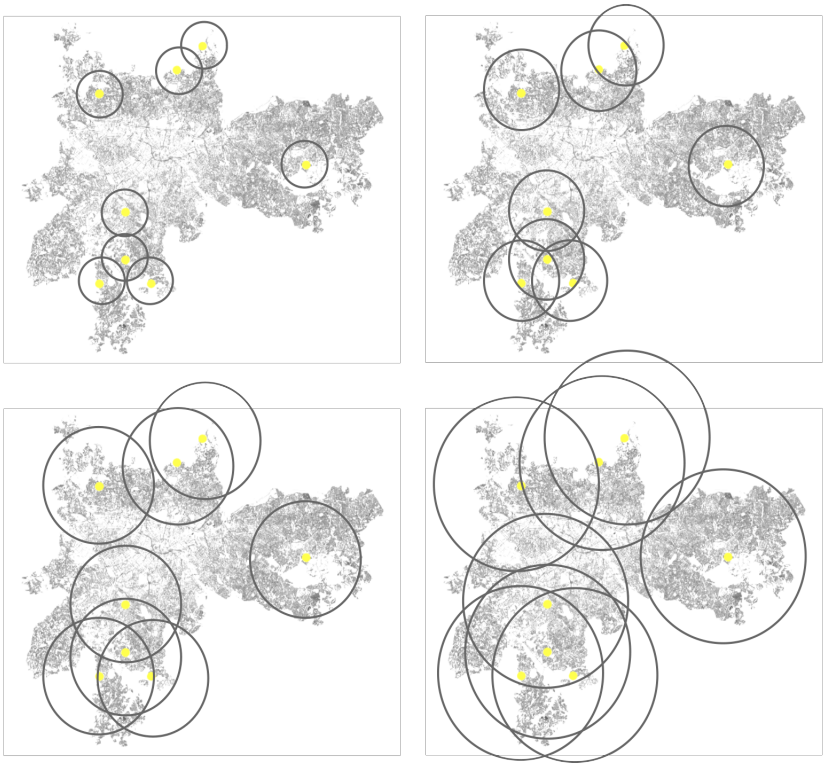

Source: Own authorship.

1. Choose a fraction of points inside the fractal or nearby points and, for each point chosen, calculate the number of elements inside a ball of a specific radius. Repeat this procedure varying the radii and on the chosen points;

2. Define a probability measure with the fractal elements on the spatial support (normalize with size or number of fractal elements, e.g., number of nodes in the network, number of people, etc.) raised to a real number q (moments of order), e.g., $q \in [-\infty, \infty]$;

3. Calculate the average value of the probability measure obtained in the previous step between all the points and for each radius;

4. Plot the list of average values against the list of chosen radii on a log-log graph and extract the sequence of slopes with the same number of elements as the sequence

of q values; interpret each slope as the generalized fractal dimension $D_{q=q'}$ of order q'.

In order to rule out abnormalities in the fractal dimension data and the multifractal spectrum, the above procedures were repeated 20 times for each city. These abnormalities are related to the poor choice of points chosen at random and where the measurements will be taken. Depending on the points chosen, it is possible to obtain a very deformed spectrum of singularities .

Figure 4.3 – Singularity spectra of the street network (SN) in blue and the population (Pop) of the city of São Paulo, SP, in orange. a) Singularity spectra as a function of the order moments q for SN. b) Singularity spectra as a function of the order moments q for Pop. c) and d) Singularity spectra as a function of the singularity indexes α. Shown in blue and orange are the spectra satisfying the $\min\{f^a(\alpha_{-\infty})\}_{i=1}^{n=20}$ criterion for $a = \{SN, Pop\}$ and, in gray, those that do not.

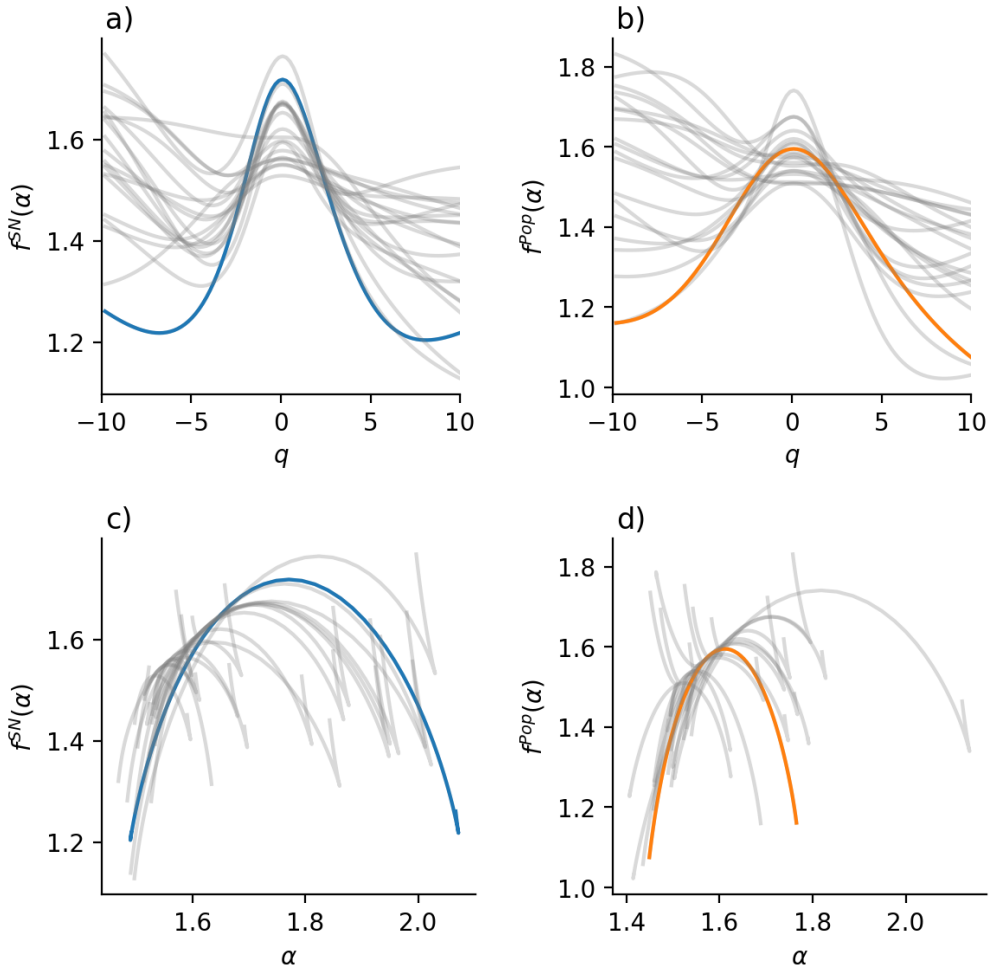

Source: Own authorship.

To eliminate abnormal samples from the spectra of SN and Pop, we search within the sample sequences of spectra $\{f_i^a(\alpha_{-\infty})\}_{i=1}^n$ with $a = \{SN, Pop\}$. n is the number of samples for a given city and $f^a(\alpha_{-\infty})$ the value of the singularity spectrum at $q = -\infty$, see Figure 4.3 a) of the city of São Paulo, SP, as an example. In particular, we used $n = 20$, i.e. 20 samples for each city. Once this was done, the configuration satisfying $\min\{f_i^a(\alpha_{-\infty})\}_{i=1}^n$ was selected.

This criterion was used based on the fact that the singularity spectrum must be increasing to the left and decreasing to the right of $q = 0$, i.e, we must have

$$\begin{cases} \dfrac{df^a(\alpha(q'))}{dq} > 0, & q < q' < 0; \\ \dfrac{df^a(\alpha(q'))}{dq} < 0, & 0 < q' < q. \end{cases} \tag{4.3.2}$$

The sample that satisfied $\min\{f_i^a(\alpha_{-\infty})\}_{i=1}^n$ was the one that best captured the conditions around $q = 0$, and it was possible to obtain spectra with little or no abnormalities.

Below are the parameters chosen for the simulations. The reason for choosing these parameters is that we were interested in making as few inferences as possible about the cities analyzed. We wanted a way to apply the simulations to each city in an automated way.

The value of R_{min} was chosen to be equal to one over fiftyths of the value of the diagonal of the lattice. If a lattice has side L, then its diagonal is given by $diag = \sqrt{2}L$ and therefore $R_{min} = \frac{diag}{50}$. In Appendix C we show the mathematical formulation used to estimate the fractal dimensions for SN and Pop according to the *sandbox* method. The value of R_{max} was chosen to be equal to half the diagonal of the lattice, so $R_{max} = \frac{diag}{2}$. We considered a linear space with 50 elements in the closed interval $[R_{min}, R_{max}]$, defined to account for the number of elements (nodes or persons) of the fractal structures (SN or Pop) studied. To generate the values of q, we define a linear space in the closed interval $[-10, 10]$ with 100 points, so $q = -\infty$ is the same as $q = -10.0$, etc. In the section 2.1.4 we show the theoretical foundations involved in the construction of the generalized dimensions and the multifractal spectrum.

5 RESULTS AND DISCUSSION

In this Chapter, we present the main results of this work. With regard to the multifractal analysis, we calculated the parameters of the multifractal modeling carried out with the aim of recovering the spectrum of generalized dimensions with as few parameters as possible (4 parameters), without having to store them in files. We calculated the generalized dimensions of the street network (SN) and the population (Pop), their respective standard deviations and the coefficients of determination. We calculated the spatial completion, redundancy, and correlation rates u, v and w for both and built hierarchical classification dendrograms for each; we calculated the skewedness index of the spectra χ and the aggregation-diffusion index ξ, satisfying $\xi = 1/\chi$. In particular, the ξ index allowed us to find out which cities show patterns of aggregation and diffusion. We suggest that the phenomenon of aggregation is a consequence of the presence of natural resources, for example lakes, forests and rock formations within cities, and of internal interference occurring from above, such as urban planning, thus delimiting and interfering in the urban space where people live.

We also present the results involving intra-city models, for example, we show that only Betterncourt's model and Molinero and Thurner's macroscopic model (M&T) could be extended *ad hoc* by exchanging the fractal dimensions of the model for some generalized dimensions, but they require further investigation with a larger number of cities. We present the results of linear regressions of M&T's macroscopic model and perform an analysis similar to theirs, confirming that the urban scaling laws can be determined through geometry. Using this approach, it was possible to see two growth regimes in the relative spatial complexity between SN and Pop. We observed that there is a kind of phase transition that occurs around cities with Pop of 10,000 inhabitants. Below this regime, this relative complexity grows linearly with time and above, it grows non-linearly, asymptotically approaching a limit value that we use to test the validity of the model.

In addition, we present scaling laws involving network measures as a function of city size and their distributions. We show that the number of nodes n, the links e and the cyclomatic number μ scale sub-linearly with city size. We provide the average distributions of the numbers of degrees k, α, β and γ, as well as two linear relationships between the measures for each network. In addition, we illustrate the scaling laws of the urban area and the perimeter with the size of the city. Finally, we present the power law relationships

between the averages of centralities, including betweenness, closeness and Bonacich, and city size.

5.1 Multifractal Analysis and Modeling

In this section, we present the results of the multifractal modeling of the estimated multifractal measures of street network (SN) and population (Pop), namely: generalized dimensions D_q, mass exponents $\tau(q)$, indexes $\alpha(q)$ and spectrum $f(\alpha(q))$ of singularities in terms of moments of order q and spectrum of singularities or multifractal spectrum $f(\alpha(q))$, for the 15 largest Brazilian cities in 2010. We show that this modeling allows us to make predictions of the abnormalities found in the singularity spectra. Long and Chen (2021) argue that these abnormalities result from uncontrolled development in peripheral and sparse areas, as well as degradation of the fractal structure in central and high-density regions.

First, we emphasize that mathematical modeling[1] plays a very important role in different areas of science, for example, climate, epidemic, city system modeling, to name a few (ROSENBLUETH; WIENER, 1945) (QUARTERONI, 2009) (SAYAMA, 2015) (FRIGG; HARTMANN, 2020). In the context of multifractal analysis it is also possible to model as we will see below.

Observing the behavior of the inverted "S" type of generalized dimensions, see Figure 5.1 a), an interesting *ansatz* that we can use to model this quantity is from a sigmoid function

$$f(x) = a + \frac{b}{1 + ce^{dx}}, \tag{5.1.1}$$

widely used in economics and computing (KYURKCHIEV; MARKOV, 2015), which we use to model the multifractal quantities. For the mathematical construction of multifractal modeling, see Appendix B.

Figure 5.1 presents as an example the modeling of multifractal functions of the SN and the Pop in the city of São Paulo. The SN and the map of the census sectors Pop of the city of São Paulo can be seen in Figures 5.3 and 5.4, respectively. It is possible to observe that the model perfectly explains the generalized dimensions, the mass exponents, and the

[1] Mathematical modeling enables: i) forecasting and planning; ii) decision-making; iii) optimization; iv) control and automation; v) simulation and experimentation; vi) risk analysis; vii) education and research, to name a few.

Figure 5.1 – Multifractal quantities: the blue and orange balls refer to empirical values for the street network (SN) and population (Pop) of the city of São Paulo, SP. The solid lines refer to the points captured by the models. The dashed lines refer to the 90% confidence intervals. a) generalized dimensions, b) mass exponents, c) singularity exponents, d) singularity spectrum as a function of order moments, e) singularity spectra.

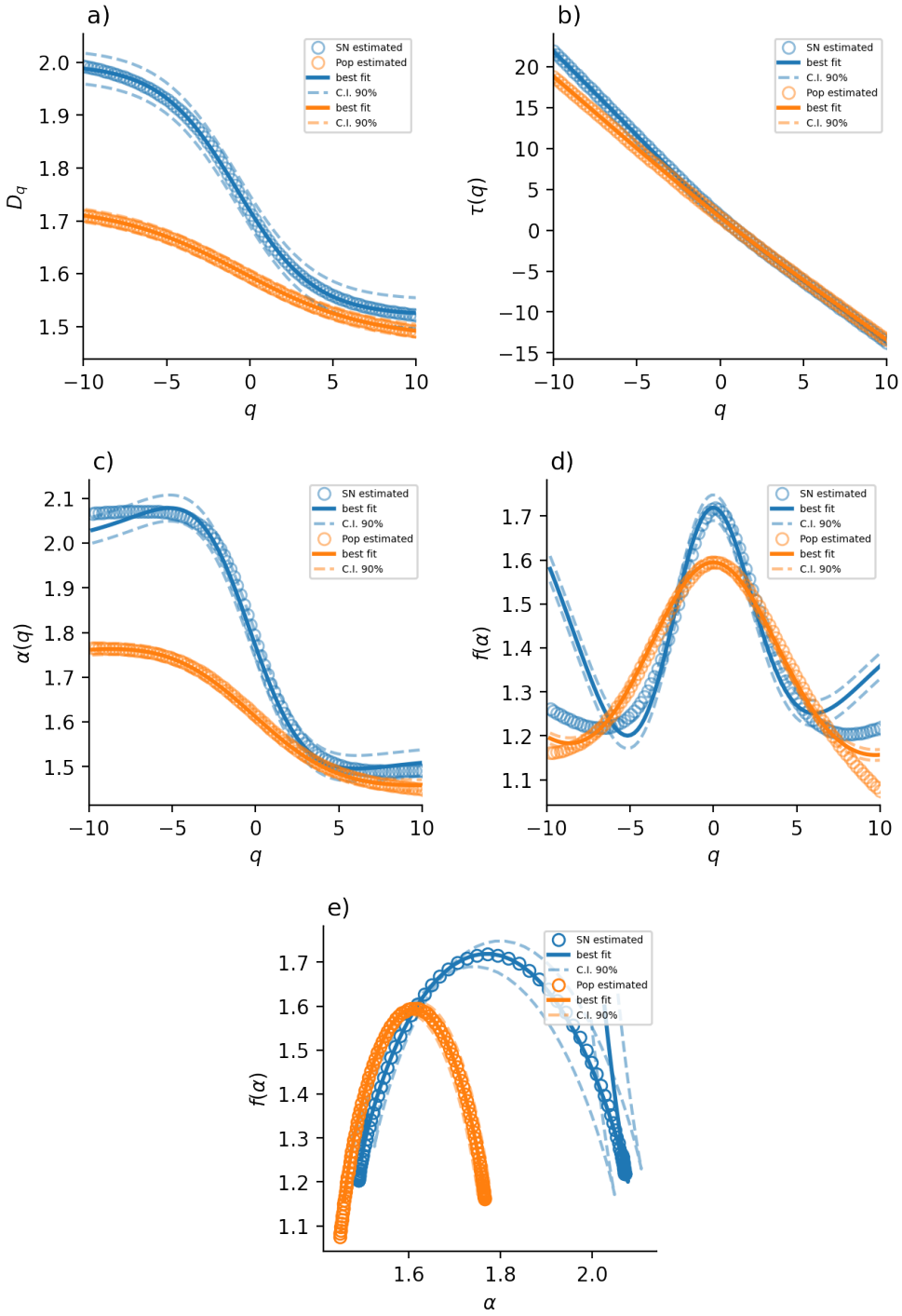

Source: Own authorship.

singularity spectrum only. The exponents of singularity, of the SN, and the spectrums depending on the moments of order, of the SN and of the Pop, deviate from the rule at the extremes, but are explained reasonably well in the most central parts.

But why does this deviate from the norm? A first insight into this is that in the denser regions, with no or almost no potholes, and in the more sparse ones, with the presence of potholes of various sizes, there is a preponderance and an absence of streets and people, respectively. In the case where these quantities are absent, the generalized dimension $D_{-\infty}$ can, in some cases, exceed spatial dimension 2, which means that the slope of the curve used to measure this dimension is quite steep, with a very small linear coefficient, see Figure 5.2. b).

The parameters of the multifractal modeling can be found in Table 5.1. The intention to obtain these parameters was based on the fact that, once these parameters are known, we can recover and predict the generalized dimensions considering a larger space in relation to the moments of order q. Also in Figure 5.1, the empty balls correspond to the estimated empirical values, the continuous lines correspond to the modeling, while the dashed lines correspond to the confidence interval 90%.

We can see in Figure 5.1 e) that the multifractal spectrum of SN exhibits abnormal behavior at the left and right ends, which has been captured and predicted by the model.

Figure 5.5 shows the multifractal SN and Pop spectra of the 15 largest Brazilian cities in 2010.

The capacity, information, correlation, minus and plus infinity dimensions of SN and Pop can be found in Tables 5.2 and 5.3, respectively. For the results of the fractal measurements of the 15 cities analyzed, access the `multifractal-analysis-br-renan.djvu` file via the link[2].

In relation to SN, the cities with the lowest and highest capacity dimension were Campinas with 1.319 and São Paulo with 1.712; those with the lowest and highest information dimension were Campinas with 1.311 and São Paulo with 1.663; those with the lowest and highest correlation dimension were Campinas with 1.303 and São Paulo with 1.624. In terms of the least infinite dimension, with the lowest and highest values, Camp-

[2] <https://www.dropbox.com/scl/fi/pevlue8vlp1tax519f1t2/FractalCity-code-and-graphs.zip?rlkey=nflraas61jrcjfr4yhtq941hm&dl=0>.

Figure 5.2 – Scaling regime for different moments of order. Scaling regimes for: a) the street network (SN) and b) the population (Pop) of the city of Brasilia. Note that in b) for $q = -10$ the line whose slope gives the generalized dimension $D_{q=-10}$ is quite steep in relation to the line whose generalized dimension is $D_{q=10}$, but the same is not true in a). The vertical circles of the same color correspond to the data obtained at different points in the fractal structure for the same radius R. The curve in black gives the average value between these points for the same value of R.

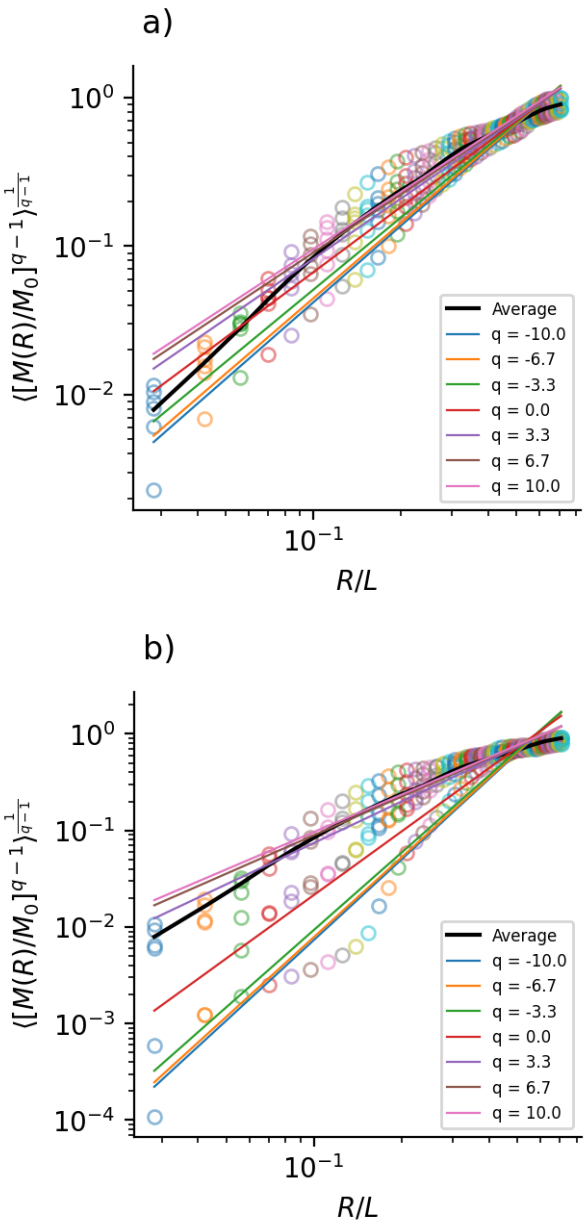

Source: Own authorship.

inas again had 1.392 and São Paulo 1.993, while in terms of the most infinite dimension, with the lowest and highest values, Campinas again had 1.266 and Fortaleza 1.583.

Figure 5.3 – Street network (SN) in the city of São Paulo, SP. In gray we have the geographical locations of the SN nodes and in yellow the locations of the points where measurements were taken.

Source: Own authorship.

On the other hand, in relation to Pop, the cities with the lowest and highest capacity dimensions were Porto Alegre with 1.377 and Brasília with 2.146; those with the lowest and highest information dimensions were Porto Alegre with 1.354 and Fortaleza with 1.739; those with the lowest and highest correlation dimensions were Guarulhos with 1.329 and Fortaleza with 1.705. Taking into account the limit dimensions, in particular the dimension of less infinity, the cities with the lowest and highest values were Salvador with 1.528 and Brasília with 2.772, while the cities with the lowest and highest values for the dimension of more infinity were Rio de Janeiro with 1.21 and Fortaleza with 1.629.

We can see that São Paulo in relation to SN is the city with the largest capacity dimension, while in relation to Pop, Brasília is the city with the highest value for this quantity.

Figure 5.4 – Sensitivity map of the city of São Paulo, SP. In yellow are the locations of the points where measurements were taken. Each sector has been colored according to the resident population (*Pop*) according to data from the 2010 IBGE census. The legend indicates the number of people living in each sector.

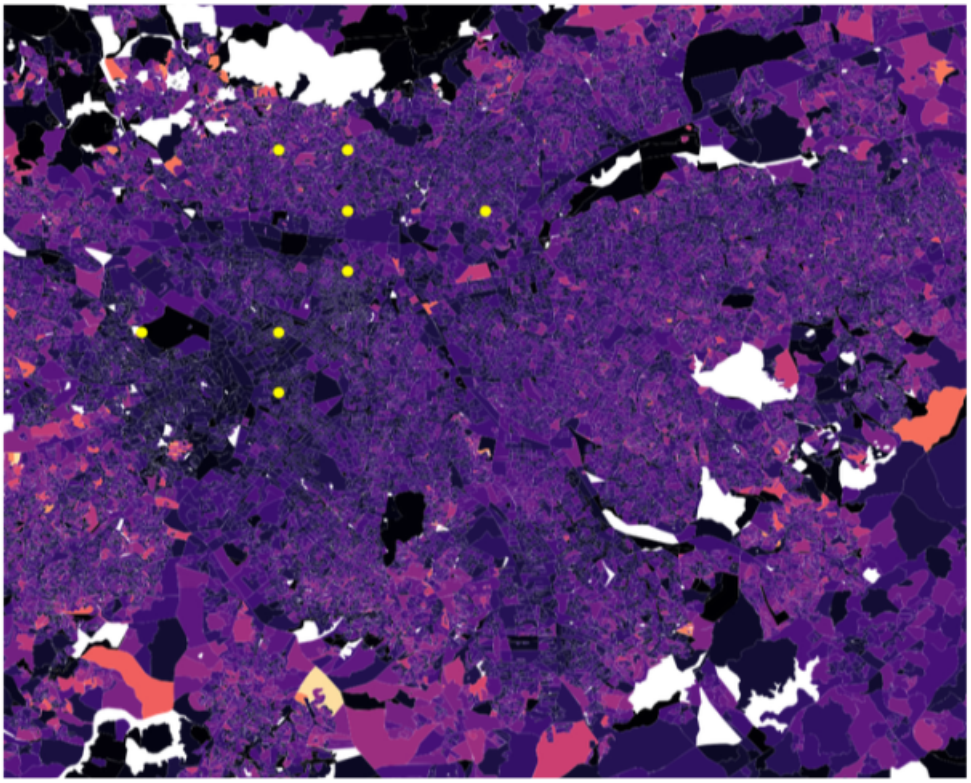

Source: Own authorship.

Figure 5.5 – Multifractal spectra of the largest Brazilian cities in 2010: a) street network (SN), b) population (Pop).

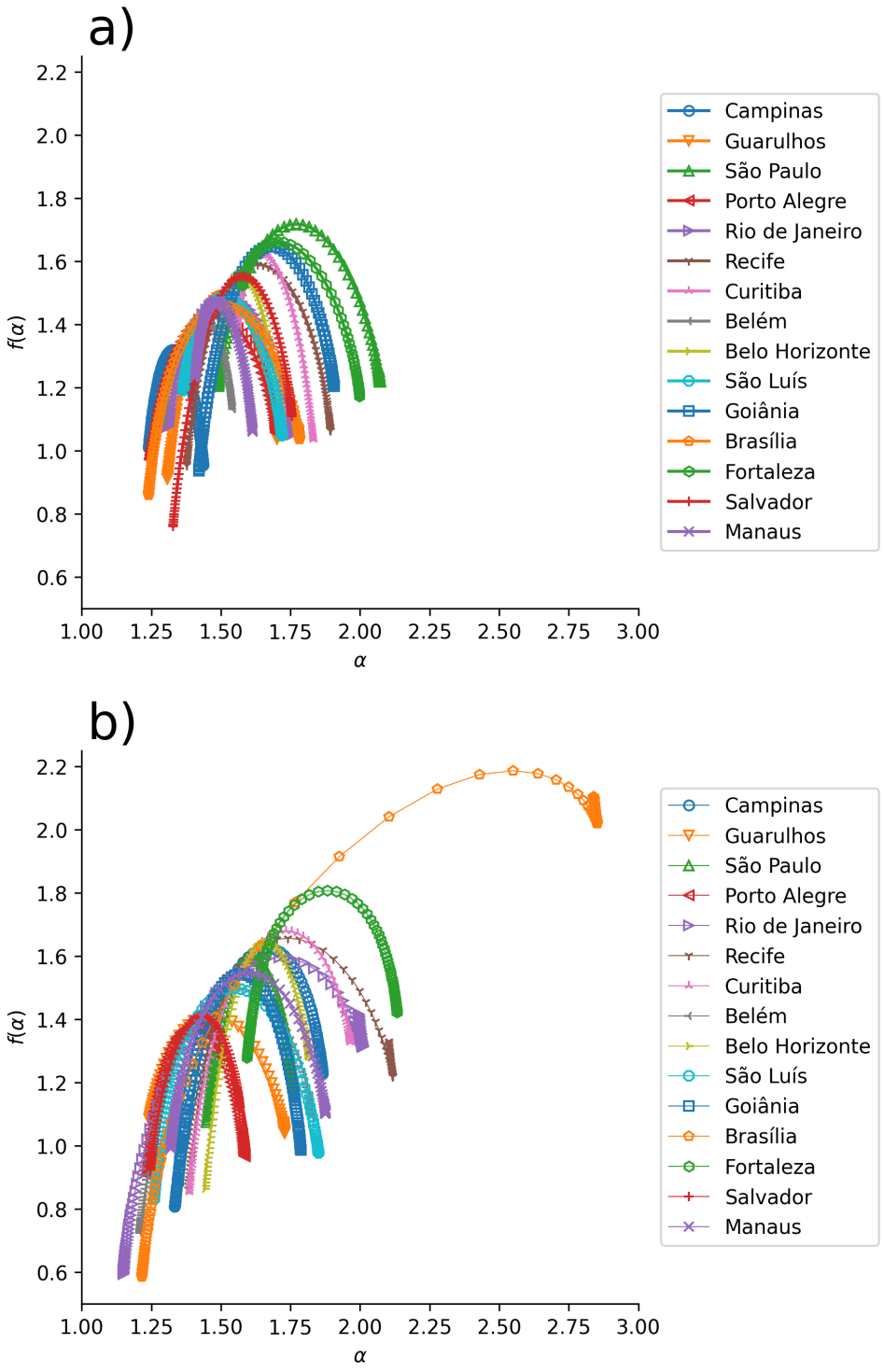

Source: Own authorship.

Table 5.1 – Parameters obtained from the multifractal model for the 15 largest Brazilian cities according to the 2010 census. With these parameters and with the help of the model equations it is possible to reproduce the generalized dimensions, the mass exponents, the singularity exponents, the singularity spectra depending on moments of order and multifractal spectrums of the population (Pop) and the street network (SN). In Appendix B we present the mathematical formulas for obtaining these parameters.

City	UF	Region	a (Pop)	a (SN)	b (Pop)	b (SN)	c (Pop)	c (SN)	d (Pop)	d (SN)
Campinas	SP	Sudeste	1.385	1.257	0.423	0.155	0.784	1.453	0.39	0.23
Guarulhos	SP	Sudeste	1.264	1.341	0.398	0.314	1.608	1.082	0.517	0.305
São Paulo	SP	Sudeste	1.477	1.521	0.253	0.476	1.137	1.395	0.263	0.437
Porto Alegre	RS	Sul	1.271	1.279	0.268	0.366	1.418	1.353	0.355	0.43
Rio de Janeiro	RJ	Sudeste	1.221	1.331	0.714	0.363	0.905	1.363	0.569	0.417
Recife	PE	Nordeste	1.456	1.427	0.572	0.398	1.705	1.371	0.558	0.395
Curitiba	PR	Sul	1.446	1.578	0.463	0.195	0.97	2.752	0.427	0.353
Belém	PA	Norte	1.265	1.306	0.499	0.204	1.09	0.898	0.436	0.337
Belo Horizonte	MG	Sudeste	1.486	1.51	0.3	0.175	0.881	2.403	0.253	0.275
São Luís	MA	Nordeste	1.311	1.383	0.464	0.281	1.439	1.686	0.428	0.393
Goiânia	GO	Centro-Oeste	1.391	1.47	0.333	0.383	1.175	1.143	0.333	0.354
Brasília	DF	Centro-Oeste	1.318	1.287	1.42	0.429	0.725	1.439	0.943	0.452
Fortaleza	CE	Nordeste	1.637	1.582	0.422	0.333	1.439	2.944	0.564	0.582
Salvador	BA	Nordeste	1.275	1.37	0.259	0.344	0.921	0.866	0.342	0.278
Manaus	AM	Norte	1.358	1.427	0.447	0.148	1.357	2.129	0.461	0.319

Source: Own authorship.

Table 5.2 – Generalized dimensions, standard error and R^2 of the street network (SN) for the 15 largest Brazilian cities according to the 2010 census.

City	D_0^{SN}	std	R^2	D_1^{SN}	std	R^2	D_2^{SN}	std	R^2	$D_{-\infty}^{SN}$	std	R^2	D_{∞}^{SN}	std	R^2
Campinas	1.319	0.088	0.949	1.311	0.088	0.949	1.303	0.089	0.948	1.392	0.089	0.954	1.266	0.094	0.939
Guarulhos	1.489	0.059	0.982	1.465	0.06	0.98	1.442	0.061	0.979	1.641	0.041	0.993	1.352	0.068	0.971
São Paulo	1.712	0.041	0.993	1.663	0.044	0.992	1.624	0.047	0.99	1.993	0.044	0.994	1.522	0.061	0.982
Porto Alegre	1.428	0.066	0.975	1.39	0.064	0.976	1.361	0.063	0.975	1.642	0.065	0.982	1.278	0.067	0.969
Rio de Janeiro	1.481	0.061	0.98	1.444	0.059	0.98	1.413	0.058	0.98	1.691	0.065	0.983	1.334	0.059	0.977
Recife	1.585	0.065	0.98	1.548	0.061	0.982	1.52	0.058	0.983	1.818	0.085	0.975	1.425	0.053	0.984
Curitiba	1.626	0.05	0.989	1.614	0.051	0.988	1.605	0.053	0.987	1.76	0.054	0.989	1.577	0.068	0.978
Belém	1.413	0.068	0.973	1.395	0.071	0.97	1.378	0.074	0.967	1.506	0.051	0.987	1.315	0.075	0.963
Belo Horizonte	1.56	0.053	0.986	1.551	0.054	0.986	1.544	0.056	0.985	1.662	0.05	0.989	1.514	0.064	0.979
São Luís	1.484	0.04	0.991	1.459	0.044	0.989	1.439	0.048	0.987	1.658	0.047	0.991	1.384	0.069	0.972
Goiânia	1.643	0.045	0.991	1.609	0.047	0.99	1.581	0.048	0.989	1.842	0.06	0.988	1.475	0.055	0.984
Brasília	1.454	0.059	0.981	1.409	0.058	0.98	1.375	0.059	0.978	1.714	0.064	0.984	1.283	0.076	0.96
Fortaleza	1.658	0.044	0.992	1.626	0.039	0.993	1.609	0.037	0.994	1.923	0.082	0.979	1.583	0.047	0.99
Salvador	1.55	0.077	0.972	1.526	0.077	0.971	1.503	0.077	0.97	1.697	0.081	0.974	1.391	0.075	0.967
Manaus	1.472	0.076	0.969	1.462	0.075	0.97	1.455	0.074	0.97	1.564	0.088	0.964	1.427	0.076	0.968

Source: Own authorship.

Table 5.3 – Generalized dimensions, standard error and R^2 of the population for the 15 largest Brazilian cities according to the 2010 census.

City	D_0^{Pop}	std	R^2	D_1^{Pop}	std	R^2	D_2^{Pop}	std	R^2	$D_{-\infty}^{Pop}$	std	R^2	D_{∞}^{Pop}	std	R^2
Campinas	1.621	0.059	0.984	1.576	0.063	0.981	1.534	0.07	0.976	1.807	0.064	0.985	1.393	0.099	0.944
Guarulhos	1.409	0.063	0.977	1.363	0.062	0.976	1.329	0.063	0.974	1.666	0.059	0.986	1.262	0.071	0.964
São Paulo	1.593	0.057	0.985	1.576	0.057	0.985	1.561	0.056	0.985	1.71	0.054	0.988	1.491	0.054	0.985
Porto Alegre	1.377	0.094	0.947	1.354	0.091	0.949	1.336	0.089	0.949	1.53	0.109	0.943	1.272	0.087	0.947
Rio de Janeiro	1.583	0.043	0.991	1.474	0.046	0.989	1.392	0.055	0.982	1.942	0.097	0.971	1.21	0.087	0.942
Recife	1.648	0.058	0.985	1.582	0.054	0.986	1.543	0.054	0.986	2.033	0.08	0.982	1.441	0.064	0.977
Curitiba	1.675	0.051	0.989	1.623	0.055	0.987	1.578	0.058	0.984	1.907	0.048	0.993	1.446	0.072	0.972
Belém	1.494	0.08	0.967	1.438	0.076	0.968	1.395	0.075	0.967	1.761	0.1	0.963	1.263	0.093	0.94
Belo Horizonte	1.641	0.044	0.992	1.622	0.045	0.991	1.605	0.047	0.99	1.764	0.045	0.992	1.508	0.062	0.98
São Luís	1.493	0.082	0.965	1.446	0.082	0.963	1.41	0.083	0.961	1.771	0.081	0.976	1.308	0.092	0.945
Goiânia	1.541	0.09	0.961	1.512	0.086	0.963	1.487	0.083	0.964	1.714	0.104	0.958	1.397	0.077	0.965
Brasília	2.146	0.133	0.957	1.734	0.09	0.969	1.524	0.079	0.969	2.772	0.171	0.957	1.286	0.097	0.937
Fortaleza	1.799	0.062	0.986	1.739	0.049	0.991	1.705	0.046	0.991	2.068	0.109	0.968	1.629	0.06	0.984
Salvador	1.407	0.059	0.98	1.384	0.066	0.974	1.363	0.071	0.969	1.528	0.036	0.993	1.283	0.085	0.951
Manaus	1.541	0.062	0.981	1.491	0.063	0.979	1.451	0.064	0.977	1.806	0.055	0.989	1.356	0.083	0.958

Source: Own authorship.

5.2 Urban Spatial Rates

In this section we present the results of the space-filling u, redundancy v and correlation w spatial rates of the 15 largest Brazilian cities according to the 2010 census. We also built dendograms (Hierarchical clustering) to find out which cities were most and least similar to each other in terms of this spatial rates. Our results show that São Paulo and Brasília are the most spatially complete cities in terms of street network (SN) and population (Pop), respectively.

We can see from Table 5.4 that the average values for the u rate, for the SN and the Pop, were around 0.76 ± 0.05 and 0.80 ± 0.09, respectively, revealing quite slightly different values. We can attribute this slight difference to the outlier represented by the city of Brasília.

With regard to the v rate, for the SN and the Pop, the average values were 0.25 ± 0.05 and 0.24 ± 0.06, revealing even closer values.

On the other hand, with regard to the w rate, for the SN and the Pop, the average values were 0.26 ± 0.05 and 0.26 ± 0.06, respectively, revealing identical values. Then, we can see that on average the SN fills the space slightly less than the Pop, because of the presence of an outlier represented by the Pop of Brasília.

Furthermore, we can see that the SN and Pop are quite similar at the various spatial scales and that on average the degree of correlation between them is the same.

In relation to SN and Pop, the cities with the highest u were São Paulo and Brasília, with values equal to 0.856 and 1.073, respectively. The cities with the highest v were Campinas and Porto Alegre with values of 0.344 and 0.323. Those with the highest correlation rate w were Campinas and Guarulhos with values of 0.348 and 0.335.

On the other hand, those with the lowest u were Campinas and Porto Alegre with values of 0.659 and 0.688, respectively. Those with the lowest v were São Paulo and Fortaleza with values of 0.168 and 0.131. Finally, those with the lowest w were São Paulo and Fortaleza with values of 0.188 and 0.147.

Furthermore, we can see that in relation to the spatial completion rate of the u^{SN} , Figure 5.6 a), the most similar cities were São Luís and Rio de Janeiro. We can also see that Salvador, Belo Horizonte, Recife, Fortaleza, Goiânia, Curitiba and São Paulo belong to the same cluster, while São Luís, Rio de Janeiro, Guarulhos, Manaus, Brasília, Belém

Table 5.4 – Space-filling u, spatial redundancy v and spatial correlation w rates of the street network (SN) and population (Pop) for the 15 largest Brazilian cities according to the 2010 census.

City	UF	u^{SN}	v^{SN}	w^{SN}	u^{Pop}	v^{Pop}	w^{Pop}
Campinas	SP	0.659	0.345	0.349	0.81	0.212	0.233
Guarulhos	SP	0.745	0.268	0.279	0.705	0.319	0.335
São Paulo	SP	0.856	0.168	0.188	0.797	0.212	0.22
Porto Alegre	RS	0.714	0.305	0.32	0.688	0.323	0.332
Rio de Janeiro	RJ	0.74	0.278	0.293	0.792	0.263	0.304
Recife	PE	0.793	0.226	0.24	0.824	0.209	0.228
Curitiba	PR	0.813	0.193	0.197	0.838	0.189	0.211
Belém	PA	0.707	0.302	0.311	0.747	0.281	0.303
Belo Horizonte	MG	0.78	0.224	0.228	0.821	0.189	0.198
São Luís	MA	0.742	0.27	0.28	0.746	0.277	0.295
Goiânia	GO	0.821	0.195	0.21	0.771	0.244	0.256
Brasília	DF	0.727	0.296	0.313	1.073	0.133	0.238
Fortaleza	CE	0.829	0.187	0.196	0.9	0.131	0.147
Salvador	BA	0.775	0.237	0.248	0.704	0.308	0.318
Manaus	AM	0.736	0.269	0.273	0.771	0.255	0.274

Source: Own authorship.

and Porto Alegre belong to another cluster and Campinas was the most dissimilar of all the cities analyzed.

In relation to the spatial redundancy rate of the v^{SN}, Figure 5.6 c), the most similar cities were Manaus and Guarulhos. We can also see that Goiânia, Curitiba, Fortaleza and São Paulo belong to the same cluster and that Campinas was also the most dissimilar of all the cities analyzed.

As for the spatial correlation rate of the w^{SN} , Figure 5.6 d), the most similar cities were Fortaleza and Curitiba, São Luís and Guarulhos, as well as Brasília and Belém. It was also possible to see that Fortaleza, Curitiba, São Paulo, Goiânia, Salvador, Recife and Belo Horizonte belong to the same cluster and that Campinas, once again, was the most dissimilar of all the cities analyzed.

On the other hand, in relation to the space-filling rate u^{Pop} , Figure 5.6 b), the most similar cities were São Luís and Belém, as well as Salvador and Guarulhos. We can also see that all the cities except Brasilia belong to the same cluster, with Fortaleza being the most dissimilar city in this cluster.

Regarding the spatial redundancy rate v^{Pop}, Figure 5.6 d), the most similar cities were Belo Horizonte and Curitiba, as well as São Paulo and Campinas. We can also see

Figure 5.6 – Hierarchical clustering of the 15 largest Brazillian cities in 2010 in terms of space-filling u, spatial redundancy v and spatial correlation w rates of the street network (SN) a), c) and e) and population (Pop) b), d) and f).

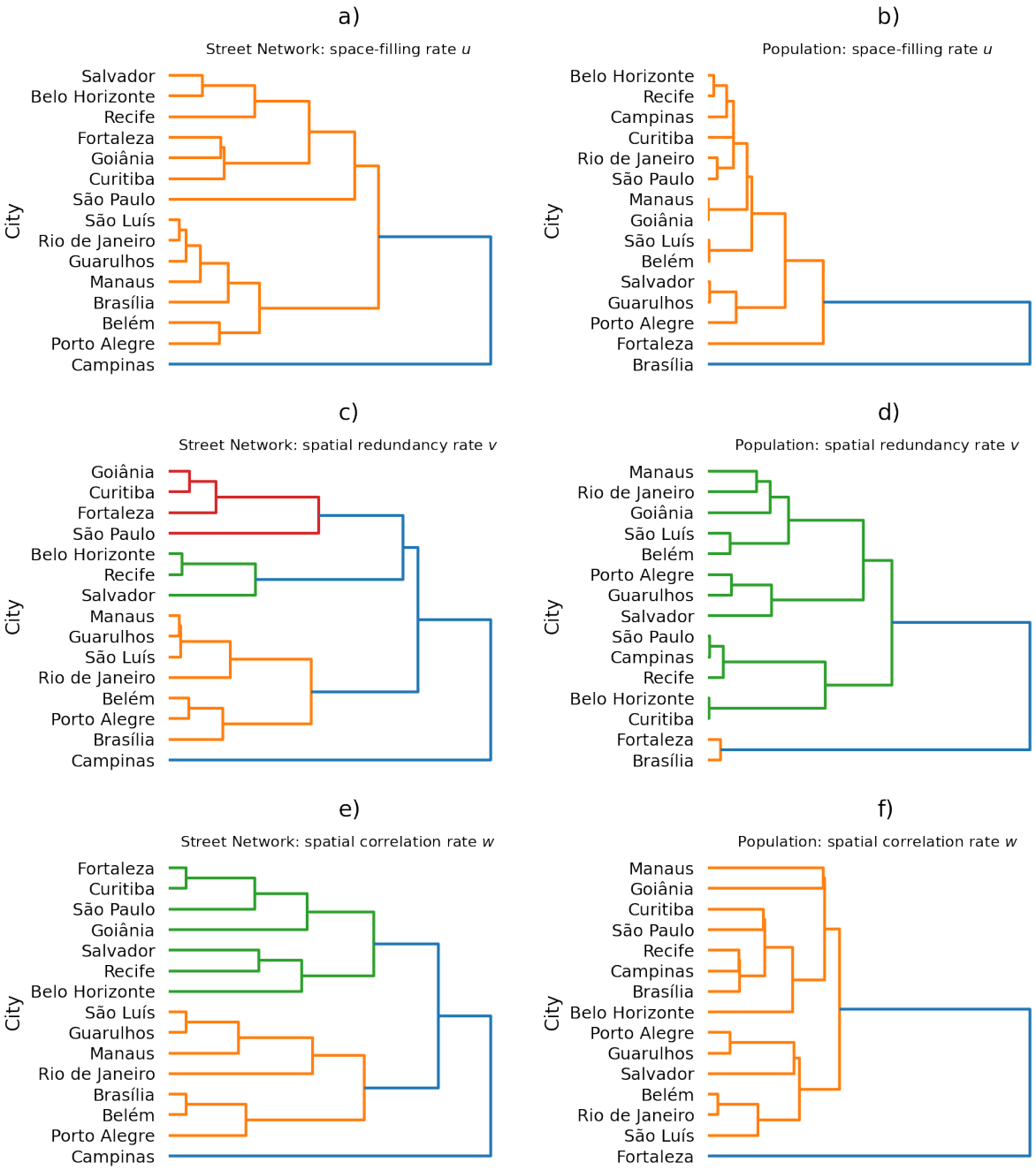

Source: Own authorship.

that all the cities except Brasilia and Fortaleza belong to the same cluster, with Fortaleza and Brasilia being similar to each other.

Finally, in relation to the spatial correlation rate w^{Pop}, Figure 5.6 f), the most similar cities were Belém and Rio de Janeiro. Furthermore, all the cities except Fortaleza

belong to the same cluster, with Fortaleza being the most dissimilar among the other cities.

5.3 Skewness and Aggregation-Diffusion Analysis

In this Section process of diffusion and aggregation taking place in these cities, respectively. In particular, São Paulo's street network (SN) diffusion process exhibits small scale fluctuations and its peripheral regions are denser and larger than the central parts, which are more sparse and relatively smaller. The population (Pop) aggregation process in Brasilia, on the other hand, exhibits large fluctuations in scale, with the peripheral regions being less dense and smaller than the central parts, which are denser and larger.

The calculation of the skewness index χ, eq. (2.1.30), and aggregation-diffusion index ξ, eq. (2.1.31), of the singularity spectra for the 15 largest Brazilian cities can be visualized in Figure 5.7. Examples of right-skewed asymmetry are stock market index, foreign exchange market (forex or FX), variability in sentence length in texts, Missouri River Discharge (DROZDZ; OSWIECIMKA, 2015); and examples of left-skewed asymmetry are: times between transactions, variability in the number of sunspots (DROZDZ; OSWIECIMKA, 2015).

In Figure 5.7 a) the blue and green bars correspond to the spectra of the SN and the Pop with left-skewed ($\chi < 1$) and right-skewed ($\chi > 1$), respectively. Also in the same figure, in b), red and orange bars correspond to the spectra of the SN and Pop with spatial diffusion ($\xi < 1$) and aggregation ($\xi > 1$), respectively. Values of $\chi = \xi \approx 1$ correspond to perfectly symmetrical spectra. The measurements obtained for each city can be viewed in Table 5.5.

With regard to the χ index, for SN and Pop, the average values were 1.29 ± 0.53 and 0.82 ± 0.25, which are surprising in their uncertainty.

On the other hand, with regard to the ξ aggregation-diffusion index, for SN and Pop, the average values were 0.88 ± 0.3 and 1.44 ± 0.88, also revealing quite large values in the deviations.

In relation to SN and Pop, the cities with the highest χ were Fortaleza with 2.289 and Guarulhos with 1.161, and the cities with the highest ξ were Salvador with 1.399 and Brasília with 4.417, respectively.

Figure 5.7 – Skewness χ and aggregation-diffusion ξ spectrum of the street network (SN) and population (Pop) of the 15 largest Brazilian cities. a) Skewness of the SN, left, and the Pop, right. b) Aggregation-diffusion of the SN (left) and the Pop (right).

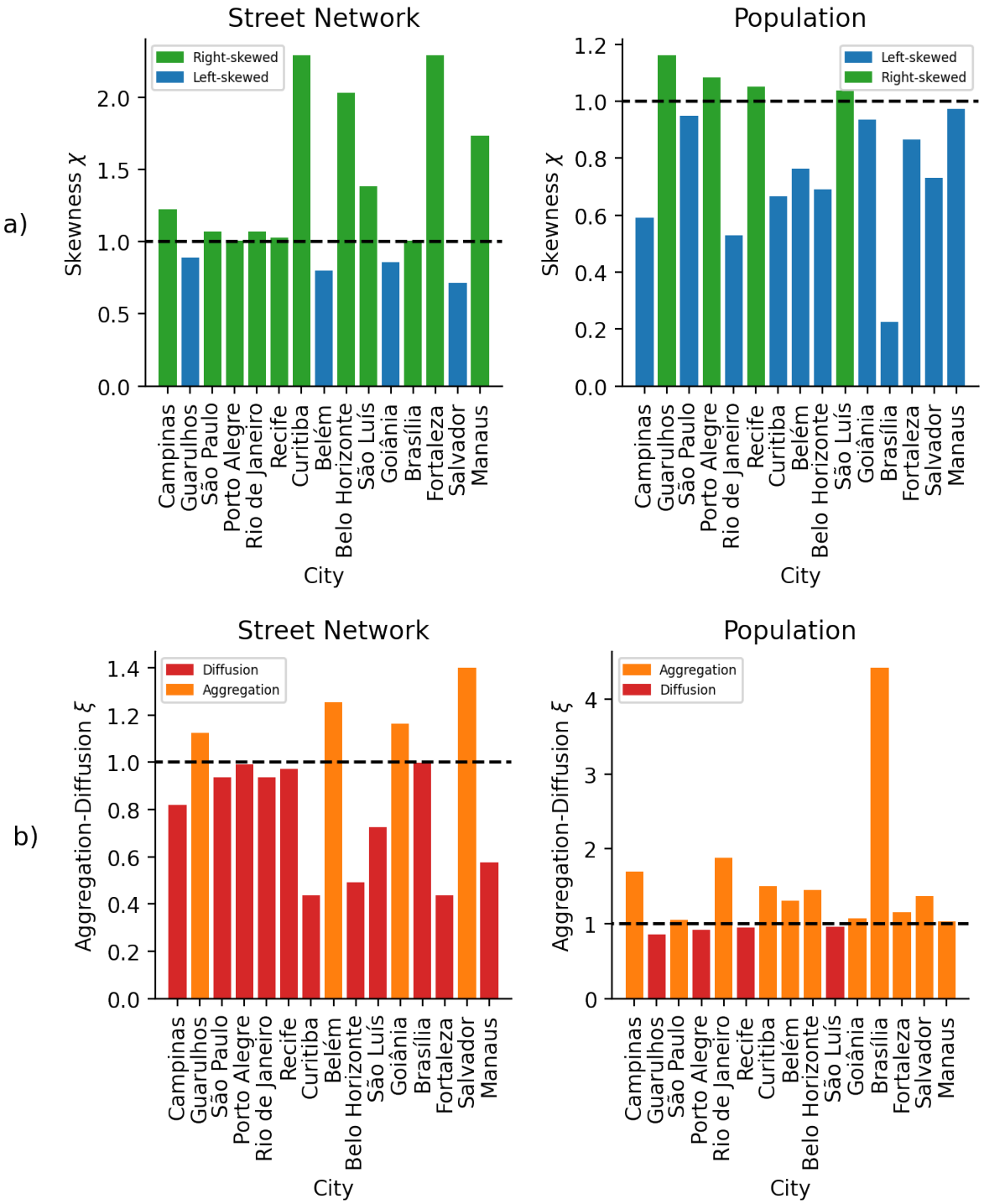

Source: Own authorship.

On the other hand, in relation to SN and Pop, those with the lowest χ were Salvador with 0.715 and Brasília with 0.226, respectively. Those with the lowest ξ were Fortaleza and Curitiba with 0.437 and Guarulhos with 0.862.

Table 5.5 – Skewness χ and spatial aggregation-diffusion process ξ of the street network (SN) and the population (Pop) singularity spectra for the 15 largest Brazilian cities according to the 2010 census.

City	UF	χ^{SN}	χ^{Pop}	ξ^{SN}	ξ^{Pop}
Campinas	SP	1.222	0.591	0.818	1.693
Guarulhos	SP	0.890	1.161	1.124	0.862
São Paulo	SP	1.070	0.948	0.935	1.055
Porto Alegre	RS	1.007	1.084	0.993	0.923
Rio de Janeiro	RJ	1.068	0.530	0.937	1.885
Recife	PE	1.029	1.051	0.972	0.951
Curitiba	PR	2.288	0.665	0.437	1.504
Belém	PA	0.797	0.762	1.254	1.312
Belo Horizonte	MG	2.031	0.689	0.492	1.451
São Luís	MA	1.380	1.038	0.724	0.963
Goiânia	GO	0.860	0.936	1.163	1.069
Brasília	DF	1.004	0.226	0.996	4.417
Fortaleza	CE	2.289	0.866	0.437	1.154
Salvador	BA	0.715	0.731	1.399	1.368
Manaus	AM	1.732	0.973	0.578	1.028

Source: Own authorship.

However, we believe that one of the probable causes of Braslia having a very high value for $\xi^{Pop} = 4.417$ compared to the other cities is the presence of potholes in the census tracts. These holes are due to the absence of sectors (Brasilia National Park and areas of dense forest around the city) , the presence of continental waters (Lake Paranoá) that are stored in depressions surrounded by land and urban planning or its absence, see spatial distribution of Brasilia's Pop in Appendix D and Brasília's map[3]. This means that from a physical point of view, the presence of lakes, rivers, forests, rock formations, and urban planning found within cities can be seen as the agents influencing the aggregation process that takes place in SN or Pop. In the same way that two massive bodies attract each other in the presence of a gravitational field, people and streets can become more concentrated in the presence of lakes, rivers, forests, parks, rock formations, and external forces such as employment opportunities, access to services and education, economic growth, accessibility in terms of infrastructure, cultural diversity, demand for innovation and investment, and networking, tourism and leisure, all of which contribute to increasing local interaction processes.

[3] <https://maps.app.goo.gl/HmNXZsLgbJCsh1rC7>.

In addition, we can see that in relation to SN, 4 cities showed spectra with left-skewed $\chi < 1$, that is, the system's scaling is dominated by large fluctuations and aggregation $\xi > 1$, while 11 cities showed spectra with right-skewed $\chi > 1$, i.e. the system's scaling is dominated by small fluctuations, and diffusion $\xi > 1$.

On the other hand, with regard to Pop, 11 cities showed spectra with left-skewed $\chi < 1$ and aggregation $\xi > 1$, while 4 cities showed spectra with right-skewed $\chi > 1$ and diffusion $\xi > 1$.

5.4 Intra-city Models

The aim of this section is to try to extend some of the intra-city models, which take into account the notion of fractal dimension, by considering, even if *ad hoc*, some of the generalized dimensions D_0, D_1, D_2, $D_{-\infty}$ and D_{∞} of the street network (SN) and the population (Pop) instead of the fractal dimensions previously considered in the construction of the models.

Nest, we present the results of the intra-city models, and should be noted that the only models that allowed us to conduct an analysis in relation to the explanation of the sub-linear and super-linear scale exponents were the Bettencourt model, eq. (2.2.14), and the M&T macroscopic model, eq. (2.2.18). In the Betterncourt model, the fractal dimensions used were those of SN and those of Pop, although the construction of the model takes into account the fractal dimension of the urban area A. In both models, our intention from the outset was to try to explain the total length of the streets, L, and the Gross Domestic Product (GDP), Y, the infrastructure and socioeconomic variables, respectively, in terms of endogenous properties of cities, a different approach to that of M&T, who consider the asymptotic and transversal limit of the sublinear exponent given by the ratio between the fractal dimensions of SN and Pop to explain laws of urban scale (MOLINERO; THURNER, 2021).

In Figure 5.8 a) and b) we show L and Y in terms of N for the 15 largest Brazilian cities in 2010 using the generalized dimension of SN. In Figure 5.9 a) and b) we show L and Y in terms of N using the generalized dimension of Pop. This figure shows an attempt to extend Bettencourt's model (2.2.14), but with caveats.

In this sense, we considered the endogenous properties of each city, namely N and D_i^a with $a = \{SN, Pop\}$ and $i = \{0, 1, 2, -\infty, \infty\}$, obtained the predictions for

Figure 5.8 – Bettencourt model for generalized dimension of street network (SN) D_i^{SN} for $i = (0, 1, 2, \infty, -\infty)$. a) Sub-linear scaling between total street length L and city size N with D_i^{SN}. b) Super-linear scaling between gross domestic product (GPD) Y and city size N with D_i^{SN}. The blue circles are the empirical data and the lines are the predictions of the model.

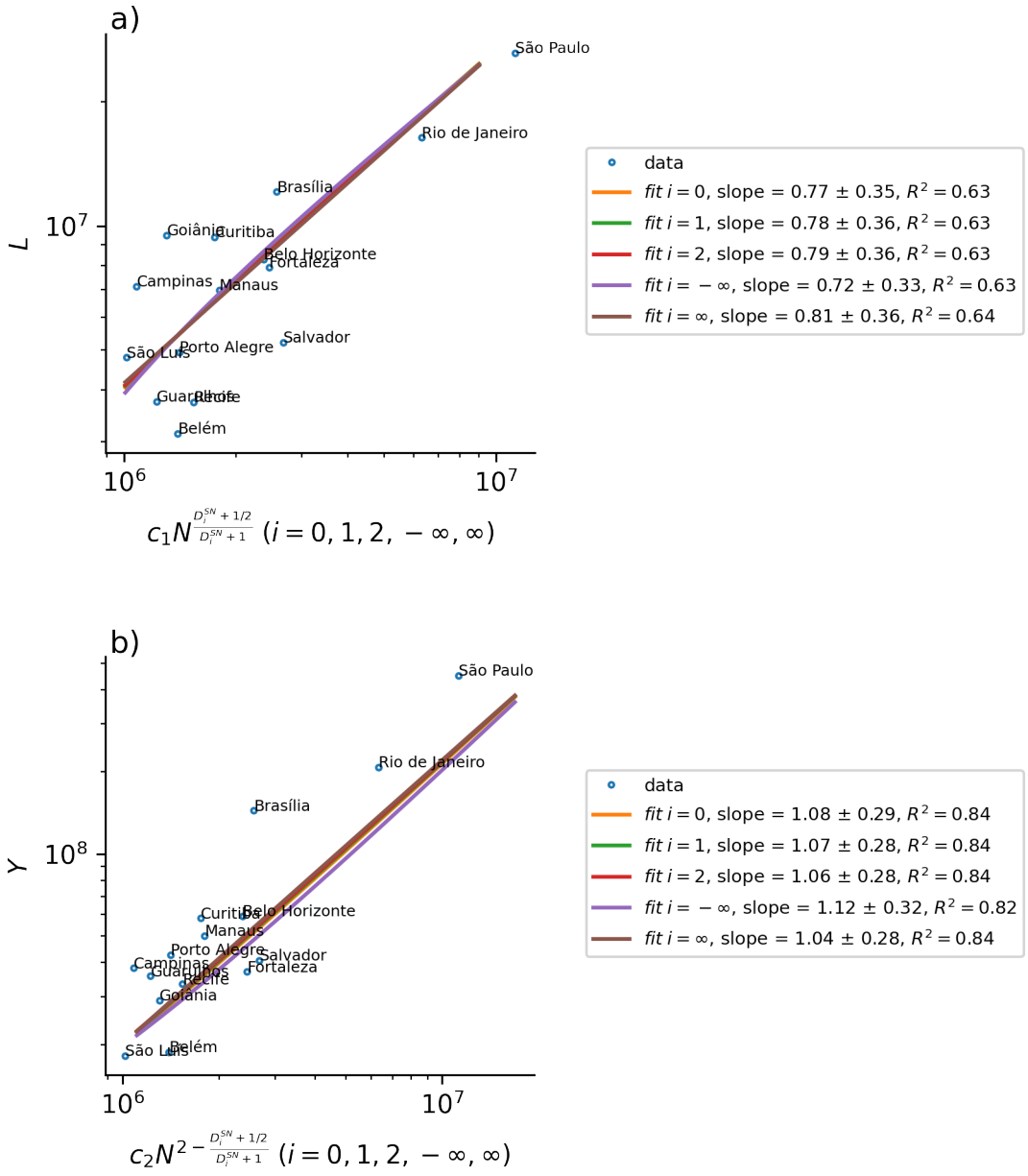

Source: Own authorship.

the empirical variables under study L and Y and made log-log scale graphs considering their respective theoretical predictions, eq. (2.2.14) and considering the multiplicative constants c_1 and c_2. The values found are shown in Table 5.6.

Figure 5.9 – Bettencourt model for generalized dimension of population (Pop) D_i^{Pop} for $i = (0, 1, 2, \infty, -\infty)$. a) Sub-linear scaling between total street length L and city size N with D_i^{Pop}. b) Super-linear scaling between gross domestic product (GPD) Y and city size N with D_i^{Pop}. The blue circles are the empirical data and the lines are the predictions of the model.

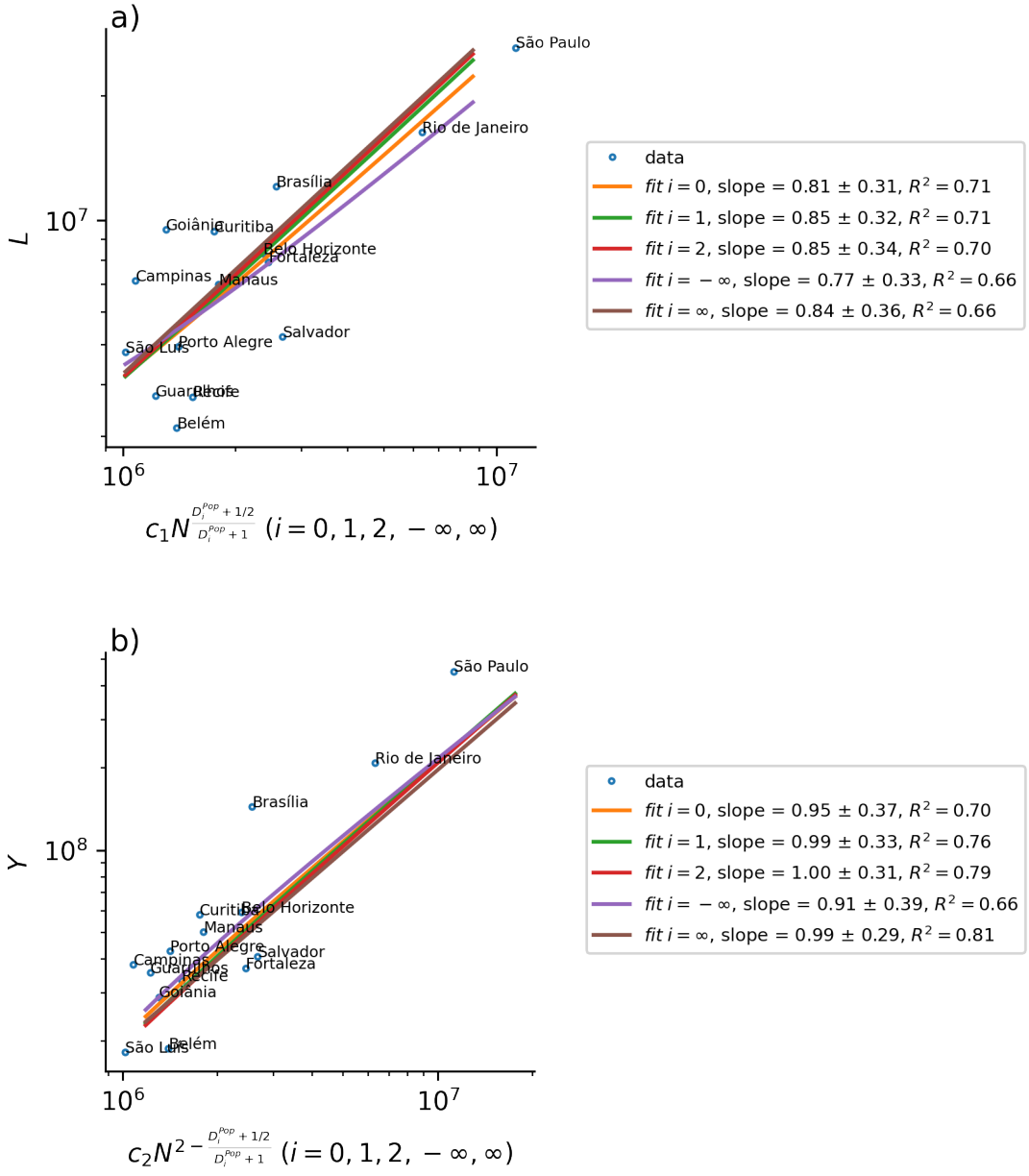

Source: Own authorship.

In particular, considering $a = SN$ and $i = \{0, 1, 2, -\infty, \infty\}$, the exponents of the best linear regressions of the L data against N had an average slope of 0.77 ± 0.03, while

Table 5.6 – Bettencourt linear regression summary for the street network (SN) and population (Pop). i represents the moment of order q of the generalized dimension D_q.

		SN			Pop		
Variable	i	slope	std	R^2	slope	std	R^2
L with $c_1 = 20$	0	0.77	0.35	0.63	0.81	0.31	0.71
	1	0.78	0.36	0.63	0.85	0.32	0.71
	2	0.79	0.36	0.63	0.85	0.34	0.70
	$-\infty$	0.72	0.33	0.63	0.77	0.33	0.66
	∞	0.81	0.36	0.64	0.84	0.36	0.66
Y with $c_2 = 0.06$	0	1.08	0.29	0.84	0.95	0.37	0.70
	1	1.07	0.28	0.84	0.99	0.33	0.76
	2	1.06	0.28	0.84	1.00	0.31	0.79
	$-\infty$	1.12	0.32	0.82	0.91	0.39	0.66
	∞	1.04	0.28	0.84	0.99	0.29	0.81

Source: Own authorship.

the exponents of the best linear regressions of the Y data against N had an average slope of 1.07 ± 0.03.

On the other hand, considering $a = Pop$ and $i = \{0, 1, 2, -\infty, \infty\}$, the exponents of the best linear regressions of the L data against N had an average slope of 0.82 ± 0.03, while the exponents of the best linear regressions of the Y data against N had an average slope of 0.97 ± 0.03. Note that this value was higher than the 0.77 ± 0.03 obtained when we considered $a = SN$.

However, considering the dimensions of $a = \{SN, Pop\}$ for each i, the slopes of the individual linear regressions varied little from each other, but showed very significant standard deviations in the first decimal place, compromising the estimates. We can attribute these significant deviations in the individual estimate to the size of the sample. This means that, in order to obtain a more conclusive result and to know whether the present approach can explain the infrastructure and socioeconomic variables only from endogenous factors, considering a longitudinal point of view, it is necessary to obtain the generalized dimensions i for all cities and repeat the analysis. Furthermore, we can see that on average the generalized dimensions considered with $a = \{SN, Pop\}$ are able to explain Y and L, the latter with some caveats.

On the other hand, in relation to the macroscopic model of M&T, eq. (2.2.18), in which L, N and A were taken into account to obtain the expression of both sub- and superlinear exponents, the slopes obtained, graphing only the 15 largest Brazilian cities in

Figure 5.10 – Macroscopic M&T model with fractal dimensions obtained by the eqs. (2.2.16) and (2.2.17). a) Sub-linear scaling between total street network (SN) L and city size N for 15 greater Brazilian cities, with $c_1 = 0.6$. b) Super-linear scaling between Gross Domestic Product Y and city size N for 15 greater Brazilian cities, with $c_2 = 2.1$. The blue circles are the empirical data and the line is the prediction of the model.

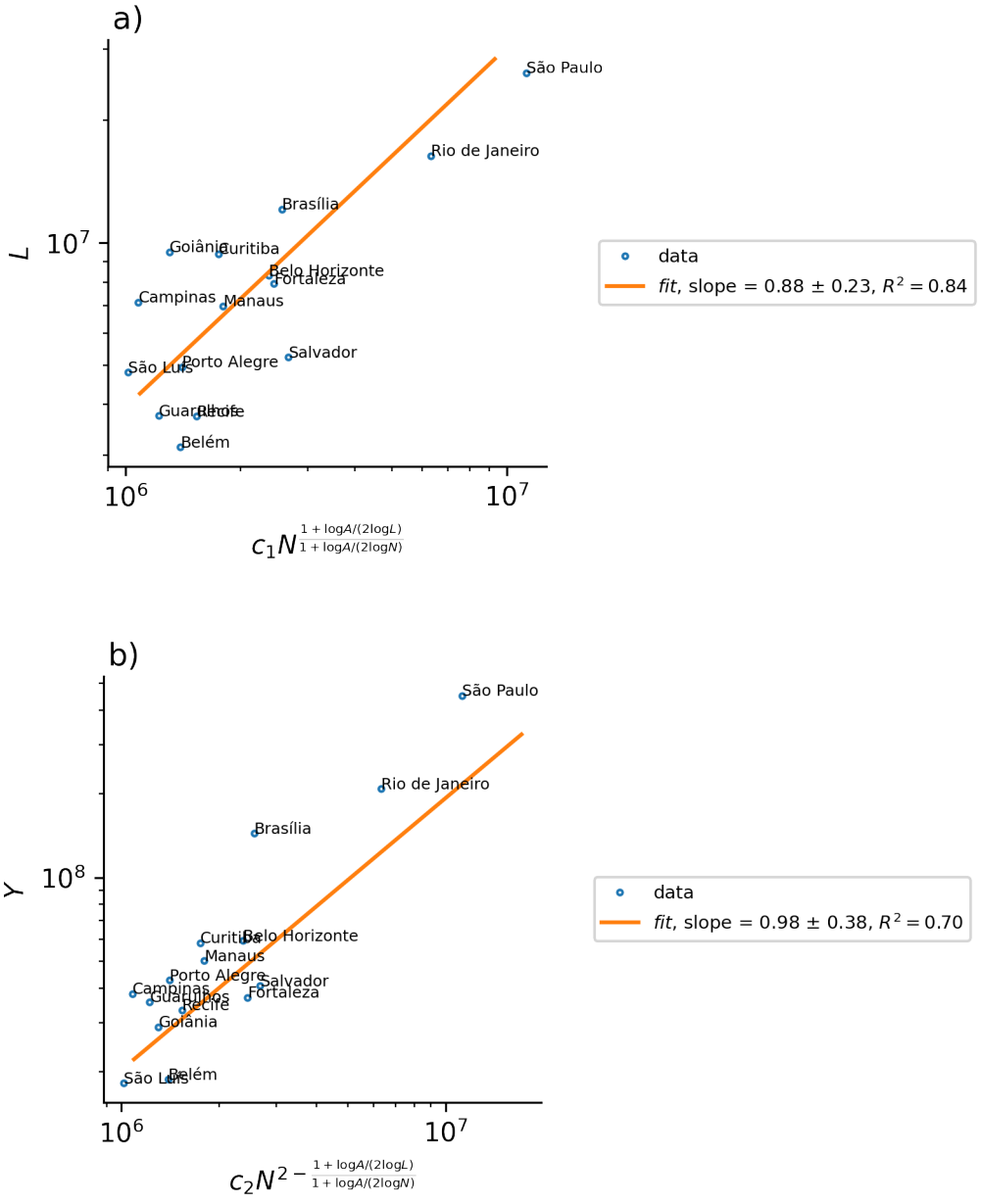

Source: Own authorship.

2010, were significantly better than in the previous analysis using the Bettencourt model and with generalized fractal dimensions; see Figure 5.10. For L against N, the exponent

Figure 5.11 – Macroscopic M&T model with fractal dimensions obtained by the eqs. (2.2.16) and (2.2.17). a) Sub-linear scaling between total street network (SN) L and city size N for 5523 Brazilian cities, with $c_1 = 0.5$. b) Super-linear scaling between Gross Domestic Product Y and city size N for 5523 Brazilian cities, with $c_2 = 2$. The blue circles are the empirical data and the line is the prediction of the model.

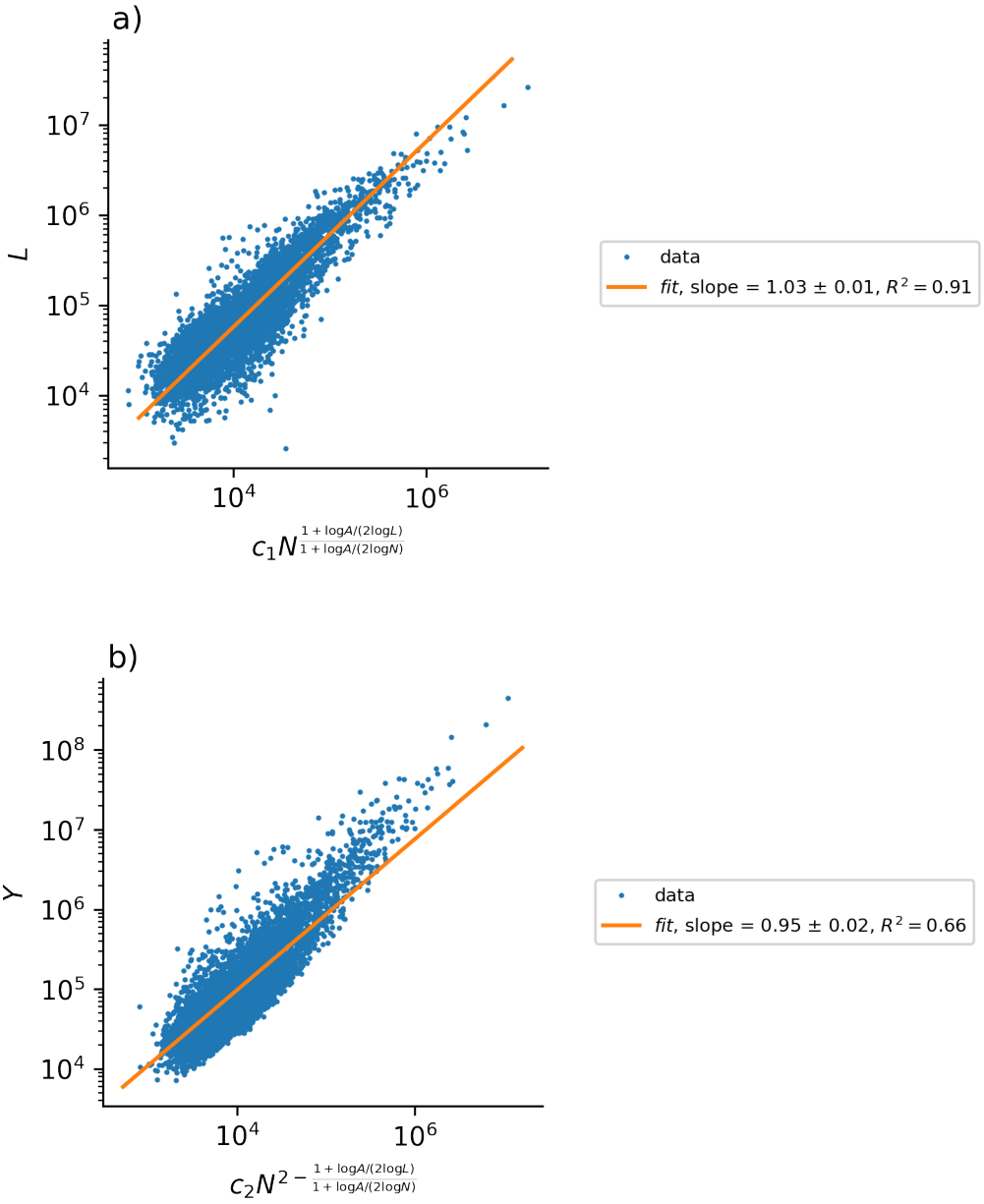

Source: Own authorship.

was 0.88 ± 0.23 with $R^2 = 0.84$, while for Y against N the exponent was 0.98 ± 0.38 with $R^2 = 0.79$.

Taking into account the 5523 cities available, for L against N the exponent was 1.03 ± 0.01 with $R^2 = 0.91$, while for Y against N the exponent was 0.95 ± 0.02 with $R^2 = 0.66$, see Figure 5.11. These results are also presented in Table 5.6 for a better comparison.

Table 5.7 – Macroscopic M&T linear regression summary for the 15 main and 5523 Brazillian cities.

# Cities	Variable	slope	std	R^2
15	L with $c_1 = 0.6$	0.88	0.23	0.84
	Y with $c_2 = 2.1$	0.98	0.38	0.79
5523	L with $c_1 = 0.5$	1.03	0.01	0.91
	Y with $c_2 = 2$	0.95	0.02	0.66

Source: Own authorship.

We stress that the difference between the latter approach and that of M&T in (MOLINERO; THURNER, 2021), is that we used macroscopic city variables such as L, N and A, while in the study presented, they obtained D_i and D_p from percolation methods, which we believe have a huge computational cost to obtain these quantities. In this sense, if the strategy presented previously, using macroscopic variables, can be verified with data from cities in other countries, we emphasize that this is simpler and faster in confirming that laws of urban scale can be explained in terms of the geometric properties of cities.

Using an approach similar to that of M&T (MOLINERO; THURNER, 2021), who calculated the fractal dimensions of SN and Pop of some European cities and the asymptotic sublinear exponent γ_{sub} equal to $a \approx 0.86$, from the model $\gamma(N) \approx a - \frac{b}{(\log N)^c}$ where N is the city Pop, see Figure 5.12, we obtain $a \approx 0.95$ for the asymptotic value, see Table 5.8.

We can see in this graph that there are two behaviors for the value of γ_{sub}. We see that below $N \approx 10,000$ inhabitants, γ_{sub} grows linearly with N, but above this value the exponent grows non-linearly converging to an asymptotic value corresponding to γ'_{sub}. Thus, our data suggest that the relative complexity between the SN and the Pop grows differently depending on the size of the city.

This suggests that the gradual increase in human occupation in urban areas, which can result in serious negative consequences - a fact already known in the literature, such as: congestion, heavy traffic, atmospheric pollution, heat islands, traffic accidents, pressure

Figure 5.12 – Graph of γ_{sub} vs. N. The green dotted curve corresponds to the fit of the model $\gamma_{sub}(N) = a - b/(\ln N)^c$ whose parameters are shown in Table 5.8. The blue dotted curve corresponds to the asymptotic value $\gamma'_{sub} = 0.95$, while the red curve corresponds to the average value $\bar{\gamma}_{sub} = 0.93$. Note the existence of two regimes around $N \approx 10^4$, the first for $\gamma_{sub} < \bar{\gamma}_{sub}$ and the second for $\gamma_{sub} < \bar{\gamma}_{sub} < \gamma'_{sub}$. This result suggests that the exponent γ_{sub} grows linearly between $0 < N < 10^4$ and grows smoothly and non-linearly for values $N > 10^4$.

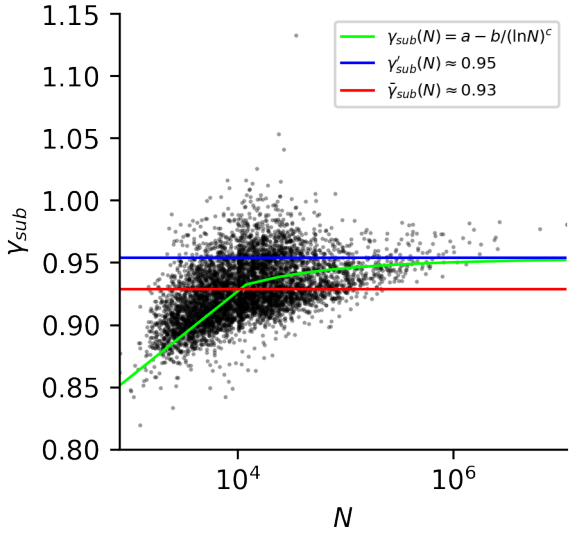

Source: Own authorship.

on public services, disorganized urban development, reduced quality of life, especially on the outskirts - also brings with it positive consequences such as new job opportunities, higher wages, innovation, networking, versatility in the local economy, leisure, to name a few. Thus, our data suggests that these consequences start to occur above of 10,000 inhabitant's.

We also find that on average the fractal dimensions of the SN are smaller than the fractal dimensions of the Pop, as they have already pointed out, see Figure 5.13 a). The average value of D_i was 1.68 ± 0.03, while the average value of D_p was 1.81 ± 0.06. In b) we see the values of D_i, D_p and the ratio γ_{sub} as a function of N.

Using the asympotic sub-linear exponent $\gamma'_{sub} = 0.95$ and average value of $\bar{\gamma}_{sub} = 0.93$, it was able to predict L and Y for the 5523 Brazilian cities. The results are shown in Figure 5.14 a) and b). Using the asymptotic approach to predict L , the slope was 0.97 ± 0.01 with $R^2 = 0.77$ and using the average approach, the slope was 0.99 ± 0.01 with $R^2 = 0.77$ and using the average approach. On the other hand, using the average approach to predict Y, the slope was 1.03 ± 0.02 with $R^2 = 0.76$ and using the asymptotic

Figure 5.13 – Macroscopic M&T model. a) histogram of the population (SN) and street network (SN) fractal dimensions obtained by the eqs. (2.2.16) and (2.2.17). b) fractal dimensions and the ratio vs. Pop

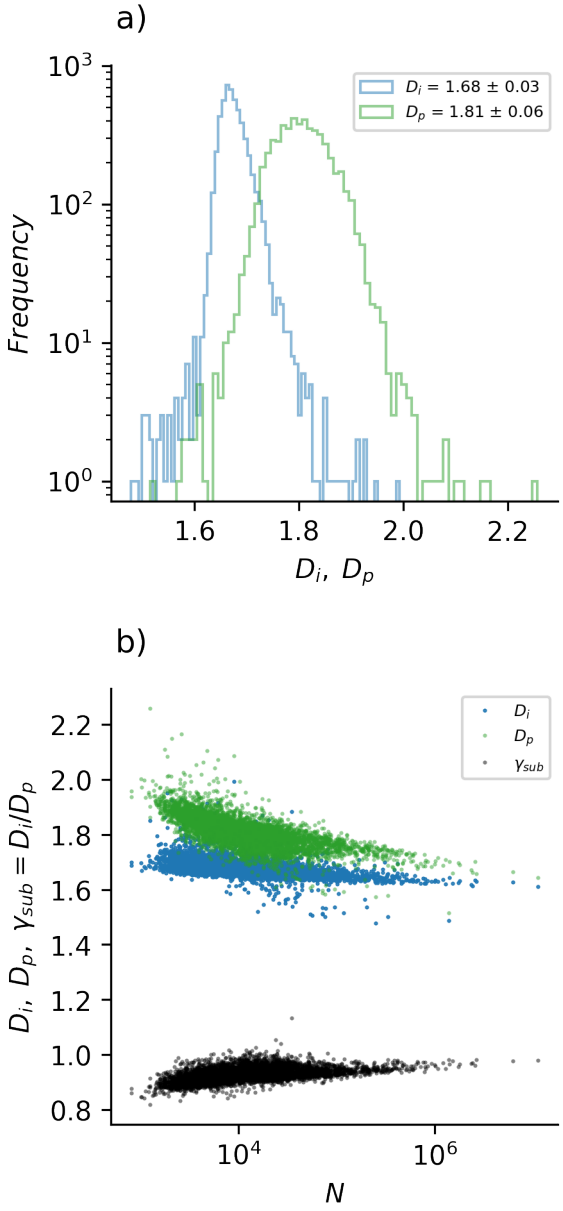

Source: Own authorship

approach the slope was 1.00 ± 0.01 with $R^2 = 0.76$. It is possible to see that the average approach is slightly better that the asymptotic approach, showing excellent predictions for L and Y. In this case, in order to confirm whether it is really valid, we need to do an analysis for cities in different countries.

Table 5.8 – Macroscopic M&T linear regression summary for the 5523 Brazilian cities.

Approach	Regime	Parameters of the model	slope	std	R^2
Asymptotic	sub-linear	$a = 0.95383,\ b = 658.79528,\ c = 4.61111$	0.97	0.01	0.77
Average		-	0.99	0.01	0.77
Asymptotic	super-linear	$a = 0.95383,\ b = 658.79528,\ c = 4.61111$	1.03	0.02	0.76
Average		-	1.00	0.01	0.76

Source: Own authorship.

Figure 5.14 – M&T model with fractal dimensions obtained by the eqs. (2.2.16) and (2.2.17). a) Sub-linear scaling between total road network L and city size N for 5523 Brazilian cities raised by $\gamma^{'}_{sub}$ and $\bar{\gamma}_{sub}$ which are the asymptotic and average sub-linear exponents obtained. b) Super-linear scaling between Gross Domestic Product (GDP) Y and city size N for 5523 Brazilian cities raised by $\gamma^{'}_{sup}$ and $\bar{\gamma}_{sup}$ which are the asymptotic and average super-linear exponents obtained. We see that the average exponent fits the data well because the slopes are equal to 1.

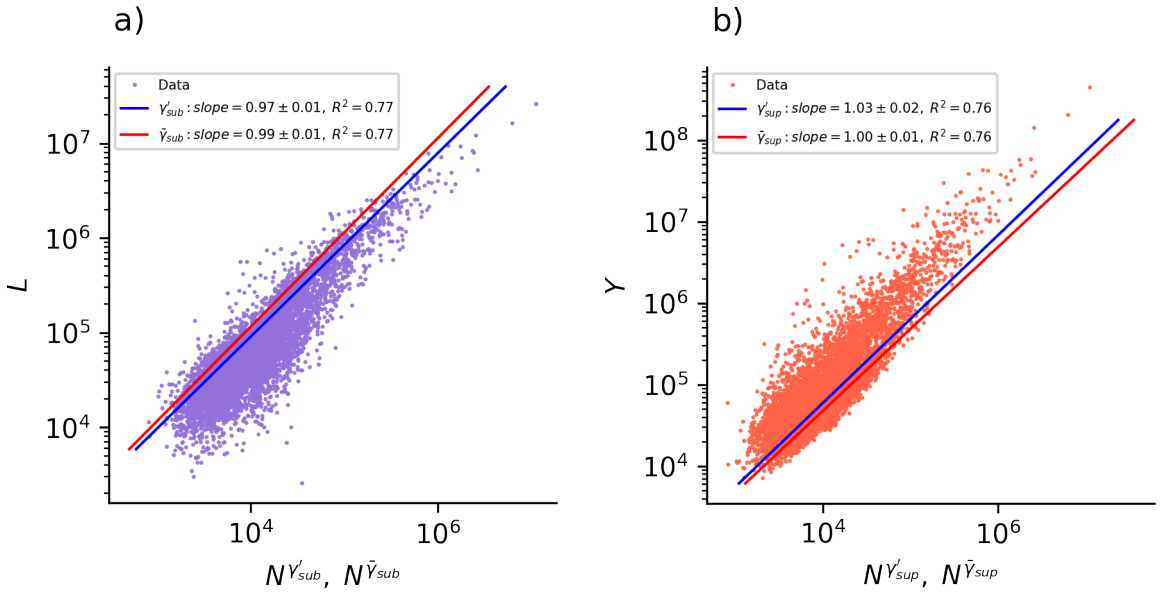

Source: Own authorship.

Table 5.9 shows some urban metrics for the 15 largest cities in 2010, namely: A urban area in square meters, P urban perimeter in meters, N the Pop, Y Gross Domestic Product, L total street length, n number of nodes and e number of links in the SN.

5.5 Street Networks Measures

In this section we present the results obtained from the analysis of the network metrics chosen in our work, namely: number of nodes n, number of links e, cyclomatic

Table 5.9 – Urban metrics of the 15 largest Brazilian cities in 2010. A urban area in square meters, P urban perimeter in meters, the Pop N, Gross Domestic Product Y, total street length L, number of nodes n and number of links e of the street network (SN).

City	UF	A (m^2)	P (m)	N	Y	L	n	e
Campinas	SP	421222664.01	278459.69	1080113	38195022	7135108.46	29381	73496
Guarulhos	SP	230179544.27	124657.6	1221979	35671510	3757246.98	15136	38171
São Paulo	SP	1135636458.51	612979.51	11253503	450491988	26190538.13	113272	281872
Porto Alegre	RS	410625345.52	223398.31	1409351	42724992	4944750.08	19069	45405
Rio de Janeiro	RJ	1095789894.42	482420.5	6320446	208153595	16355990.84	70329	170490
Recife	PE	146142086.37	126564.58	1537704	33369681	3738115.6	18469	47130
Curitiba	PR	507657895.71	115778.09	1751907	58122788	9393066.64	34887	90749
Belém	PA	2114684.66	8928.36	1393399	18801039	3140062.58	14311	35708
Belo Horizonte	MG	357285541.72	123905.92	2375151	59203074	8302358.58	32358	83388
São Luís	MA	285835641.08	222185.26	1014837	18211488	4798184.39	20899	55277
Goiânia	GO	461923803.55	180765.48	1302001	29038011	9492848.46	38079	98491
Brasília	DF	965744106.0	806426.03	2570160	144174102	12084570.64	60385	139205
Fortaleza	CE	288216767.71	118255.71	2452185	37001831	7934034.72	36728	96359
Salvador	BA	274876314.45	162741.36	2675656	40762687	5225368.12	27482	63209
Manaus	AM	431152233.65	139381.42	1802014	50168821	6988648.03	28652	74878

Source: Own authorship.

number μ and the average values of betweenness, closeness and Bonacich, see Figure 5.15. We present the results taking into account the perimeter and the urban area. All of the above quantities were analyzed as a function of the Pop, N, and we were able to observe that they all scale with the Pop, but with different behaviors and exponents. In addition, we analyzed the average values of the number of links $\langle k \rangle$ and the numbers α, β and γ, which are closely related.

We start by pointing out that the number of nodes n, the number of links e and the cyclomatic number μ have the same fractal dimension. To show this, we can assume that these quantities scale with the Euclidean distance r with positive exponents and given by the respective fractal dimensions, d_n, d_e and d_μ, respectively. We must also assume that the Pop follows this same pattern but with an exponent given by the fractal dimension of the Pop, i.e. d_p. Therefore, we have

$$N_a(r) \sim r^{d_a} \qquad N(r) \sim r^{d_p} \tag{5.5.1}$$

where $N_a(r)$ with $a = (n, e, \mu)$ are the number of each quantity in a radii r. Under these conditions, you can show that

$$N_a^{1/d_a} \sim N^{1/d_p} \tag{5.5.2}$$

in such a way that

$$N_a \sim N^{d_a/d_p}, \tag{5.5.3}$$

which means

$$\frac{d_a}{d_p} \approx \frac{17}{20} \Longrightarrow d_n = d_e = d_\mu \tag{5.5.4}$$

Figure 5.15 – Street network (SN) in Curitiba, PR, with nodes colored according to: a) degree. b) betweenness, c) closeness and d) Bonacich centrality. Red nodes have higher values and blue nodes have lower values.

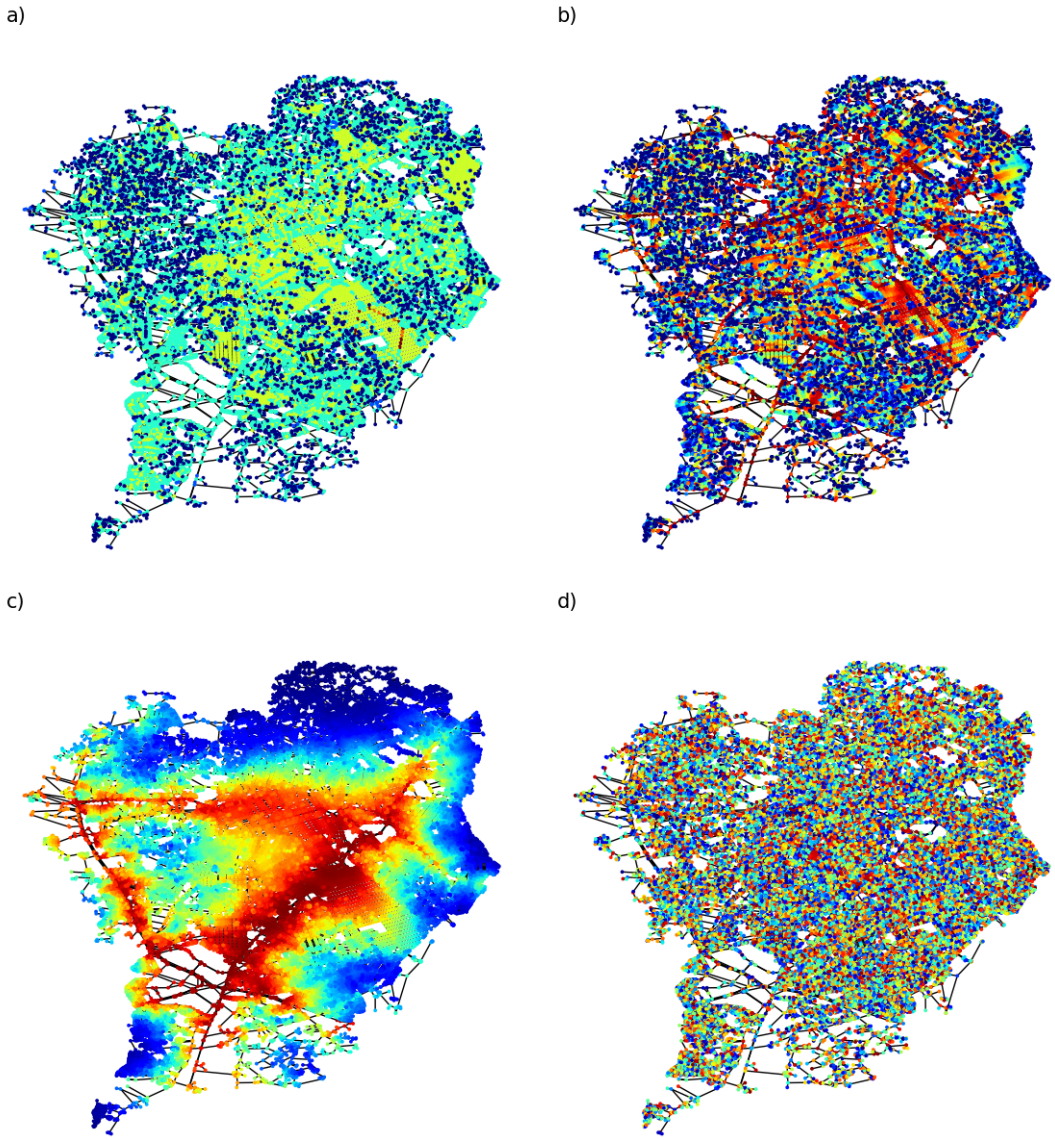

Source: Own authorship.

a consequence of the following results

$$N_a \sim N^{c_a},\ c_a \approx \frac{17}{20},\ a = (n, e, \mu), \tag{5.5.5}$$

and the eq. 2.3.9.

We can use the same arguments to estimate the fractal dimension of the urban area A and its perimeter P, so that

$$A(r) \sim r^{d_A}, \qquad P(r) \sim r^{d_o} \tag{5.5.6}$$

where d_A and d_o are the fractal dimensions of the urban area and perimeter. Therefore, we have the following equivalence between these quantities

$$A^{1/d_A} \sim P^{1/d_o}, \tag{5.5.7}$$

with

$$\frac{d_o}{d_A} \sim \frac{3}{5}. \tag{5.5.8}$$

This can be confirmed by noting that

$$A \sim N^{c_4}, \;\; c_4 = \frac{97}{100}\,; \qquad P \sim N^{c_5}, \;\; c_5 = \frac{31}{50}, \tag{5.5.9}$$

then we have $P \sim A^{c_5/c_4}$ with $\frac{c_5}{c4} = \frac{3007}{5000} \approx \frac{3}{5}$.

We can see that the average values of the measures of betweenness, closeness, and Bonacich scale with the *Pop* with a negative exponent and less than 1. This means that these quantities tend to decrease sublinearly as the city grows. For the case of betweenness, the exponent was 0.44 ± 0.01 with $R^2 = 0.65$, see Figure 5.22 a). In the case of closeness, the exponent value was 0.39 ± 0.01 with $R^2 = 0.68$, see Figure 5.23 a), while for the Bonacich measure we obtained a value of 0.85 ± 0.01 with $R^2 = 0.71$, see Figure 5.24 a). In addition, also we present the exponents of the distibution following the power law (ALSTOTT; BULLMORE; PLENZ, 2014)

$$p(x) \sim (\alpha \pm \sigma - 1) x_{min}^{\alpha \pm \sigma - 1} x^{-\alpha \pm \sigma}, \tag{5.5.10}$$

where $p(x)$ is a probability associated with the variable x, x_{min} is the cutoff for adjusting this quantity by depressing its heavy tail. α is the exponent and σ is the uncertainty associated with this exponent. The summary results are in the Table 5.10.

Table 5.10 – Power law expoents.

measure	α	σ	x_{min}
n	1.716	0.002	1.0
e	1.164	0.002	1.0
μ	1.202	0.003	1.0
A	1.052	0.001	0.016
P	1.073	0.001	0.016
$\langle c_B(v)\rangle$	5.736	0.224	0.085
$\langle c_C(v)\rangle$	7.202	0.398	0.178
$\langle c_i(\theta,\phi)\rangle$	4.007	0.167	0.016

Source: Own authorship.

Furthermore, considering that the average value of Bonacich, see Figure 5.24, centrality scales with r with an exponent given by the fractal dimension d_c, we have

$$\langle c_i(\theta,\phi)\rangle(r) \sim r^{-d_c}, \tag{5.5.11}$$

providing

$$\langle c_i(\theta,\phi)\rangle \sim N^{-d_c/d_p} \tag{5.5.12}$$

where d_p is the fractal dimension of the population. But we know that $\frac{d_c}{d_p} = \frac{17}{20}$, which implies that

$$d_c = d_n = d_e = d_\mu. \tag{5.5.13}$$

This result shows that the spatial complexity associated with Bonacich's centrality is the same as that associated with the number of nodes, links, and cyclomatic number, making it possible to say that they belong to the same universality class.

Another interesting result that can be observed is that the numbers α, β, γ are closely related to the average value of the degree of nodes $\langle k\rangle$, which can be seen in the relationship

$$\frac{\langle k\rangle}{\langle\beta\rangle} \approx \frac{\langle\gamma\rangle}{\langle\alpha\rangle} \approx 2, \tag{5.5.14}$$

which suggests that the ratio between these quantities is constant regardless of the size of the network, see Figure 5.19. According with Barthelemy (2009), the ratio $\frac{\langle k\rangle}{\langle\beta\rangle}$ is in line with two-dimensional spatial networks, which have strong physical constraints, which in turn prevent hubs from appearing. However, considering the ratio $\frac{\langle\gamma\rangle}{\langle\alpha\rangle}$, we have something new.

The following are some of the contributions of this work:

- application of generalized dimensions in intra-city models, initially based on a monofractal approach, in an attempt to predict urban indicators;
- joint multifractal analysis of the SN and the Pop of the most populous cities in a developing country and South America;
- proposition of the spatial correlation rate in analogy to the special filling and redundancy rates;
- proposing an index to characterize the process of aggregation and diffusion in terms of the inverse of the skewness of the multifractal spectrum;
- heuristic urban scale model (in analogy to the Molinero & Thurner model) using macroscopic city variables such as Pop, total street length and urban area in an attempt to predict urban indicators;
- demonstration that intra-city models can be obtained via Shannon entropy maximization;
- demonstration of the equivalence between the generalized dimension of order 2 via the *sandbox* method and the correlation dimension;
- demonstration that the generalized dimensions of orders other than 0 and 1 are normalized versions of the correlation dimension.

Figure 5.16 – Number of nodes e vs. city size N and histogram associated to this measure.

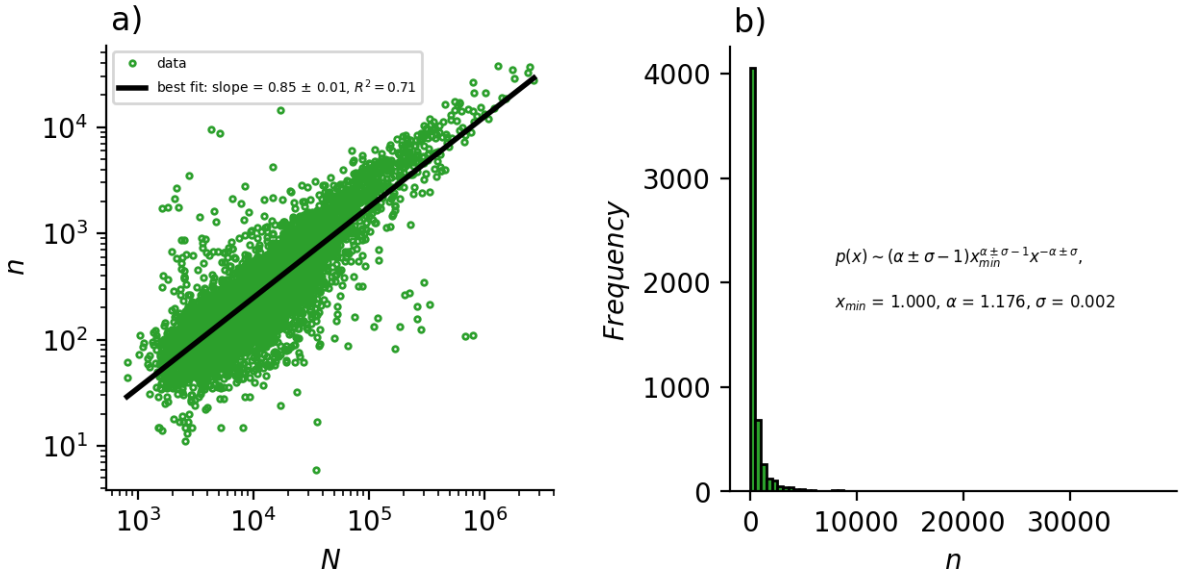

Source: Own authorship.

Figure 5.17 – Number of edges or links e vs. city size N and histogram associated to this measure.

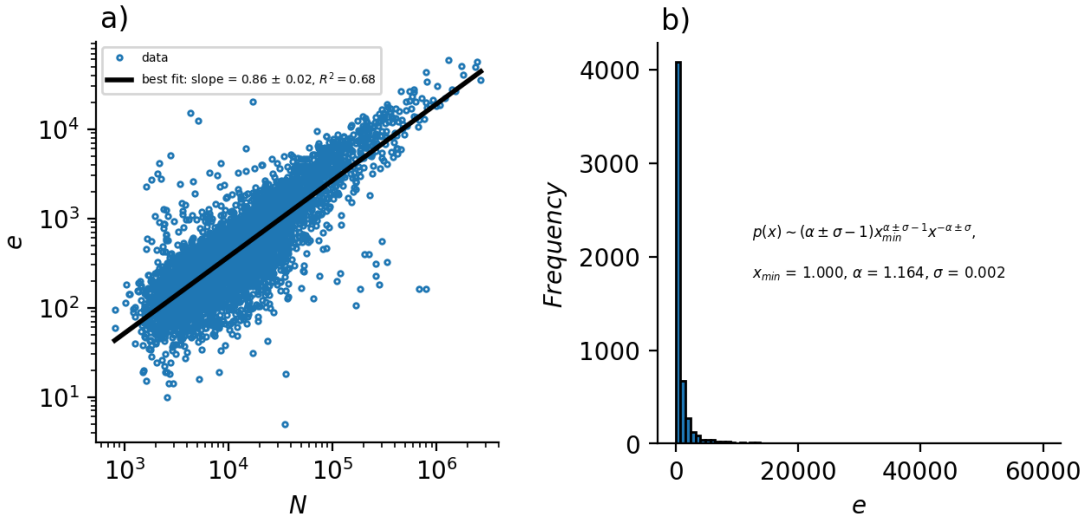

Source: Own authorship.

Figure 5.18 – Cyclomatic number μ vs. city size N and histogram associated to this measure.

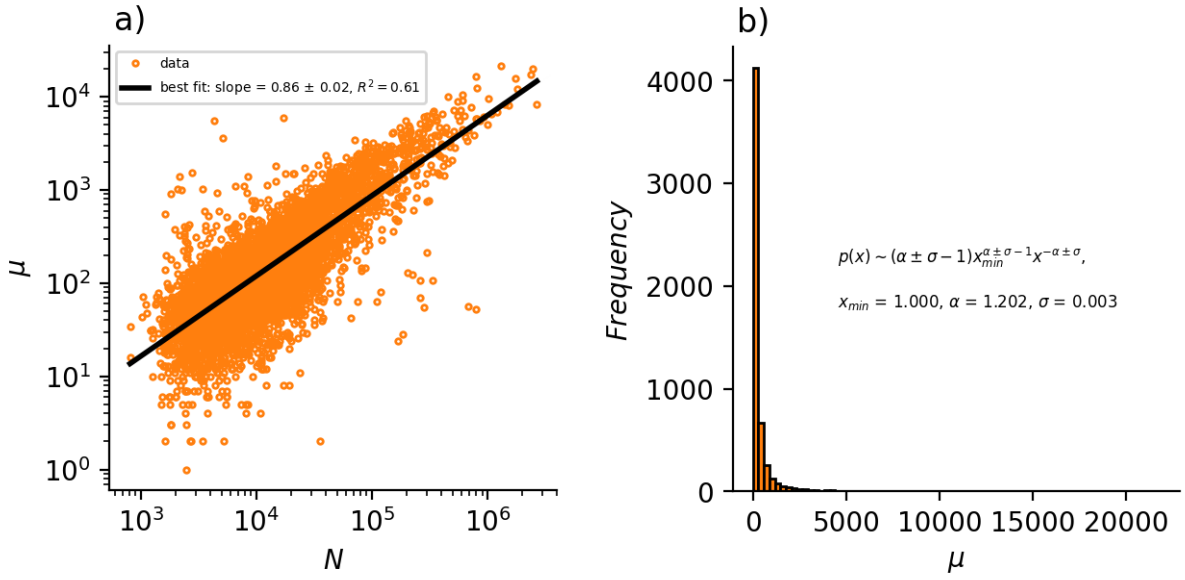

Source: Own authorship.

Figure 5.19 – Street network (SN) histograms. a) degree centrality. b) α number. c) β number. γ number. Note that the $\langle k \rangle / \langle \beta \rangle \approx \langle \gamma \rangle / \langle \alpha \rangle \approx 2$.

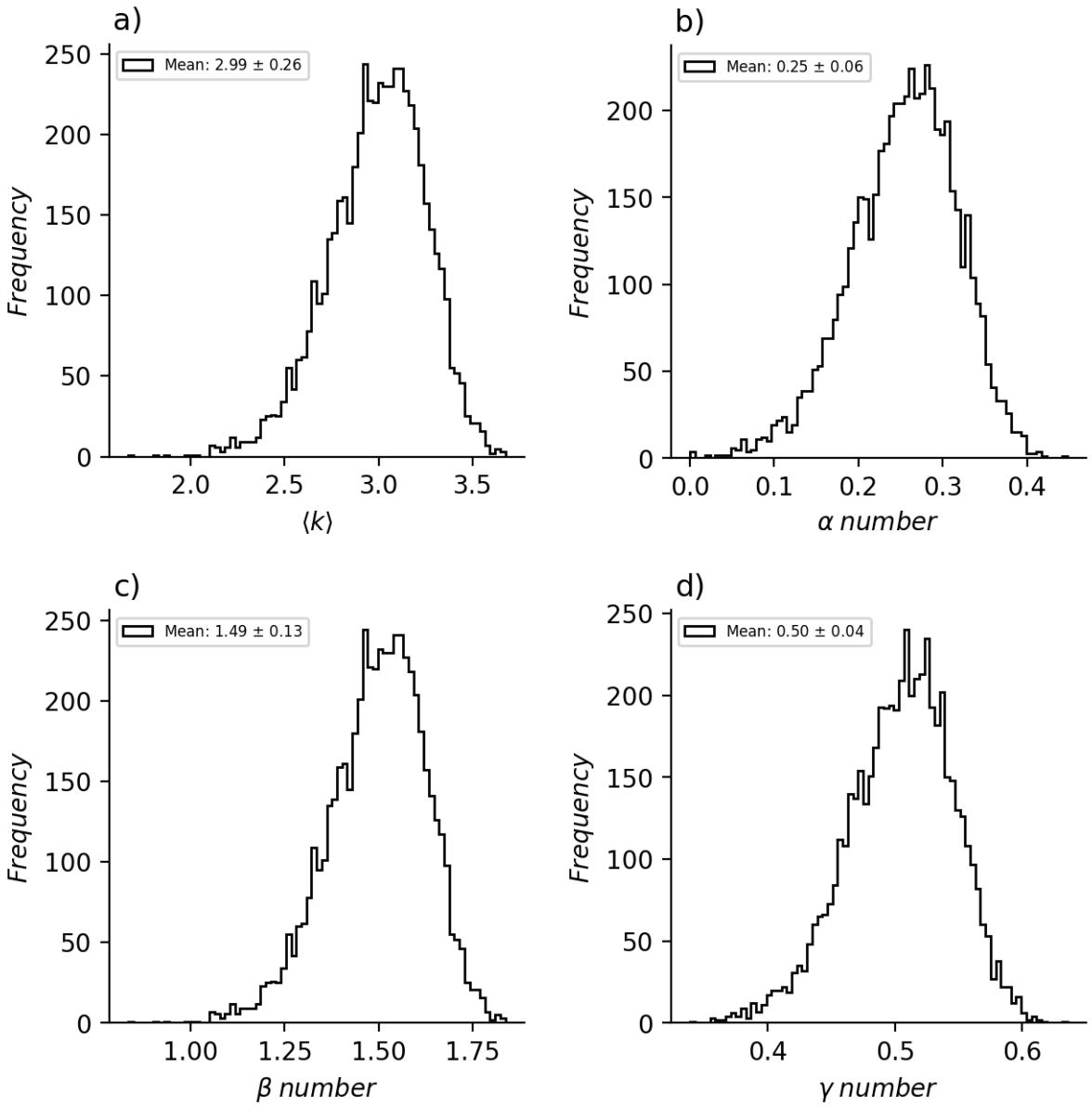

Source: Own authorship.

Figure 5.20 – Urban area A vs. city size N and histogram associated to this quantity.

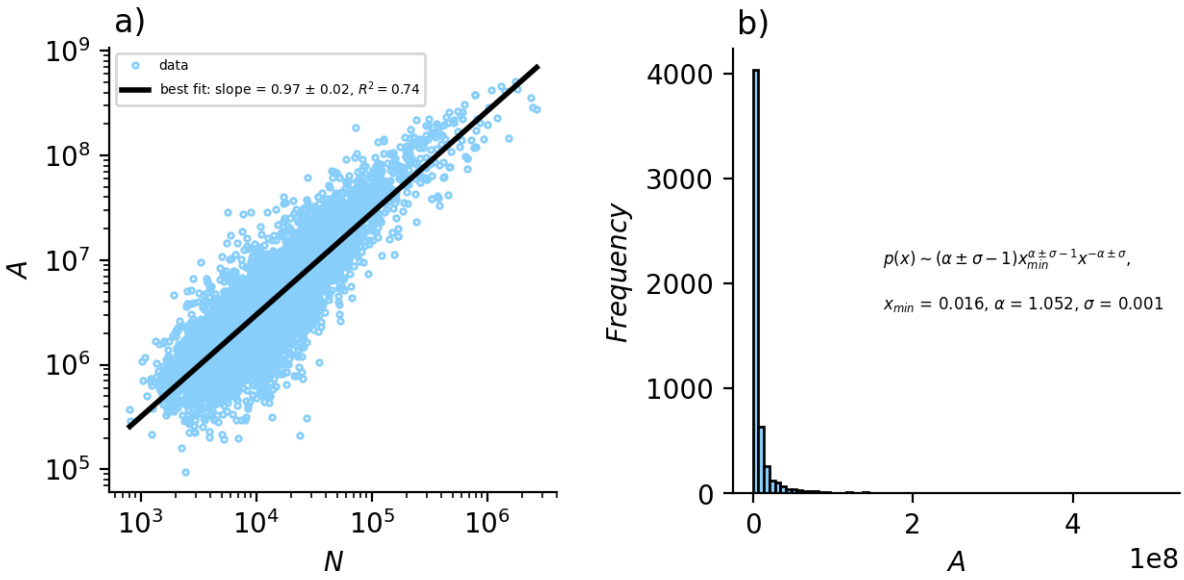

Source: Own authorship.

Figure 5.21 – Urban perimeter P vs. city size N and histogram associated to this quantity.

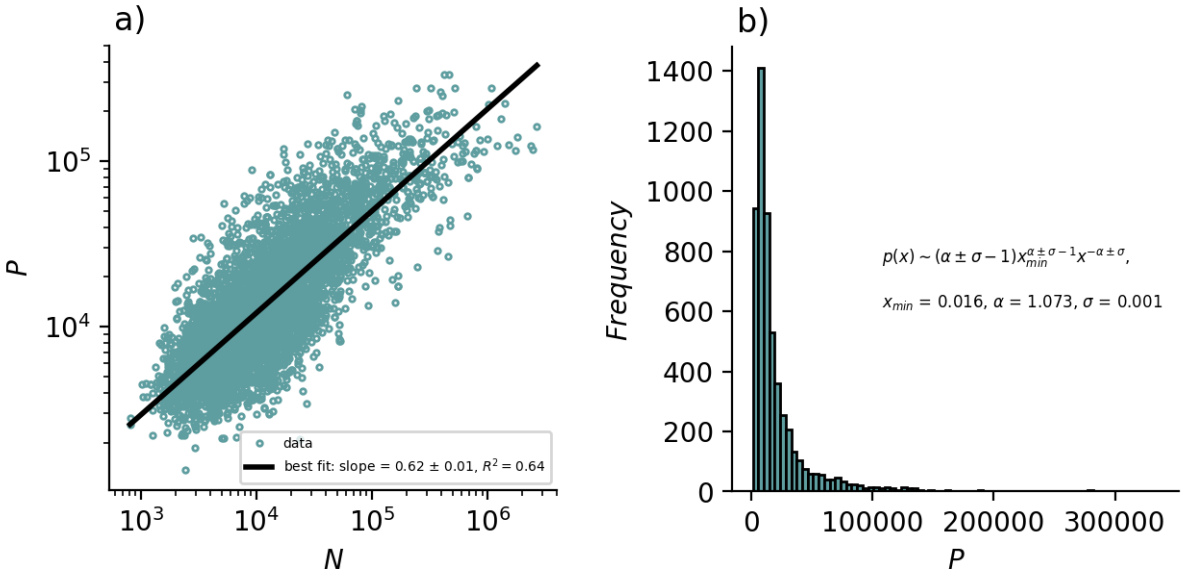

Source: Own authorship.

Figure 5.22 – Average betweenness centrality $\langle c_B(v) \rangle$ vs. city size N and histogram associated to this centrality.

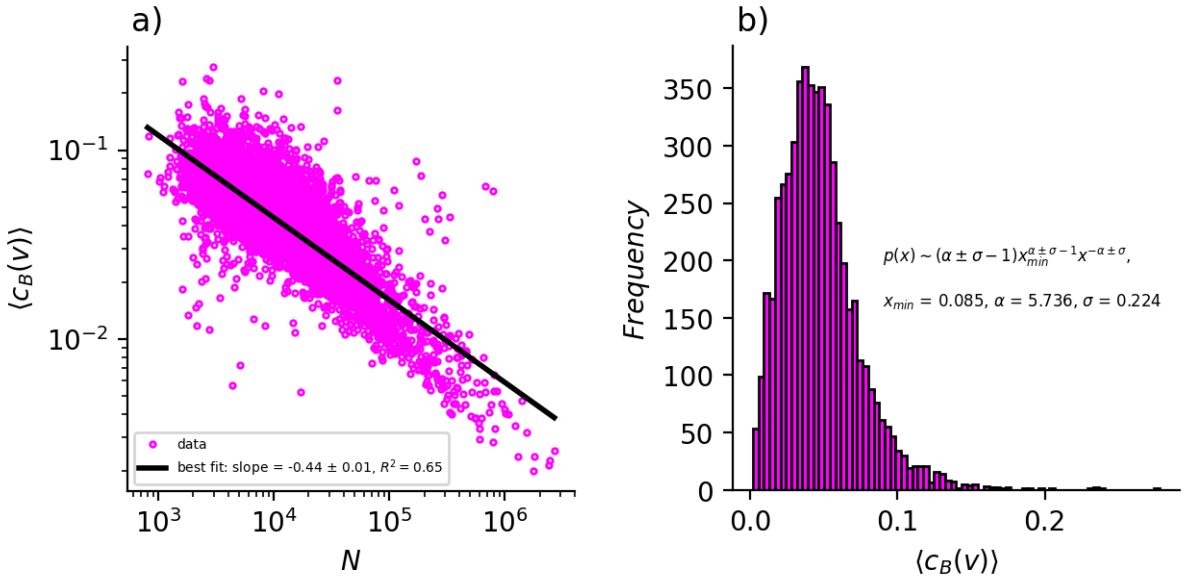

Source: Own authorship.

Figure 5.23 – Average closeness centrality $\langle c_C(v) \rangle$ vs. city size N and histogram associated to this centrality.

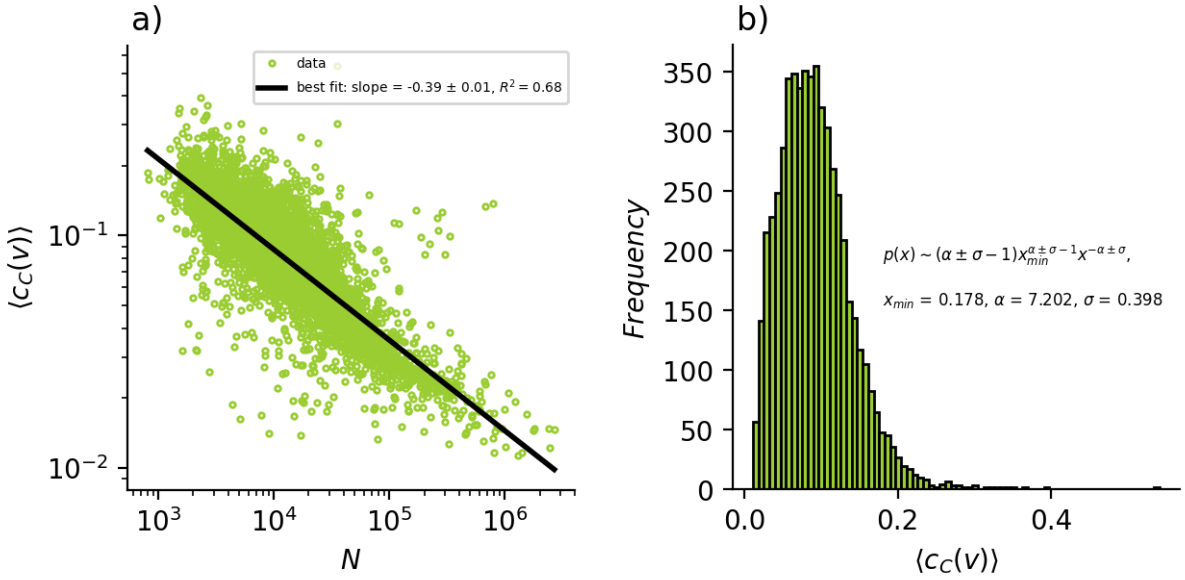

Source: Own authorship.

Figure 5.24 – Average Bonacich centrality $\langle c_i(\phi, \theta) \rangle$ vs. city size N and histogram associated to this centrality.

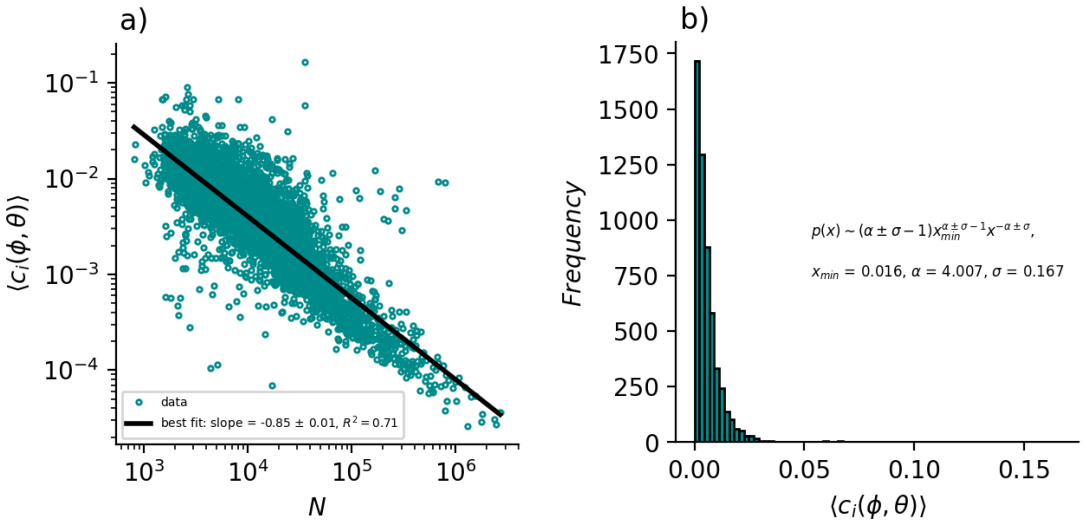

Source: Own authorship.

6 CONCLUSIONS

In this Chapter we present some conclusions about this work.

Firstly, the street network (SN) and the spatial distribution of the population (Pop) of the 15 largest Brazilian cities in 2010 showed: i) properties of multifractal structures, ii) a tendency towards aggregation and diffusion phenomena, iii) disordered development in the peripheral regions and in the most sparse areas, in addition to showing degradation of the fractal structure in the central regions and in high-density areas. Our results show that São Paulo is the city with the highest rate of spatial completion in relation to SN, while Brasília is the city with the highest value in relation to Pop. In the case of São Paulo, our result was not surprising, as it has the highest number of nodes and links compared to the other cities, see Figure 5.9. On the other hand, although Brasília does not have a larger Pop than São Paulo, we can attribute its higher space-filling rate in relation to Pop to its geography, which has regions with the presence of forest (Brasilia National Park) and continental waters (Paranoá Lake). We can see that these cities showed phenomena of diffusion and aggregation, respectively.

In relation to the Bettencourt model, we see that in order to obtain more satisfactory results, if we want to extend this model and the others, even if *ad hoc*, it is necessary to carry out a multifractal analysis of all the cities in order to obtain the spectra and the generalized dimensions. With this, the uncertainties of the exponents could be significantly improved, improving the predictions of indicators related to infrastructure and those related to socioeconomic activities. The idea is that the generalized dimensions, which have different meanings, can provide some additional information when used to develop intra-city models. This is justified by the fact that the Pop and SN are distributed in space in a non-uniform way and only a multifractal approach can capture the spatial complexity of these structures.

In relation to intra-city models, the Molinero & Thurner (M&T) model and the ratio between the fractal dimensions of SN and Pop, using the (CHEN, 2020) approximation, allowed us to observe that the total length of streets, L, and the gross domestic product (GDP), Y, can be explained via the geometric properties of cities. Using the asymptotic limit of the exponent $\gamma_{sub} = D_i/D_p$, which in (MOLINERO; THURNER, 2021) is approximately 0.86, in our case, on the other hand, the exponent that best answered the predictions of L *vs.* N and Y *vs.* N was the average value of $\gamma_{sub} = 0.93$,

providing slopes of 0.99 ± 0.01 with $R^2 = 0.77$ and 1.00 ± 0.01 with $R^2 = 0.76$, respectively. Then, we confirm that infrastructure and socio-economic variables in urban systems can be explain urban scaling via geometry, but as novelty, the geometry the cities can be easy obtained from the definition of the fractal dimensions of SN and Pop in terms of the L, N, and urban area A data. This strategy has significant implications, such as speed and simplicity in obtaining these exponents, which can often be computationally costly when using more complex methodologies to estimate fractal dimensions. We believe that this strategy can be implemented in any urban system as long as the necessary data is available for analysis. Once the data is available, a comprehensive analysis of all urban systems can be conducted within a few hours or even minutes. This knowledge can be used to create mathematical models to support local and global decision-making in cities.

Considering fractal theory and the number of nodes, links and cyclomatics, as well as Bonacich's centrality, it was possible to show that the spatial complexity captured by the fractal dimension of each of these quantities is the same. In relation to the number of nodes, links and the cyclomatic number this conclusion is trivial, but when we include Bonacich's centrality this result, whose meaning is completely different from these quantities, is not so trivial, which suggests future research.

Regarding the centrality measures estimated for the SN, we see that some of them do not present typical values, for example, betweenness, closeness, Bonacich, but others do, for example, the number of links and the topological measures α, β and γ. In particular, it was observed that there is a relationship whose value is constant and independent of the size of the network.

Furthermore, it is essential to understand how cities work in order to promote quality of life in urban environments. This requires the use of computational tools, a theoretical foundation derived from various topics of complex systems, and a close relationship between decision-makers and the knowledge generated.

The work has the following limitations: i) a limited number of samples were used in the multifractal analysis, indicating the need for further procedures with more cities. ii) The calculations with census tract geometries are computationally expensive.

However, this work serves as an introduction to the application of multifractal analysis in urban systems, particularly in developing countries. Additionally, it contributes to the study of urban scale laws by considering the fractal properties of their constituents.

The author hopes to publish at least one article presenting the results of this work and plans to continue their studies in a doctoral program.

REFERENCES

ABID, R. I.; TORTUM, A.; ATALAY, A. Fractal dimensions of road networks in amman metropolitan districts. **Alexandria Engineering Journal**, v. 60, n. 4, p. 4203–4212, 2021. ISSN 1110-0168. Disponível em: <https://www.sciencedirect.com/science/article/pii/S1110016821001769>.

ALBERT, R.; BARABASI, A.-L. Statistical mechanics of complex networks. **Rev. Mod. Phys.**, American Physical Society, v. 74, p. 47–97, Jan 2002. Disponível em: <https://link.aps.org/doi/10.1103/RevModPhys.74.47>.

ALBERTI, M. Grand challenges in urban science. **Frontiers in Built Environment**, v. 3, 2017. ISSN 2297-3362. Disponível em: <https://www.frontiersin.org/articles/10.3389/fbuil.2017.00006>.

ALEXANDER, C. **Notes on the Synthesis of Form**. [S.l.]: Harvard University Press, 1964. v. 5.

ALEXANDER, C. The city is not a tree. In: **Architectural Forum**. [S.l.: s.n.], 1965.

ALSTOTT, J.; BULLMORE, E.; PLENZ, D. powerlaw: A python package for analysis of heavy-tailed distributions. **PLOS ONE**, Public Library of Science, v. 9, n. 1, p. 1–11, 01 2014. Disponível em: <https://doi.org/10.1371/journal.pone.0085777>.

ALVES, L. G. A. et al. Scale-adjusted metrics for predicting the evolution of urban indicators and quantifying the performance of cities. **PLOS ONE**, Public Library of Science, v. 10, n. 9, p. 1–17, 09 2015. Disponível em: <https://doi.org/10.1371/journal.pone.0134862>.

AMIT, G. et al. Percolation in fractal spatial networks with long-range interactions. **Phys. Rev. Res.**, American Physical Society, v. 5, p. 023129, May 2023. Disponível em: <https://link.aps.org/doi/10.1103/PhysRevResearch.5.023129>.

APPLEBY, S. Multifractal characterization of the distribution pattern of the human population. **Geographical Analysis**, v. 28, n. 2, p. 147–160, 1996. Disponível em: <https://onlinelibrary.wiley.com/doi/abs/10.1111/j.1538-4632.1996.tb00926.x>.

ARCAUTE, E. et al. Constructing cities, deconstructing scaling laws. **Journal of the Royal Society interface**, v. 12, n. 102, 2015.

ARCAUTE, E.; RAMASCO, J. J. Recent advances in urban system science: Models and data. **PLOS ONE**, Public Library of Science, v. 17, n. 8, p. 1–16, 08 2022. Disponível em: <https://doi.org/10.1371/journal.pone.0272863>.

ARVIDSSON, M.; LOVSJO, N.; KEUSCHNIGG, M. Urban scaling laws arise from within-city inequalities. **Nat Hum Behav**, v. 7, p. 365–374, 2013.

BAEZ, J. C. Renyi entropy and free energy. **Entropy**, MDPI, v. 24, n. 5, p. 706, 2022.

BAKER, G. L.; GOLLUB, J. P. **Chaotic Dynamics: an introduction**. 2. ed. [S.l.]: Cambridge University Press, 1996.

BARABASI, A.-L. **Linked: The New Science of Networks.** [S.l.]: Perseus Books Group, 2002.

BARABASI, A.-L. **Network Science**. [S.l.]: Cambridge University Press, 2016.

BARABASI, A.-L.; ALBERT, R. Albert, r.: Emergence of scaling in random networks. **Science (New York, N.Y.)**, v. 286, p. 509–12, 11 1999.

BARNSLEY, M. F.; DEMKO, S. Iterated function systems and the global construction of fractals. **Proceedings of the Royal Society of London. Series A, Mathematical and Physical Sciences**, The Royal Society, v. 399, n. 1817, p. 243–275, 1985. ISSN 00804630. Disponível em: <http://www.jstor.org/stable/2397690>.

BARTHELEMY, M. Modeling cities. **Comptes Rendus Physique**, v. 20, n. 4, p. 293–307, 2019. ISSN 1631-0705. Disponível em: <https://www.sciencedirect.com/science/article/pii/S1631070519300337>.

BARTHELEMY, M. The statistical physics of cities. **Nature Reviews Physics**, Nature Publishing Group, v. 1, n. 6, p. 406–415, 2019.

BARTHELEMY, M.; FLAMMINI, A. Co-evolution of density and topology in a simple model of city formation. **Netw Spat Econ 9**, p. 401–425, 2009.

BARTOLO, S. G. D.; GAUDIO, R.; GABRIELE, S. Multifractal analysis of river networks: Sandbox approach. **Water Resources Research**, v. 40, n. 2, 2004. Disponível em: <https://agupubs.onlinelibrary.wiley.com/doi/abs/10.1029/2003WR002760>.

BASSETT, D.; GAZZANIGA, M. Understanding complexity in the human brain. **Trends in cognitive sciences**, v. 15, p. 200–9, 05 2011.

BATTY, M. The size, scale, and shape of cities. **Science (New York, N.Y.)**, v. 319, p. 769–71, 03 2008.

BATTY, M. Building a science of cities. **Cities**, v. 29, p. S9–S16, 2012. ISSN 0264-2751. Current Research on Cities. Disponível em: <https://www.sciencedirect.com/science/article/pii/S0264275111001375>.

BATTY, M. **The New Science of Cities**. The MIT Press, 2013. ISBN 9780262019521. Disponível em: <http://www.jstor.org/stable/j.ctt9qf7m6>.

BATTY, M. City systems and complexity. In: PORTUGALI, J. (Ed.). **Handbook on Cities and Complexity**. Cheltenham: Edward Elgar Publishing, 2021. p. 48–64.

BATTY, M.; LONGLEY, M. **Fractal Cities - A Geometry of Form and Function**. [S.l.: s.n.], 1994. 432 p.

BATTY, M.; XIE, Y. Self-organized criticality and urban development. **Discrete Dynamics in Nature and Society**, Hindawi Publishing Corporation, New York, v. 3, n. 2-3, p. 109–124, 1999. Disponível em: <http://eudml.org/doc/125502>.

BAVELAS, A. A mathematical model for group structures. **Human Organization**, v. 7, p. 16–30, 1948.

BAVELAS, A. Communication patterns in task oriented group. **Journal of the Acoustical Society of America**, v. 22, p. 271–282, 1950.

BECK, C. Generalised information and entropy measures in physics. **Contemporary Physics**, Taylor and Francis, v. 50, n. 4, p. 495–510, 2009. Disponível em: <https://doi.org/10.1080/00107510902823517>.

BENZI, R. et al. On the multifractal nature of fully developed turbulence and chaotic systems. **Journal of Physics A: Mathematical and General**, v. 17, n. 18, p. 3521, dec 1984. Disponível em: <https://dx.doi.org/10.1088/0305-4470/17/18/021>.

BERRY, B. J. L.; GARRISON, W. L. Alternate explanations of urban rank–size relationships. **Annals of the Association of American Geographers**, v. 48, n. 1, p. 83–91, 1958.

BETTENCOURT, L.; WEST, G. A unified theory of urban living. **Nature**, v. 467, p. 912–3, 10 2010.

BETTENCOURT, L. M. A. The origins of scaling in cities. **Science**, v. 340, n. 6139, p. 1438–1441, 2013. Disponível em: <https://www.science.org/doi/abs/10.1126/science.1235823>.

BIANCONI, G. et al. Complex systems in the spotlight: next steps after the 2021 nobel prize in physics. **Journal of Physics: Complexity**, IOP Publishing, v. 4, n. 1, p. 010201, jan 2023. Disponível em: <https://dx.doi.org/10.1088/2632-072X/ac7f75>.

BOEING, G. Osmnx: New methods for acquiring, constructing, analyzing, and visualizing complex street networks. **Computers, Environment and Urban Systems**, v. 65, p. 126–139, 2017. ISSN 0198-9715. Disponível em: <https://www.sciencedirect.com/science/article/pii/S0198971516303970>.

BONACICH, P. Power and centrality: A family of measures. **American Journal of Sociology**, v. 92, n. 5, p. 1170–1182, 1987.

BORUVKA, O. O jistem problemu minimalním. **Prace Moravske prirodovedecke spolecnosti, sv. III, spis 3**, p. 37–58, 1926.

BRANDES, U.; BORGATTI, S. P.; FREEMAN, L. C. Maintaining the duality of closeness and betweenness centrality. **Social Networks**, v. 44, p. 153–159, 2016. ISSN 0378-8733. Disponível em: <https://www.sciencedirect.com/science/article/pii/S0378873315000738>.

BUNDE, A.; HAVLIN, S. **Fractals and Disordered System**. [S.l.: s.n.], 1992. ISBN 978-3-642-51437-1.

BUNDE, A.; HAVLIN, S. **Fractals in Science**. [S.l.]: Springer Berlin, Heidelberg, 1994. ISBN 978-3-642-77953-4.

CALLAWAY, D. S. et al. Network robustness and fragility: Percolation on random graphs. **Physical review letters**, APS, v. 85, n. 25, p. 5468, 2000.

CAPOANI, L. Review of the gravity model: origins and critical analysis of its theoretical development. **SN Business and Economics**, v. 3, p. 43, 04 2023.

CAVES, R. W. **Encyclopedia of the City**. [S.l.]: Routledge, 2004.

CHANUI, A. L. et al. Analysis of the structural complexity of crab nebula observed at radio and infrared frequencies using a multifractal approach. **arXiv preprint arXiv:2206.04717**, 2022.

CHEN, Y. A set of formulae on fractal dimension relations and its application to urban form. **Chaos, Solitons and Fractals**, v. 54, p. 150–158, 2013. ISSN 0960-0779. Disponível em: <https://www.sciencedirect.com/science/article/pii/S0960077913001343>.

CHEN, Y. Defining urban and rural regions by multifractal spectrums of urbanization. **Fractals**, v. 24, n. 01, p. 1650004, 2016. Disponível em: <https://doi.org/10.1142/S0218348X16500043>.

CHEN, Y. Two sets of simple formulae to estimating fractal dimension of irregular boundaries. **Mathematical Problems in Engineering**, 2020.

CHEN, Y.; HUANG, L. Spatial measures of urban systems: from entropy to fractal dimension. **Entropy**, v. 20, n. 12, 2018. ISSN 1099-4300. Disponível em: <https://www.mdpi.com/1099-4300/20/12/991>.

CHEN, Y.; WANG, J. Multifractal characterization of urban form and growth: the case of beijing. **Environment and Planning B: Planning and Design**, v. 40, p. 884 – 904, 2013.

CHEN, Y.; ZHOU, Y. Scaling laws and indications of self-organized criticality in urban systems. **Chaos, Solitons and Fractals**, v. 35, n. 1, p. 85–98, 2008. ISSN 0960-0779. Disponível em: <https://www.sciencedirect.com/science/article/pii/S0960077906004577>.

CHEN, Y.-G. Logistic models of fractal dimension growth of urban morphology. **Fractals**, v. 26, n. 03, p. 1850033, 2018. Disponível em: <https://doi.org/10.1142/S0218348X18500330>.

CHLOUVERAKIS, K.; SPROTT, J. C. A comparison of correlation and lyapunov dimensions. **Physica D: Nonlinear Phenomena**, v. 200, 01 2005.

CORRAL, A.; BOLEDA, G.; FERRERI-CANCHO, R. Zipf's law for word frequencies: Word forms versus lemmas in long texts. **PLOS ONE**, Public Library of Science, v. 10, n. 7, p. 1–23, 07 2015. Disponível em: <https://doi.org/10.1371/journal.pone.0129031>.

COSTA, L. da F. et al. Characterization of complex networks: A survey of measurements. **Advances in Physics**, v. 1, n. 56, p. 167–242, 2007.

COURTAT, T.; GLOAGUEN, C.; DOUADY, S. Mathematics and morphogenesis of cities: A geometrical approach. **Physical Review E**, APS, v. 83, n. 3, p. 036106, 2011.

CRUCITTI, P.; LATORA, V.; PORTA, S. Centrality in networks of urban streets. **Chaos: An Interdisciplinary Journal of Nonlinear Science**, v. 16, n. 1, p. 015113, 03 2006. ISSN 1054-1500. Disponível em: <https://doi.org/10.1063/1.2150162>.

CZYŻA, S. et al. An analysis of the spatial development of european cities based on their geometry and the corine land cover (clc) database. **International Journal of Environmental Research and Public Health**, v. 20, n. 3, 2023. ISSN 1660-4601. Disponível em: <https://www.mdpi.com/1660-4601/20/3/2049>.

DEPPMAN, A.; MEGÍAS, E.; MENEZES, D. P. Fractals, nonextensive statistics, and qcd. **Phys. Rev. D**, American Physical Society, v. 101, p. 034019, Feb 2020. Disponível em: <https://link.aps.org/doi/10.1103/PhysRevD.101.034019>.

DEPREZ, P.; WÜTHRICH, M. V. Networks, random graphs and percolation. In: _____. **Theoretical Aspects of Spatial-Temporal Modeling**. Tokyo: Springer Japan, 2015. p. 95–124. ISBN 978-4-431-55336-6. Disponível em: <https://doi.org/10.1007/978-4-431-55336-6_4>.

DIJKSTRA, E. A note on two problems in connexion with graphs. **Numer. Math. 1,**, p. 269–271, 1959.

DING, R. et al. Application of complex networks theory in urban traffic network researches. **Networks and Spatial Economics**, v. 19, 12 2019.

DROZDZ, S.; OSWIECIMKA, P. Detecting and interpreting distortions in hierarchical organization of complex time series. **Phys. Rev. E**, American Physical Society, v. 91, p. 030902, Mar 2015. Disponível em: <https://link.aps.org/doi/10.1103/PhysRevE.91.030902>.

ERDÖS, P.; RÉNYI, A. On random graphs i. **Publ. Math.**, p. 290, December 1959.

ERDOS, P.; RENYI, A. On the evolution of random graphs. **Publication of the Mathematical Institute of the Hungarian Academy of Sciences**, v. 5, p. 17–60, 1960.

EVANS, T. S.; CHEN, B. Linking the network centrality measures closeness and degree. **Commun Phys**, v. 172, n. 5, 2022.

FALCONER, K. **Fractal geometry: mathematical foundations and applications**. [S.l.]: John Wiley and Sons, 2004.

FALCONER, K. **Fractals**. [S.l.]: Oxford University Press, 2013. ISBN 978–0–19–967598–2.

FALCONER, K. J.; LAMMERING, B. Fractal properties of generalized sierpiński triangles. **Fractals**, v. 06, n. 01, p. 31–41, 1998. Disponível em: <https://doi.org/10.1142/S0218348X98000055>.

FARMER, J. D. Information dimension and the probabilistic structure of chaos. **Zeitschrift für Naturforschung A**, v. 37, p. 1304 – 1326, 1982. Disponível em: <https://api.semanticscholar.org/CorpusID:3502678>.

FEDER, J. **Fractals**. [S.l.]: Springer Science Business Media, 1988.

FERNANDES, T.; FILHO, J.; LOPES, I. Fractal signature of coronaviruses related to severe acute respiratory syndrome. **Research on Biomedical Engineering**, v. 38, 06 2020.

FILHO, A. C. da S.; MAGANINI, N. D.; ALMEIDA, E. W. A. D. Multifractal analysis of bitcoin market. **Physica A: Statistical Mechanics and its Applications**, 2018.

FRAME, M.; NEGER, N. **Kitchen Science Fractals: A Lab Manual for Fractal Geometry**. [S.l.]: World Scientific, 2022.

FRANKHAUSER, P. Fractal geometry for measuring and modelling urban patterns. In: _____. **The dynamics of complex urban systems: an interdisciplinary approach**. Heidelberg: Physica-Verlag HD, 2008. p. 213–243. ISBN 978-3-7908-1937-3. Disponível em: <https://doi.org/10.1007/978-3-7908-1937-3_11>.

FRIGG, R.; HARTMANN, S. Models in Science. In: ZALTA, E. N. (Ed.). **The Stanford Encyclopedia of Philosophy**. Spring 2020. [S.l.]: Metaphysics Research Lab, Stanford University, 2020.

GARRISON, W. Connectivity of the interstate highway system. **Papers of the Regional Science Association**, p. 121–137, 6 1960.

GIACOMUCCI, S. Sociometry and social work theory. In: _____. **Social Work, Sociometry, and Psychodrama: Experiential Approaches for Group Therapists, Community Leaders, and Social Workers**. Singapore: Springer Singapore, 2021. p. 83–100. ISBN 978-981-33-6342-7. Disponível em: <https://doi.org/10.1007/978-981-33-6342-7_5>.

GLERIA, I.; MATSUSHITA, R.; SILVA, S. D. Sistemas complexos, criticalidade e leis de potência. **Revista Brasileira de Ensino de Física**, Sociedade Brasileira de Física, v. 26, n. 2, p. 99–108, 2004. ISSN 1806-1117. Disponível em: <https://doi.org/10.1590/S0102-47442004000200004>.

GRANDJEAN, M. Social network analysis and visualization: Moreno's sociograms revisited. 2015. Disponível em: <http://www.martingrandjean.ch/social-network-analysis-visualization-morenos-sociograms-revisited/>.

GRANOVETTER, M. S. The strength of weak ties. **AJS**, v. 78, 1973.

GUO, M. et al. Impact of socio-economic environment and its interaction on the initial spread of COVID-19 in mainland China. **Geospatial Health**, v. 17, n. s1, Mar. 2022. Disponível em: <https://www.geospatialhealth.net/index.php/gh/article/view/1060>.

HALSEY, T. C. et al. Fractal measures and their singularities: The characterization of strange sets. **Phys. Rev. A**, American Physical Society, v. 33, p. 1141–1151, Feb 1986. Disponível em: <https://link.aps.org/doi/10.1103/PhysRevA.33.1141>.

HARTE, D. **Multifractals Theory and Applications**. [S.l.]: Chapman and Hall/CRC, 2001.

HE, H. Multifractal analysis of interactive patterns between meteorological factors and pollutants in urban and rural areas. **Atmospheric Environment**, v. 149, p. 47–54, 2017.

HERRMANN, H.; STANLEY, H. The fractal dimension of the minimum path in two-and three-dimensional percolation. **Journal of Physics A: Mathematical and General**, v. 21, p. L829, 01 1999.

HIDALGO, C. **How Information Grows: The Evolution of Order, from Atoms to Economies**. [S.l.]: Basic Books, 2015.

HILLIER, B.; HANSON, J. **The social logic of space**. [S.l.]: Cambridge university press, 1989.

HUBERT, P. Multifractals as a tool to overcome scale problems in hydrology. **Hydrological Sciences Journal**, v. 46, p. 897 – 905, 2001.

HUFF, D. L. A probabilistic analysis of shopping center trade areas. **Land Economics**, [Board of Regents of the University of Wisconsin System, University of Wisconsin Press], v. 39, n. 1, p. 81–90, 1963. ISSN 00237639. Disponível em: <http://www.jstor.org/stable/3144521>.

IHLEN, E. Multifractal analyses of response time series: A comparative study. **Behavior Research Methods**, v. 45, p. 928–945, 2013.

JOHNSON, N. F. **Simplify Complexity: A Clear Guide to Complexity Theory**. [S.l.]: Oneworld Oxford, 2009.

JOHNSON, N. F.; JEFFERIES, P.; HUI, P. M. **Financial Market Complexity**. Oxford University Press, 2003. ISBN 9780198526650. Disponível em: <https://doi.org/10.1093/acprof:oso/9780198526650.001.0001>.

KAK, S. Information theory and dimensionality of space. **Sci. Rep.**, v. 10, n. 1, p. 20733, 2020.

KANSKY., K. The structure of transportation networks: Relationships between network geography and regional characteristics. **Chicago: University of Chicago, 1963. Research Paper No. 84.**, 1963.

KEUSCHNIGG, M. Scaling trajectories of cities. **Proceedings of the National Academy of Sciences**, v. 116, n. 28, p. 13759–13761, 2019. Disponível em: <https://www.pnas.org/doi/abs/10.1073/pnas.1906258116>.

KYURKCHIEV, N.; MARKOV, S. **Sigmoid Functions: some approximation, and modelling aspects**. AP Lambert Academic Publishing, 2015. Disponível em: <http://www.biomath.bg/s%20markov%20publications/B2015-Kyurkchiev_Markov_Lambert.pdf>.

LEE, M.; BARBOSA, H.; YOUN, H. Morphology of travel routes and the organization of cities. **Nat Commun**, v. 8, n. 2229, 12 2017. Disponível em: <https://doi.org/10.1038/s41467-017-02374-7>.

LIU, D. et al. Precipitation complexity measurement using multifractal spectra empirical mode decomposition detrended fluctuation analysis. **Water Resources Management**, v. 30, p. 505–522, 2015.

LOBO, J. et al. Urban science: Integrated theory from the first cities to sustainable metropolises. **SSRN Electronic Journal**, 01 2020.

LONG, Y.; CHEN, Y. Multifractal scaling analyses of urban street network structure: The cases of twelve megacities in china. **PLOS ONE**, Public Library of Science, v. 16, n. 2, p. 1–23, 02 2021. Disponível em: <https://doi.org/10.1371/journal.pone.0246925>.

LOPES, R.; BETROUNI, N. Fractal and multifractal analysis: A review. **Medical Image Analysis**, v. 13, n. 4, p. 634–649, 2009. ISSN 1361-8415. Disponível em: <https://www.sciencedirect.com/science/article/pii/S1361841509000395>.

LOVEJOY, S. The 2021 “complex systems” nobel prize: The climate, with and without geocomplexity. **AGU Advances**, v. 3, n. 6, p. e2021AV000640, 2022. E2021AV000640 2021AV000640. Disponível em: <https://agupubs.onlinelibrary.wiley.com/doi/abs/10.1029/2021AV000640>.

LUCAS, R. E. On the mechanics of economic development. **Journal of Monetary Economics**, v. 22, n. 1, p. 3–42, 1988. ISSN 0304-3932. Disponível em: <https://www.sciencedirect.com/science/article/pii/0304393288901687>.

LYRA, M. L.; TSALLIS, C. Nonextensivity and multifractality in low-dimensional dissipative systems. **Phys. Rev. Lett.**, American Physical Society, v. 80, p. 53–56, Jan 1998. Disponível em: <https://link.aps.org/doi/10.1103/PhysRevLett.80.53>.

MALLION, R. B. The six (or seven) bridges of kaliningrad: a personal eulerian walk, 2006. **MATCH Commun. Math. Comput. Chem.**, n. 58, p. 529–556, 2007.

MANDELBROT, B. **Les Objects Fractals: Forme, hasard et dimenion**. 4. ed. [S.l.]: Flammarion, 1995.

MANDELBROT, B.; FREEMAN, W. H.; COMPANY. **The Fractal Geometry of Nature**. Henry Holt and Company, 1983. (Einaudi paperbacks). ISBN 9780716711865. Disponível em: <https://books.google.com.br/books?id=SWcPAQAAMAAJ>.

MANDELBROT, B. B. Self-affine fractal sets, i: The basic fractal dimensions. In: PIETRONERO, L.; TOSATTI, E. (Ed.). **Fractals in Physics**. Amsterdam: Elsevier, 1986. p. 3–15. ISBN 978-0-444-86995-1. Disponível em: <https://www.sciencedirect.com/science/article/pii/B9780444869951500044>.

MARSILI, M.; ZHANG, Y.-C. Interacting individuals leading to zipf’s law. **Phys. Rev. Lett.**, American Physical Society, v. 80, p. 2741–2744, Mar 1998. Disponível em: <https://link.aps.org/doi/10.1103/PhysRevLett.80.2741>.

MARTÍNEZ, F.; SEPÚLVEDA, B.; MANRÍQUEZ, H. Fractal organization of chilean cities: Observations from a developing country. **Land**, 2023. Disponível em: <https://api.semanticscholar.org/CorpusID:256142773>.

MATA, A. S. d. Complex networks: a mini-review. **Brazilian Journal of Physics**, v. 50, n. 5, p. 658–672, oct 2020. Disponível em: <https://ui.adsabs.harvard.edu/abs/2020BrJPh..50..658M>.

MERTON, R. K. The matthew effect in science: The reward and communication systems of science are considered. **Science**, 1968.

MILGRAM, S. The small-world problem. **Psychology Today**, v. 1, n. 1, p. 61–67, 1967.

MOLINERO, C. A fractal theory of urban growth. **Frontiers in Physics**, v. 10, 2022. ISSN 2296-424X. Disponível em: <https://www.frontiersin.org/articles/10.3389/fphy.2022.861678>.

MOLINERO, C.; THURNER, S. How the geometry of cities determines urban scaling laws. **Journal of the Royal Society interface**, The Royal Society, v. 18, n. 176, p. 20200705, 2021.

MOLONTAY, R. **Fractal Characterization of Complex Networks.** 2015. Disponível em: <https://math.bme.hu/~molontay/Msc_MolontayR.pdf>.

MOORE, B.; DASI, L. P. Multi-fractal nature of human left ventricular trabeculae: Possible biomechanical role? **Chaos, Solitons and Fractals**, v. 57, p. 19–23, 2013. ISSN 0960-0779. Disponível em: <https://www.sciencedirect.com/science/article/pii/S0960077913001586>.

MORENO, J. L. **Who shall survive?: A new approach to the problem of human interrelations.** [S.l.]: Nervous and Mental Disease Publishing Co., 1934.

MORENO, J. L. et al. **Application of the group method to classification**. 2. ed. [S.l.]: National committee on prisons and prison labor, 1932.

MUNROE, D. K.; BILES, J. J. Regional science. In: KEMPF-LEONARD, K. (Ed.). **Encyclopedia of Social Measurement**. New York: Elsevier, 2005. p. 325–335. ISBN 978-0-12-369398-3. Disponível em: <https://www.sciencedirect.com/science/article/pii/B0123693985003650>.

MURCIO, R. et al. Multifractal to monofractal evolution of the london street network. **Phys. Rev. E**, American Physical Society, v. 92, p. 062130, Dec 2015. Disponível em: <https://link.aps.org/doi/10.1103/PhysRevE.92.062130>.

NAKAYAMA, T.; YAKUBO, K. **Fractal Concepts in Condensed Matter Physics**. [S.l.: s.n.], 2003. v. 140. ISBN 978-3-642-05711-3.

NATALIA, Y. et al. Fractal dimension based geographical clustering of covid-19 time series data. **Scientific Reports**, v. 13, 03 2023.

NATIONS, U. **New urban agenda: H III: Habitat III: Quito 17-20**. 2016. Disponível em: <https://habitat3.org/the-new-urban-agenda>.

NATIONS, U. **World Population Prospects: The 2017 Revision, Key Findings and Advance Tables.** New York, 2017. Disponível em: <https://population.un.org/wpp/publications/files/wpp2017_keyfindings.pdf>.

NEWMAN., M. E. J. **Networks: An Introduction.** [S.l.]: Oxford University Press, 2016.

NEWMAN, M. E. J.; WATTS, D. J.; STROGATZ, S. H. Random graph models of social networks. **Proceedings of the National Academy of Sciences**, v. 99, n. suppl_1, p. 2566–2572, 2002. Disponível em: <https://www.pnas.org/doi/abs/10.1073/pnas.012582999>.

NGAI, S.-M.; XU, Y. Existence of lq-dimension and entropy dimension of self-conformal measures on riemannian manifolds. **Nonlinear Analysis**, Elsevier, v. 230, p. 113226, 2023.

NICHOLS, J. M. et al. Controlling system dimension: A class of real systems that obey the kaplan–yorke conjecture. **Proceedings of the National Academy of Sciences**, v. 100, n. 26, p. 15299–15303, 2003. Disponível em: <https://www.pnas.org/doi/abs/10.1073/pnas.2535197100>.

OTT, E. **Chaos in Dynamical Systems**. 2. ed. [S.l.]: Cambridge University Press, 2002.

PALADIN, G.; VULPIANI, A. Anomalous scaling laws in multifractal objects. **physrep**, v. 156, n. 4, p. 147–225, dec 1987.

PARETO, V. Cours d'economie politique. **F. Rouge Lausanne**, v. 2, 1897.

PAVÓN-DOMÍNGUEZ, P.; JIMÉNEZ-HORNERO, F. J.; RAVÉ, E. G. de. Joint multifractal analysis of the influence of temperature and nitrogen dioxide on tropospheric ozone. **Stochastic Environmental Research and Risk Assessment**, v. 29, p. 1881–1889, 2015.

PERES, Y.; SOLOMYAK, B. Existence of lq dimensions and entropy dimension for self-conformal measures. **Indiana University Mathematics Journal**, Indiana University Mathematics Department, v. 49, n. 4, p. 1603–1621, 2000. ISSN 00222518, 19435258. Disponível em: <http://www.jstor.org/stable/24901114>.

PITSIANIS, N.; BLERIS, L.; ARGYRAKIS, P. Information dimension in fractal structures. **Physical review. B - Condensed matter**, v. 39, p. 7097–7100, 05 1989.

PRICE, D. J. de S. Networks of scientific papers: The pattern of bibliographic references indicates the nature of the scientific research front. **Science**, v. 149, n. 3683, p. 510–515, 1965. Disponível em: <https://www.science.org/doi/abs/10.1126/science.149.3683.510>.

QUARTERONI, A. Mathematical models in science and engineering. **Notices of the AMS**, v. 56, n. 1, 2009.

RAPOPORT, A. Contribution to the theory of random and biased nets. **Bulletin of Mathematical Biophysics**, v. 19, p. 257–277, 1957.

RÉNYI, A. On a new axiomatic theory of probability. **Acta Mathematica Academiae Scientiarum Hungarica**, v. 6, p. 285–335, 1955. Disponível em: <https://api.semanticscholar.org/CorpusID:121218256>.

RIBEIRO, F. L. et al. A model of urban scaling laws based on distance dependent interactions. **R. Soc. Open Sci.**, v. 4, n. 160926, 2017.

RIBEIRO, F. L.; RYBSKI, D. Mathematical models to explain the origin of urban scaling laws. **Physics Reports**, v. 1012, p. 1–39, 2023. ISSN 0370-1573. Mathematical models to explain the origin of urban scaling laws. Disponível em: <https://www.sciencedirect.com/science/article/pii/S0370157323000650>.

RODRIGUE, J.-P. **The Geography of Transport Systems**. [S.l.]: Routledge, 2020. 456 p.

ROSENBERG, E. **Fractal Dimensions of Networks**. 1. ed. [S.l.]: Springer Cham, 2021.

ROSENBLUETH, A.; WIENER, N. The role of models in science. **Philosophy of Science**, [The University of Chicago Press, Philosophy of Science Association], v. 12, n. 4, p. 316–321, 1945. ISSN 00318248, 1539767X. Disponível em: <http://www.jstor.org/stable/184253>.

ROSNI, N. A.; NOOR, N. M. A review of literature on urban sprawl: Assessment of factors and causes. **JOURNAL OF ARCHITCTURE, PLANNING and CONSTRUCTION MANAGEMENT**, v. 6, 2016.

RYBSKI, D.; CICCONE, A. Auerbach, lotka, and zipf: pioneers of power-law city-size distributions. **Arch. Hist. Exact Sci.**, 2023.

RYBSKI, D.; GONZALEZ, M. C. Cities as complex systems—collection overview. **PLOS ONE**, Public Library of Science, v. 17, n. 2, p. 1–6, 02 2022. Disponível em: <https://doi.org/10.1371/journal.pone.0262964>.

SACHS, H.; STIEBITZ, M.; WILSON, R. J. An historical note: Euler's konigsberg letters. **Journal of Graph Theory**, v. 12, n. 1, p. 133–139, 1988.

SALAT, H.; MURCIO, R.; ARCAUTE, E. Multifractal methodology. **Physica A: Statistical Mechanics and its Applications**, v. 473, p. 467–487, 2017. ISSN 0378-4371. Disponível em: <https://www.sciencedirect.com/science/article/pii/S0378437117300341>.

SALLIS, P. et al. Use of science to guide city planning policy and practice: How to achieve healthy and sustainable future cities. **The Lancet**, v. 388, 09 2016.

SAMOYLENKO, I. et al. Why are there six degrees of separation in a social network? **Phys. Rev. X**, American Physical Society, v. 13, p. 021032, May 2023. Disponível em: <https://link.aps.org/doi/10.1103/PhysRevX.13.021032>.

SANTOS, F. S. D. et al. Multifractal analysis of solar radiation in the northeastern region of brazil. **Fractals**, v. 31, n. 03, p. 2350026, 2023. Disponível em: <https://doi.org/10.1142/S0218348X23500263>.

SANTOS, P. H. N.; CRUZ, M. G.; SANTOS, W. F. S. City science and urban planning: geoprocessing as an instrument for municipal strategic planning. v. 6, 2022. Disponível em: <https://doi.org/10.22481/rg.v6.e2022.e9180>.

SAYAMA, H. **Introduction to the Modeling and Analysis of Complex Systems**. SUNY, 2015. ISBN 13: 9781942341093. Disponível em: <https://open.umn.edu/opentextbooks/textbooks/233>.

SCHERTZER, D.; LOVEJOY, S.; HUBERT, P. An introduction to stochastic multifractal fields. In: HIGHER EDUCATION PRESS BEIJING. **ISFMA Symposium on Environmental Science and Engineering with related Mathematical Problems**. [S.l.], 2002. v. 4, p. 106–179.

SCHROEDER, M. **Fractal Chaos and Power Laws: Minutes from Infinite Paradise.** [S.l.]: W. H. Freeman and Company, 1991.

SEMECURBE, F.; TANNIER, C.; ROUX, S. G. Spatial distribution of human population in france: exploring the modifiable areal unit problem using multifractal analysis. **Geographical Analysis**, v. 48, n. 3, p. 292–313, 2016. Disponível em: <https://onlinelibrary.wiley.com/doi/abs/10.1111/gean.12099>.

SEVTSUK, A.; MEKONNEN, M. Urban network analysis. a new toolbox for arcgis. **Revue internationale de géomatique**, v. 22, p. 287–305, 06 2012.

SEVTSUK, A.; RATTI, C. Does urban mobility have a daily routine? learning from the aggregate data of mobile networks. **Journal of Urban Technology**, Routledge, v. 17, n. 1, p. 41–60, 2010. Disponível em: <https://doi.org/10.1080/10630731003597322>.

SHARIFI, A. Resilient urban forms: A review of literature on streets and street networks. **Building and Environment**, v. 147, p. 171–187, 2019. ISSN 0360-1323. Disponível em: <https://www.sciencedirect.com/science/article/pii/S0360132318305985>.

SIEGENFELD, A. F.; BAR-YAM, Y. An introduction to complex systems science and its applications. **Complexity**, Hindawi, v. 2020, 2020.

SILVA, A. S. A. da et al. Multifractal analysis of standardized precipitation index in northeast brazil. **Chaos, Solitons and Fractals**, v. 172, p. 113600, 2023. ISSN 0960-0779. Disponível em: <https://www.sciencedirect.com/science/article/pii/S0960077923005015>.

SKKUMAR, K. K. Fractal dimension for data mining. In: . [s.n.], 2003. Disponível em: <https://api.semanticscholar.org/CorpusID:16847233>.

SONG, Z.; CHEN, Y.; BO, M. Multifractal characteristics analysis of spatial state of prefecture-level cities in china. **Appl. Spatial Analysis**, 2023.

STANLEY, H.; MEAKIN, P. Multifractal phenomena in physics and chemistry. **Nature**, v. 335, p. 405–409, 09 1988.

STEINDL, J. **Random Processes and the Growth of Firms: A Study of the Pareto Law**. [S.l.]: Ashgate Publishing Limited, 1965.

STEPINSKI, T. F.; DMOWSKA, A. Complexity in patterns of racial segregation. **Chaos, Solitons and Fractals**, v. 140, p. 110207, 2020. ISSN 0960-0779. Disponível em: <https://www.sciencedirect.com/science/article/pii/S0960077920306032>.

STRANO, E. et al. The scaling structure of the global road network. **Royal Society Open Science**, v. 4, n. 10, p. 170590, 2017. Disponível em: <https://royalsocietypublishing.org/doi/abs/10.1098/rsos.170590>.

TAKAYASU, H. **Fractals in physical sciences**. 2. ed. [S.l.]: Machester University Press, 1990.

TEL, T.; FULOP, A.; VICSEK, T. Determination of fractal dimensions for geometrical multifractals. **Physica A: Statistical Mechanics and its Applications**, v. 159, n. 2, p. 155–166, 1989. ISSN 0378-4371. Disponível em: <https://www.sciencedirect.com/science/article/pii/0378437189905633>.

TEL, T.; GRUIZ, M. **Chaotic Dynamics: An Introduction Based on Classical Mechanics**. [S.l.]: Cambridge University Press, 2006.

TEL, T.; VICSEK, T. Geometrical multifractality of growing structures. **Journal of Physics A: Mathematical and General**, IOP Publishing, v. 20, n. 13, p. L835, 1987.

TERO, A. et al. Rules for biologically inspired adaptive network design. **Science**, v. 327, n. 5964, p. 439–442, 2010. Disponível em: <https://www.science.org/doi/abs/10.1126/science.1177894>.

THEILER, J. Estimating fractal dimension. **JOSA A**, n. 7, p. 1055–1073, 1990.

THERAULAZ, G. et al. Spatial patterns in ant colonies. **Proceedings of the National Academy of Sciences**, v. 99, n. 15, p. 9645–9649, 2002. Disponível em: <https://www.pnas.org/doi/abs/10.1073/pnas.152302199>.

TOBLER, W. R. A computer movie simulating urban growth in Detroid region. **Economic Geography**, v. 46, p. 234–240, 1970.

TSALLIS, C. Possible generalization of boltzmann-gibbs statistics. **Journal of Statistical Physics**, v. 52, p. 479–487, 07 1988.

VICSEK, T. **Fractal Growth Phenomena**. 2. ed. [S.l.]: World Scientific, 1992.

WANG, D.-L.; YU, Z.-G.; ANH, V. Multifractal analysis of complex networks. **Chinese Physics B**, IOP Publishing, v. 21, n. 8, 2012.

WATTS, D.; STROGATZ, S. Collective dynamics of 'small-world' networks. **Nature**, v. 393, p. 440–442, 1998.

WEN, W.; ZHANG, W.; DENG, H. Research on urban road network evaluation based on fractal analysis. **Journal of Advanced Transportation**, 2023. Disponível em: <https://api.semanticscholar.org/CorpusID:256076535>.

WENDT, H.; ABRY, P. Bootstrap for multifractal analysis. **2006 IEEE International Conference on Acoustics Speech and Signal Processing Proceedings**, v. 3, p. III–III, 2006.

WILSON, A. A statistical theory of spatial distribution models. **Transportation Research**, v. 1, n. 3, p. 253–269, 1967. ISSN 0041-1647. Disponível em: <https://www.sciencedirect.com/science/article/pii/0041164767900354>.

WILSON, A. Entropy in urban and regional modelling: Retrospect and prospect. **Geographical Analysis**, v. 42, n. 4, p. 364–394, 2010. Disponível em: <https://onlinelibrary.wiley.com/doi/abs/10.1111/j.1538-4632.2010.00799.x>.

WOODCOCK, J. et al. Public health benefits of strategies to reduce greenhouse-gas emissions: urban land transport. **The Lancet**, Elsevier, v. 374, n. 9705, p. 1930–1943, 2009.

XIANG, J. et al. Multifractal analysis of river networks in an urban catchment on the taihu plain, china. **Water**, v. 11, p. 2283, 10 2019.

YAHIA, H. et al. Description of turbulent dynamics in the interstellar medium: Multifractal-microcanonical analysis i. application to herschel observations of the musca filament. **Astronomy and Astrophysics**, v. 649, 03 2021.

YAKUBO, K.; SAIJO, Y.; KOROVSAK, D. Superlinear and sublinear urban scaling in geographical networks modeling cities. **Phys. Rev. E**, American Physical Society, v. 90, p. 022803, Aug 2014. Disponível em: <https://link.aps.org/doi/10.1103/PhysRevE.90.022803>.

ZHAO, F.-X.; LIU, J.-L.; ZHOU, Y. Sandbox edge-based algorithm for multifractal analysis of complex networks. **Chaos, Solitons and Fractals**, v. 173, p. 113719, 2023. ISSN 0960-0779. Disponível em: <https://www.sciencedirect.com/science/article/pii/S0960077923006203>.

ZHOU, Z. et al. Shortest-path fractal dimension for percolation in two and three dimensions. **Phys. Rev. E**, American Physical Society, v. 86, p. 061101, Dec 2012. Disponível em: <https://link.aps.org/doi/10.1103/PhysRevE.86.061101>.

ZIPF, G. K. **Human behavior and the principle of least effort**. [S.l.]: Addison-Wesley, 1949.

ZMESKAL, O.; DZIK, P.; VESELY, M. Entropy of fractal systems. **Computers and Mathematics with Applications**, v. 66, n. 2, p. 135–146, 2013. ISSN 0898-1221. Nostradamus 2012. Disponível em: <https://www.sciencedirect.com/science/article/pii/S0898122113000345>.

ÖZDEMIR, O. The performance of top coronavirus vaccine stocks during covid-19 pandemic: A multifractal analysis. **Sosyoekonomi**, Sosyoekonomi Derneği, v. 31, n. 56, p. 27 – 46, 2023. ISSN 1305-5577.

APPENDIX A – Self-Similar Multifractal

In this appendix, we demonstrate how a system of iterated functions with memory can be used to study self-similar multifractals. If we consider a self-similar fractal generated from an Iteration Function System (IFS) with memory, like

$$\begin{cases} T_1(x,y) = & (sx\cos\theta, -ry\sin\theta) + (g,f), \\ T_2(x,y) = & (sx\sin\theta, ry\cos\theta) + (g,f), \\ T_3(x,y) = & (sx\cos\theta, ry\sin\theta) + (g,f), \\ T_4(x,y) = & (-sx\sin\theta, ry\cos\theta + f) + (g,f) \end{cases} \tag{A.1}$$

we can generate some beautiful multifractals. A IFS with memory is a set of similarity transformations that we can apply to an initial pair of coordinates, such as the origin of coordinates $x = 0$, $y = 0$, with restrictions on the transitions between the transformations considered, which means that some transformations are prohibited and others are not, then the term memory is because there is some prohibited transitions. If there is a set of similarity transformations $i = (1, \cdots, n)$ denoted by T_i, it is possible to associate a probability p_i with it such that some transformation can occur more likely than others (BARNSLEY; DEMKO, 1985; FRAME; NEGER, 2022).

In general, if we have an IFS with n transformation, we can define a generalized Moran's equation

$$\sum_i p_i^q r_i^{\tau(q)} = 1, \tag{A.2}$$

where r_i is the contraction factor of the similarity transformation T_i and p_i is the probability with which T_i is applied to the fractal points. $\tau(q)$ is the mass exponent, which describes how the mass of fractal change with r_i and q is the moments of order. Applying the natural logarithm to both sides of the equation follows

$$\ln\left(\sum_i p_i^q r_i^{\tau(q)}\right) = \ln\left(\sum_i p_i^q\right) + \ln\left(\sum_i r_i^{\tau(q)}\right) = 0 \tag{A.3}$$

so that the mass exponents can be written as follows

$$\tau(q) = -\frac{\ln\left(\sum_i p_i^q\right)}{\ln\left(\sum_i r_i\right)}. \tag{A.4}$$

By implicitly deriving both sides of the previous equation with respect to q, it follows

$$\frac{d}{dq}\left(\sum_i p_i^q r_i^{\tau(q)}\right) = \frac{d}{dq}\left(\sum_i p_i^q\right) r_i^{\tau(q)} + \sum_i p_i^q \frac{d}{dq}\left(r_i^{\tau(q)}\right) = 0. \tag{A.5}$$

But

$$\frac{d}{dq}\left(\sum_i p_i^q\right) = \sum_i \frac{d}{dq} p_i^q = \sum_i p_i^q \ln p_i \tag{A.6}$$

and

$$\frac{d}{dq}\left(r_i^{\tau(q)}\right) = r_i^{\tau(q)} \ln r_i \frac{d}{dq}\tau(q). \tag{A.7}$$

So, taking these results into eq. (A.5), we get

$$\sum_i p_i^q \ln p_i r_i^{\tau(q)} + \sum_i p_i^q r_i^{\tau(q)} \ln r_i \frac{d}{dq}\tau(q) = 0, \tag{A.8}$$

which solving for the derivative of the mass exponents results in

$$\frac{d}{dq}\tau(q) = -\frac{\sum_i p_i^q r_i^{\tau(q)} \ln p_i}{\sum_i p_i^q r_i^{\tau(q)} \ln r_i}. \tag{A.9}$$

Now, defining the singularity indexes by

$$\alpha(q) = -\frac{d}{dq}\tau(q) \tag{A.10}$$

and noticing that

$$d\tau(q) = -\alpha(q)dq = -\alpha(q)dq - qd\alpha(q) + qd\alpha(q), \tag{A.11}$$

we have

$$d\left(\tau(q) + q\alpha(q)\right) = qd\alpha(q), \tag{A.12}$$

making it possible to define

$$f(\alpha(q)) \equiv \tau(q) + q\alpha(q) \tag{A.13}$$

such as the multifractal spectrum associated with the generalized Moran equation or even

$$f(\alpha(q)) = \frac{\sum_i p_i^q r_i^{\tau(q)} \ln p_i^q}{\sum_i p_i^q r_i^{\tau(q)} \ln r_i} - \frac{\ln\left(\sum_i p_i^q\right)}{\ln\left(\sum_i r_i\right)}. \tag{A.14}$$

In addition, we can also define the generalized dimensions using

$$D_q = \frac{\tau(q)}{1-q}. \tag{A.15}$$

Therefore, if we impose transition rules for each transformation T_i $(i = 1, 2, 3, 4)$ of the form

$$1 \to 1, 2, 4; \quad 2 \to 1, 3, 4; \quad 3 \to 1, 2, 4; \quad 4 \to 4,$$

we can see that the forbidden transitions are: i) from 1 to 3; ii) from 2 to 2; iii) from 3 to 3; iv) from 4 to 1, 2, and 3. In particular, considering $s = 1 = -r$, $\theta = \pi/4$ and $g = f = 1$ in the eq. (A.1), we have

$$\begin{cases} T_1(x,y) &= \left(\frac{\sqrt{2}}{2}x + 1, \frac{\sqrt{2}}{2}y + 1\right) \\ T_2(x,y) &= \left(\frac{\sqrt{2}}{2}x + 1, -\frac{\sqrt{2}}{2}y + 1\right) \\ T_3(x,y) &= \left(\frac{\sqrt{2}}{2}x + 1, -\frac{\sqrt{2}}{2}y + 1\right) \\ T_4(x,y) &= \left(-\frac{\sqrt{2}}{2}x + 1, -\frac{\sqrt{2}}{2}y + 1\right) \end{cases} \tag{A.16}$$

Also, if we choose the following probabilities and contraction factor

$$p_1 = p_2 = p_3 = \frac{1}{10},\ p_4 = \frac{7}{10}, \quad r_i = r = \frac{1}{2}\ (i = 1, 2, 3, 4), \tag{A.17}$$

is not difficult to show that

$$\tau(q) = \frac{\log\left(\frac{10^q}{3+7^q}\right)}{\log r}, \qquad D_q = \frac{1}{1-q}\frac{\log\left(\frac{10^q}{3+7^q}\right)}{\log r}, \tag{A.18}$$

$$\alpha(q) = \frac{\left(\frac{7^q}{3+7^q}\right)\log 7 - \log 10}{\log r}, \qquad f(q) = \frac{\left(\frac{7^q}{3+7^q}\right)\log 7^q - \log 10^q + \log\left(\frac{10^q}{3+7^q}\right)}{\log r}. \tag{A.19}$$

In Section 2.1.4 we present the theoretical formalism of generalized dimensions and the multifractal spectrum.

APPENDIX B – Multifractal Modeling

In this appendix we present the mathematical construction of the multifractal modeling. First, by observing the behavior of the inverted "S" type of generalized dimensions, an interesting *ansatz* that we can use to model this quantity is from a sigmoid function, a function widely used in economics and computing. Therefore, assume that the generalized dimensions of the street network (SN) and population (Pop) are described by

$$D_q = a + \frac{b}{1 + ce^{dq}}. \tag{B.20}$$

We can obtain the mass exponents in terms of generalized dimensions, so we have

$$\tau(q) = (1-q)D_q = (1-q)\left[a + \frac{b}{1 + ce^{dq}}\right]. \tag{B.21}$$

Without loss of generality, we can also express the singularity exponents through

$$\alpha(q) = -\frac{d\tau(q)}{dq} = a + \frac{b}{1 + ce^{dq}} - \frac{bcd(q-1)e^{dq}}{(1 + ce^{dq})^2}, \tag{B.22}$$

while the spectrum of singularities can be written as

$$f(\alpha(q)) = q\alpha(q) + \tau(q) = a + \frac{b}{1 + ce^{dq}} - \frac{bcdq(q-1)e^{dq}}{(1 + ce^{dq})^2}. \tag{B.23}$$

However, we can obtain the dimensions of the capacity, information, correlation and the limiting dimensions, when the moments of order q approach $\pm\infty$, in terms of the parameters a, b, c and d, that is:

$$D_0 = a + \frac{b}{1+c}, \quad D_1 = a + \frac{b}{1 + ce^{d}}, \quad D_2 = a + \frac{b}{1 + ce^{2d}}, \quad D_{-\infty} = a + b, \quad D_{\infty} = a. \tag{B.24}$$

Following this same reasoning, the the respective mass exponents are given by

$$\tau(0) = a + \frac{b}{1+c}, \quad \tau(1) = 0, \quad \tau(2) = -a - \frac{b}{1 + ce^{2d}} \tag{B.25}$$

The singularity exponents by

$$\alpha(0) = a + \frac{b}{1+c} + \frac{bcd}{(1+c)^2}, \quad \alpha(1) = a + \frac{b}{1 + ce^{d}}, \tag{B.26}$$

$$\alpha(2) = a + \frac{b}{1+c} - \frac{bcde^{2d}}{(1+ce^{2d})^2}, \quad \alpha(-\infty) = a + b, \quad , \quad \alpha(\infty) = a. \tag{B.27}$$

In turn, the spectrum of singularities are given by

$$f(\alpha(0)) = a + \frac{b}{1+c}, \quad f(\alpha(1)) = a + \frac{b}{1+ce^{d}} \tag{B.28}$$

$$f(\alpha(2)) = a + \frac{b}{1+c} - \frac{2bcde^{2d}}{(1+ce^{2d})^2}, \quad f(\alpha(-\infty)) = a + b, \quad f(\alpha(\infty)) = a. \tag{B.29}$$

With the previous quantities we can obtain the mass exponents in the limit $\pm\infty$, by means of

$$\tau(-\infty) = f(\alpha(-\infty)) - \alpha(-\infty)q, \quad \tau(\infty) = f(\alpha(\infty)) - \alpha(\infty)q. \tag{B.30}$$

so that

$$\tau(-\infty) = (a+b)(1-q), \qquad \tau(\infty) = a(1-q) \tag{B.31}$$

Using the definition of multifractal correlation exponent eq. (2.1.29), we can obtain the correlation exponents from the relation

$$z(q) = 2a + \frac{b}{1+c} + (1-q)\left[\frac{2b}{1+ce^{dq}}\right] + (2q-1)\left[\frac{b}{1+ce^{2dq}}\right] \tag{B.32}$$

$$z(0) = 2D_0, \quad z(1) = D_0 + D_2, \quad z(2) = D_0 + a + \frac{3b}{1+ce^{4d}} - \frac{2b}{1+ce^{2d}}, \tag{B.33}$$

$$z(-\infty) = D_0 + (a+b)(1-q), \quad z(\infty) = D_0 + a(1-q). \tag{B.34}$$

In Section 5.1, Table 5.1, you will find the best parameters for modeling the generalized dimensions, the mass and singularity exponents, and the spectrum of singularities, the SN and Pop of the 15 largest Brazilian cities according to the 2010 census.

APPENDIX C – Sandbox Algorithm

In this appendix we highlight the points executed and the mathematical formalization for obtaining the generalized dimensions of the street network (SN) and the population (Pop) of the 15 largest Brazilian cities in 2010. We also show the equivalence between the generalized dimensions D_0, D_1, D_2 and the capacity d_B, information d_I and correlation d_C dimensions. In fact, for the case of the equivalence between D_2 and d_C, we show that by appropriately choosing a normalization factor, it is possible to interpret the generalized dimensions (for $q \neq 0, 1$) as being nothing more than the dimensions normalized by the correlation dimension d_C.

Generalized Dimensions of the SN

Below are the points taken into account when estimating street network (SN):

- to obtain information on the positions of the SN (x, y or lon, lat) of the nodes of a of size M_0 via osmnx, Figure 1;
- define the enclosing box side L (originating from the center of SN) over the nodes of the SN;
- define a lattice of size $S \times S$ (e.g., $S = 15$) with S^2 points and side L;
- find the points of the lattice at a previously specified distance d (e.g., $d = 50m$);
- Choose at random a number l $(s_1, s_2, ..., s_j, \ldots, s_l)$ of the points found;
- For each of the l points chosen, define k $(1 \leq i \leq k)$ circles of radius R_i $(R_1 = R_{min} < R_2 < ... < R_i < ... < R_k = R_{max})$ with $R_i \ll L$ and, for each of them, count the number of elements (nodes in the case of SN or people in the case of Pop) circumscribed, forming the matrix

$$M(R(s)) = \begin{pmatrix} M(R_1(s_1)) & M(R_1(s_2)) & \cdots & M(R_1(s_j)) & \cdots & M(R_1(s_l)) \\ M(R_2(s_1)) & M(R_2(s_2)) & \cdots & M(R_2(s_j)) & \cdots & M(R_2(s_l)) \\ \vdots & \vdots & \ddots & \vdots & \vdots & \vdots \\ M(R_i(s_1)) & M(R_i(s_2)) & \cdots & M(R_i(s_j)) & \cdots & M(R_i(s_l)) \\ \vdots & \vdots & \vdots & \vdots & \ddots & \vdots \\ M(R_k(s_1)) & M(R_k(s_2)) & \cdots & M(R_k(s_j)) & \cdots & M(R_k(s_l)) \end{pmatrix}. \quad \text{(C.35)}$$

- Calculate the ratio between $M(R(s))$ and M_0, raise it to the exponent $q-1$, where q are the moments of order, and obtain the average value of this ratio at each of the l points chosen for each of the R_j radii, forming the quantity

$$\left\langle \left[\frac{M(R)}{M_0}\right]^{q-1} \right\rangle = \begin{pmatrix} \frac{1}{l}\sum_{j=1}^{l}\left(\frac{M(R_1(s_j))}{M_0}\right)^{q-1} \\ \frac{1}{l}\sum_{j=1}^{l}\left(\frac{M(R_2(s_j))}{M_0}\right)^{q-1} \\ \vdots \\ \frac{1}{l}\sum_{j=1}^{l}\left(\frac{M(R_i(s_j))}{M_0}\right)^{q-1} \\ \vdots \\ \frac{1}{l}\sum_{j=1}^{l}\left(\frac{M(R_k(s_j))}{M_0}\right)^{q-1} \end{pmatrix} \quad \text{(C.36)}$$

- Building quantity

$$\left(\frac{R}{L}\right) = \begin{pmatrix} \frac{R_1}{L} \\ \frac{R_2}{L} \\ \vdots \\ \frac{R_i}{L} \\ \vdots \\ \frac{R_k}{L} \end{pmatrix}. \quad \text{(C.37)}$$

- Obtain the generalized dimensions of the SN according to eq. (2.1.27) and with the aid of a linear regression method.

Generalized Dimensions of the *Pop*

Below are the points taken into account when estimating *Pop*:

- Repeat the first 5 items to calculate the fractal dimension of the SN;
- Then carry out the following steps:

Let's consider a census grid containing t census tracts with areas $\{a_1, \ldots, a_t\}$ and populations $\{p_1, \ldots, p_t\}$ evenly distributed over them and defining k $(1 \leq i \leq k)$ circles of radius R_i $(R_1 = R_{min} < R_2 < ... < R_i < ... < R_k = R_{max})$ with $R_i \ll L$, we adopt the l $(s_1, s_2, ..., s_j, \ldots, s_l)$ points found as the origin of the k circles defined. In particular, choosing the point s_1, the areas of the k circles are given by

$$A(R_1(s_1)), A(R_2(s_1)), \ldots, A(R_i(s_1)), \ldots, A(R_k(s_1)).$$

For simplicity's sake, if we consider a census grid made up of $t = 3$ areas, and consequently $t = 3$ resident populations, then the resident Pop $M(R_1(s_1))$ within the circle of radius R_1 originating in s_1 can be obtained by adding the populations $\widetilde{p}_1$, $\widetilde{p}_2$ and $\widetilde{p}_3$ restricted to the circle of radius R_1 so that

$$\begin{aligned} M(R_1(s_1)) &= \widetilde{p}_1 + \widetilde{p}_2 + \widetilde{p}_3 \\ &= \frac{\widetilde{a}_1}{a_1}p_1 + \frac{\widetilde{a}_2}{a_2}p_2 + \frac{\widetilde{a}_3}{a_3}p_3 \\ &= \frac{A(R_1(s_1)|a_1)}{a_1}p_1 + \frac{A(R_1(s_1)|a_2)}{a_2}p_2 + \frac{A(R_1(s_1)|a_3)}{a_3}p_3 \\ &= \sum_{m=1}^{3} \frac{A(R_1(s_1)|a_m)}{a_m}p_m \end{aligned} \tag{C.38}$$

where $A(R_1(s_1)|a_m)$ is the area of the circle of radius $R_1(s_1)$ restricted to the area a_m of the mth census tract and p_m its respective Pop. In fact, for t census tracts, we have

$$M(R_1(s_1)) = \sum_{m=1}^{t} \frac{A(R_1(s_1)|a_m)}{a_m}p_m, \tag{C.39}$$

making it possible to construct a matrix, similarly to the case of the fractal dimension of the SN

However, considering the l points and the k radii chosen, it is possible to form the quantity

$$\left\langle \left[\frac{M(R)}{M_0}\right]^{q-1} \right\rangle = \begin{pmatrix} \frac{1}{l}\sum_{j=1}^{l}\left(\frac{1}{M_0}\sum_{m=1}^{t}\frac{A(R_1(s_j)|a_m)}{a_m}p_m\right)^{q-1} \\ \frac{1}{l}\sum_{j=1}^{l}\left(\frac{1}{M_0}\sum_{m=1}^{t}\frac{A(R_2(s_j)|a_m)}{a_m}p_m\right)^{q-1} \\ \vdots \\ \frac{1}{l}\sum_{j=1}^{l}\left(\frac{1}{M_0}\sum_{m=1}^{t}\frac{A(R_i(s_j)|a_m)}{a_m}p_m\right)^{q-1} \\ \vdots \\ \frac{1}{l}\sum_{j=1}^{l}\left(\frac{1}{M_0}\sum_{m=1}^{t}\frac{A(R_k(s_j)|a_m)}{a_m}p_m\right)^{q-1} \end{pmatrix} \tag{C.40}$$

- This topic is carried out analogously to topic 8 of the SN fractal dimension strategy;
- Obtain the generalized dimensions of the *Pop* according to eq. (2.1.27) and with the aid of a linear regression method.

In Section 2.1.4 we show the mathematical construction of the generalized dimensions and the multifractal spectrum.

In the Section 4.3 we present the details used to eliminate abnormal spectra and the parameters adopted in the simulations.

Figure 1 – Graphical representation of the strategy used to choose the possible points where the measurements will be taken. a) Geographical location (blue dots) of street intersections in the city of São Paulo, SP. b) Geographical location of street intersections and grid (black dots) 15×15 with equally spaced points. c) geographical location of street intersections, grid and nearest points (red dots), 50 m from the blue dots. d) geographical location of street intersections, grid, nearest points and randomly chosen points (yellow dots) where measurements will be taken.

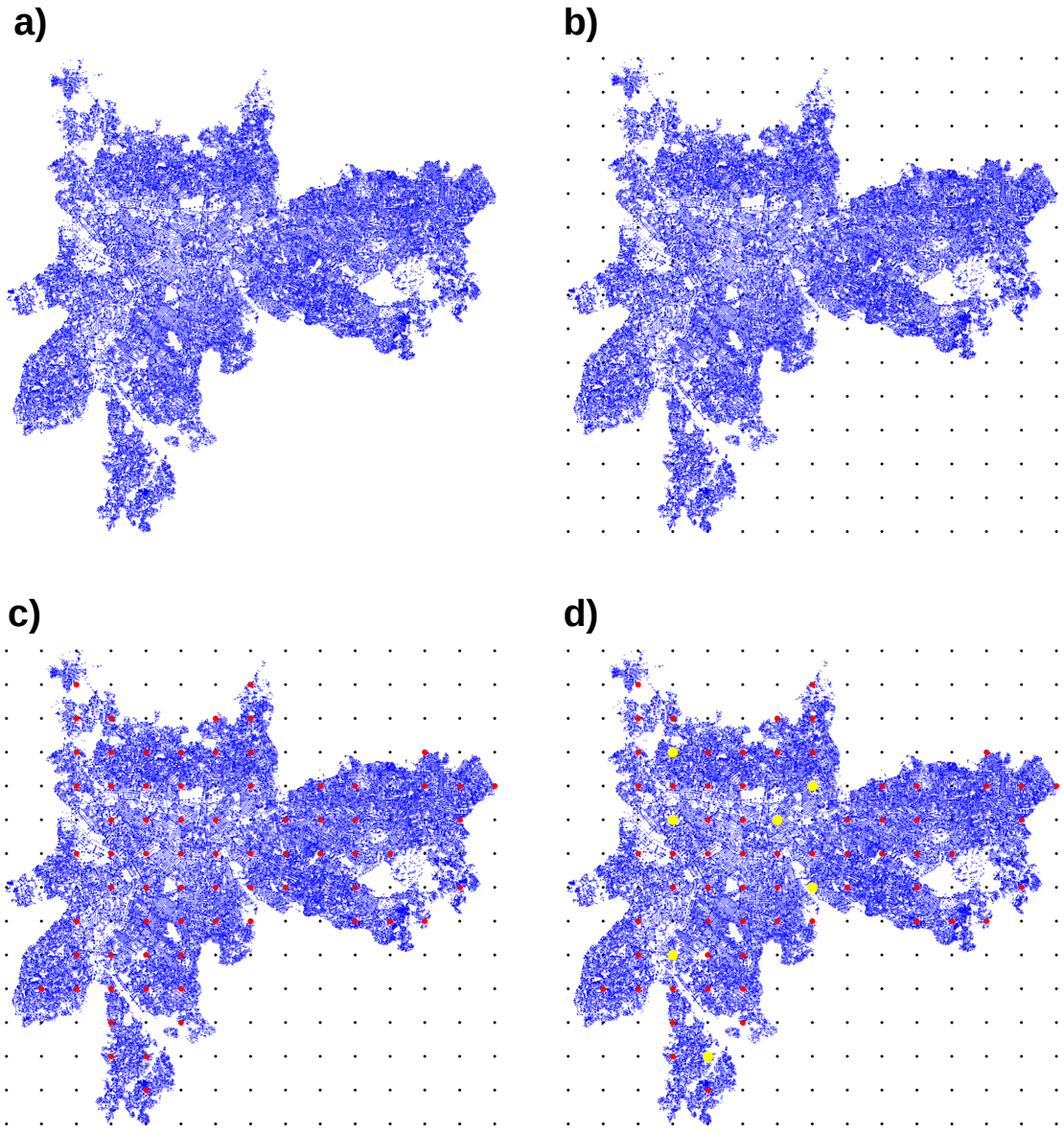

Source: Own authorship.

APPENDIX D – Equivalences for D_q

In this appendix we present the equivalences between the dimensions of capacity d_B, information d_I, correlation d_C and the generalized dimensions of order 0, 1, 2, respectively. We start by showing the equivalence between D_0 and d_B. To show this equivalence we follow Bartolo et al. (2004) and Rosenberg (2021). Calculating the limit of generalized dimensions when $q \to 0$, it follows

$$\lim_{q\longrightarrow 0} D_q = \lim_{q\longrightarrow 0}\left\{\frac{1}{q-1}\lim_{R/L\to 0}\frac{\ln\left\langle\left[\frac{M(R)}{M_0}\right]^{q-1}\right\rangle}{\ln\left(\frac{R}{L}\right)}\right\} = -\lim_{R/L\to 0}\frac{\ln\left\langle\left[\frac{M(R)}{M_0}\right]^{-1}\right\rangle}{\ln\left(\frac{R}{L}\right)} \tag{D.41}$$

In fact, the natural logarithm argument can be written as

$$\left\langle\left[\frac{M(R)}{M_0}\right]^{-1}\right\rangle = \frac{1}{M_0}\frac{M_0}{M(R)} = M(R)^{-1}. \tag{D.42}$$

where

$$\begin{aligned} D_0 &= -\lim_{R/L\to 0}\frac{\ln M(R)^{-1}}{\ln\left(\frac{R}{L}\right)} \\ &= \lim_{R/L\to 0}\frac{\ln M(R)}{\ln\left(\frac{R}{L}\right)} \end{aligned} \tag{D.43}$$

so that

$$\lim_{q\longrightarrow 0} D_q = d_B \tag{D.44}$$

provides the capacity dimension.

Now, we show the equivalence between D_1 and d_I. Making the approximation $q = 1 + dq$ where dq is an infinitesimal value of the moment order q, we can write

$$\left\langle\left[\frac{M(R)}{M_0}\right]^{1+dq-1}\right\rangle = \left\langle\left[\frac{M(R)}{M_0}\right]^{dq}\right\rangle = \left\langle e^{dq\ln\left[\frac{M(R)}{M_0}\right]}\right\rangle \propto \left(\frac{R}{L}\right)^{(1+dq-1)D_{1+dq}} = \left(\frac{R}{L}\right)^{dqD_{1+dq}}. \tag{D.45}$$

For $|dq| \ll 1$, you can use the Taylor series expansion of the exponential $e^x \approx 1+x$, which allows you to rewrite the left-hand side as

$$\langle e^{dq\ln\left[\frac{M(R)}{M_0}\right]}\rangle \approx \left\langle 1 + dq\ln\left[\frac{M(R)}{M_0}\right]\right\rangle = 1 + dq\left\langle\ln\left[\frac{M(R)}{M_0}\right]\right\rangle, \tag{D.46}$$

so we have

$$1 + dq \left\langle \ln \left[\frac{M(R)}{M_0} \right] \right\rangle \propto \left(\frac{R}{L} \right)^{dqD_{1+dq}} \tag{D.47}$$

which, taking the logarithm of both sides and using the approximation $\ln(1+x) \approx x$ for $|x| \ll 1$, follows

$$\left\langle \ln \left[\frac{M(R)}{M_0} \right] \right\rangle \propto D_{1+dq} \ln \left(\frac{R}{L} \right) \tag{D.48}$$

results in

$$D_{1+dq} = \lim_{R/L \longrightarrow 0} \frac{\left\langle \ln \left[\frac{M(R)}{M_0} \right] \right\rangle}{\ln \left(\frac{R}{L} \right)} \tag{D.49}$$

so that

$$D_1 = \lim_{dq \longrightarrow 0} D_{1+dq} = \lim_{R/L \longrightarrow 0} \frac{\left\langle \ln \left[\frac{M(R)}{M_0} \right] \right\rangle}{\ln \left(\frac{R}{L} \right)} = d_I \tag{D.50}$$

provides the information dimension.

Finally, the equivalence between D_2 and d_C follows. As a novelty, here's a way of showing the equivalence between D_2 and d_C. Starting from the integral correlation defined by

$$C(R) \equiv \lim_{M_0 \longrightarrow \infty} \frac{1}{M_0^2} \sum_{\substack{i,j=1 \\ i \neq j}}^{\infty} H(R - d_{ij}) \tag{D.51}$$

where

$$H(R - d_{ij}) = \begin{cases} 1, & R \leq d_{ij}, \\ 0, & R > d_{ij}, \end{cases} \tag{D.52}$$

is the Heaviside function and d_{ij} is the distance between two places on the fractal. Considering that

$$M(R) = M_0^2 C(R) = \sum_{\substack{i,j=1 \\ i \neq j}}^{\infty} H(R - d_{ij}), \tag{D.53}$$

so we have

$$\frac{M(R)}{M_0} = M_0 C(R) \tag{D.54}$$

so that

$$\left[\frac{M(R)}{M_0} \right]^{q-1} \frac{M(R)}{M_0} = \left[M_0 C(R) \right]^q . \tag{D.55}$$

But

$$\left[\frac{M(R)}{M_0} \right]^{q-1} \frac{M(R)}{M_0} = \left\langle \left[\frac{M(R)}{M_0} \right]^{q-1} \right\rangle \propto \left(\frac{R}{L} \right)^{(q-1)D_q} . \tag{D.56}$$

then, we have

$$[M_0 C(R)]^q \propto \left(\frac{R}{L}\right)^{(q-1)D_q} \tag{D.57}$$

which means

$$M_0 C(R) \propto \left(\frac{R}{L}\right)^{(q-1)D_q/q} \tag{D.58}$$

and

$$\frac{C(R)}{C(R')} \propto \frac{\left(\frac{R}{L}\right)^{(q-1)D_q/q}}{\left(\frac{R'}{L}\right)^{(q-1)D_q/q}} = \left(\frac{R}{R'}\right)^{(q-1)D_q/q}. \tag{D.59}$$

Applying the logarithm to both sides of the previous expression, solving for D_q and making $R, R' \longrightarrow 0$, we have

$$D_q \equiv k\left(\frac{q}{q-1}\right) \lim_{R,R' \longrightarrow 0} \frac{\ln\left[\frac{C(R)}{C(R')}\right]}{\ln\left[\frac{R}{R'}\right]} \tag{D.60}$$

where k is a normalization factor. In particular, for $q = 2$ and $k = 1/2$, it follows

$$D_2 \equiv d_C \tag{D.61}$$

where

$$d_C = \lim_{R,R' \longrightarrow 0} \frac{\ln\left[\frac{C(R)}{C(R')}\right]}{\ln\left[\frac{R}{R'}\right]} \tag{D.62}$$

is the correlation dimension. The previous result shows that the generalized dimensions are nothing more than normalized versions (for $q \neq 0, 1$) of the correlation dimension, as is expected according to Rosenberg (2021, p. 217). In Chapter 2, Section 2.1.4, we show the construction of the generalized dimensions and the multifractal spectrum.